Organocatalysis by halogen bonding donors: A promising complement to hydrogen bond-based catalysis.

A thesis presented to Trinity College Dublin, the University of Dublin for the degree of Master of Science

Marianne Rica Garcia

Under the supervision of Dr. Cristina Trujillo

March 2023 Trinity College Dublin

I declare that this thesis has not been submitted as an exercise for a degree at this or any other university and it is entirely my own work.

I agree to deposit this thesis in the University's open access institutional repository or allow the Library to do so on my behalf, subject to Irish Copyright Legislation and Trinity College Library conditions of use and acknowledgement.

I consent to the examiner retaining a copy of the thesis beyond the examining period, should they so wish (EU GDPR May 2018).

.....

Marianne Rica Garcia

1 Acknowledgements

Firstly, I would like to thank my amazing girl boss of a supervisor, Dr Cristina Trujillo for her guidance and support throughout the whole research masters. I could not have done this without her.

I would also like to express my sincerest gratitude to my research group. To Iñigo; queen of figures and a great computational chemist, who has helped me tremendously from the very beginning. To Nika, my twin; who is a fashion icon and who was by my side for the majority of my time as a master's student. To Diana, my dictionary; who helped me whenever I was lost for words and fueled my sugar addiction. I would have never had such a great and memorable post-graduate experience without them. I would also like to thank the Connon boys; Lorenzo, Ian and Lee, and, additionally, Maxime, for their friendship throughout the years.

I would like to thank the staff at the Irish Centre for High-End Computing (ICHEC) for maintaining the Kay cluster where I performed my calculations, enabling me to carry out my research.

Finally, I would like to convey my greatest appreciation to my family. My Dad, my Mom, Thea, Meil and Nicole have been the best support system for me throughout my life and, especially, throughout my master's degree. They have provided for me financially, emotionally and mentally, and without them, I would not be where I am today. I am so lucky and eternally grateful to have them by my side. I'd also like to acknowledge my fur babies; Chip and Mac, who have been and continue to be great stress relievers for me (most of the time). And lastly, I would like to thank Orán, who was an amazing boyfriend, who supported me in my journey and was there for me when I needed him.

2 Abstract

Catalytic transformations, previously dominated by metal catalysts, have seen exponential growth in the use of organocatalysts over the last two decades. The emergence of small organic molecules employed to facilitate chemical reactions has played a significant role in a more economical and sustainable synthetic approach. Examples of such molecules include the well-established hydrogen bond catalysts and their analogous halogen bond catalysts. While halogen bond catalysts are known to have more desirable features than their predecessor, such as a higher degree of directionality and tunability, there have only been a handful of reports on the use of halogen bond-based catalysts in organocatalysis.

Herein, in this project, theoretical investigations have been carried out in relation to non-covalent interactions within organocatalysis. The first study involved hydrogen bond interactions to analyse the type of binding modes that can simultaneously form and the influences cooperativity and secondary interactions have on them.

In the second part of this research project, halogen bond-based catalysis was studied and for that two different reactions were theoretically investigated. The first reaction involved a halide abstraction reaction between a benzyl bromide and acetonitrile, catalysed by two catalysts to reveal the reaction mechanism and to determine the binding modes of each catalyst. The second reaction carried out was a Michael addition reaction between a trans-crotonophenone and an indole, catalysed by five different catalysts, in order to establish the effects produced when different halogen atoms are used and to study the substituent effects on the halogen bond strength by modifying the catalytic scaffolds. A successful redesign of two new catalysts was established based on the results obtained.

List of Figures

List of Tables

Acronyms

AIM Atoms in Molecules.

BCP Bond Critical Point.

DFT Density Functional Theory.

HB Hydrogen Bonding.

HF Hartree-Fok.

LDA Local-Density Approximation.

LSDA Local Spin-Density Approximation.

meta-GGA Meta-Generalized Gradient Approximation.

NBO Natural Bond Orbitals.

PBE Perdew-Burke-Ernzerhof.

QTAIM Quantum Theory of Atoms In Molecules.

SMD Solvation Model based on Density.

XB Halogen Bonding.

Contents

3 Introduction

As a fundamental component of modern synthetic chemistry, catalysis is one of the most active fields in chemical research in pursuit of the most ideal synthetic processes for producing useful compounds with 100% selectivity in maximum yields. 'Chirality' a well-known concept where compounds can exist in two non-superimposable mirror images called enantiomers (Figure 3.1), play an important role in the recognition between biologically active molecules and their targets, having substantial effects based on which enantiomer is formed.[1,2] This was found to be paramount in drug design, where the binding affinity for a chiral drug can differ between enantiomers and the production of both counterparts may lead to devastating consequences. The drug thalidomide is a prime example of this;[3] originally developed to mitigate morning sickness in pregnant women, the drug was found to cause a fetal deformity as it consisted of equal parts of enantiomers where one was highly effective and its mirror image was highly toxic.

Synthetic research into the development of these molecules was primarily established through transition metal catalysis in the 1950s[4] and has now evolved into one of the most active homogeneous catalysis disciplines. Since then, several branches of catalysis have emerged, most notably organocatalysis.

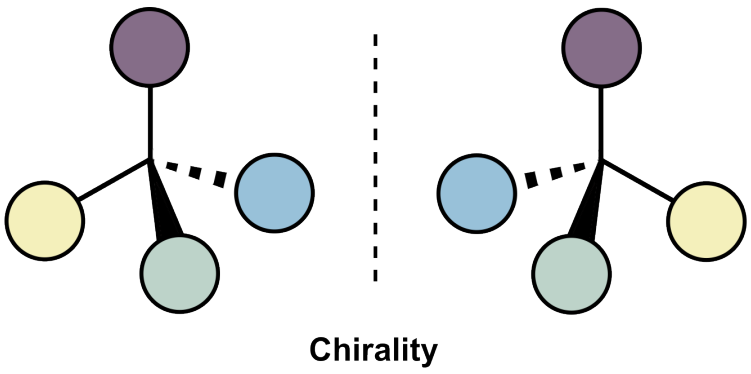

Figure 3.1: Non-superimposable mirror images.

Organocatalysis was first demonstrated in 1970s[5,6] in an asymmetric aldol reaction catalysed by proline. This was followed by decades worth of accomplishments within organocatalytic reactions, however, the great success of metal catalysis overshadowed its advancements. It was only in the late 1990s that seminal studies[7] of non-metallic catalysts; consisting of ketone, thiourea, and amine analogues, caught the attention of researchers contributing to an increase in the popularity of organocatalysts. Further discoveries of novel modes of activation have ignited the field's exponential evolutionary growth. A few examples of these include; the formation of covalent bonds in carbonyl compounds with enamine and iminium-based catalysts resulting in more stabilised LUMO/HOMO energy levels, the formation of chelating hydrogen bonds brought upon by urea/thiourea catalytic scaffolds resulting in the activation of polarised double bonds, and finally, bifunctional chiral phosphoric acid catalysts which have characteristics of both Brønsted acid and a Lewis base unit.

Additionally, organocatalysts possess several highly desirable advantages over metal catalysis making them a more desirable and 'greener' design approach; including stability in air and water, ease of experimentation, relative non-toxicity, reproducibility, versatility, availability of natural resources, and ability to access both enantiomers of the desired product.[8] Despite being a relatively stagnant field until recently, in the last two decades, organocatalysis has grown dramatically due to List[9–11] and MacMillan's[12–16] influential work inspiring other chemists to follow pursuit (some examples of famous organocatalysts can be seen in Figure 3.2), accelerating the advancement of organocatalytic research and, therefore, becoming one of the fastest growing areas of modern chemistry. This consequently awarded them the Chemistry Nobel Prize in 2021.

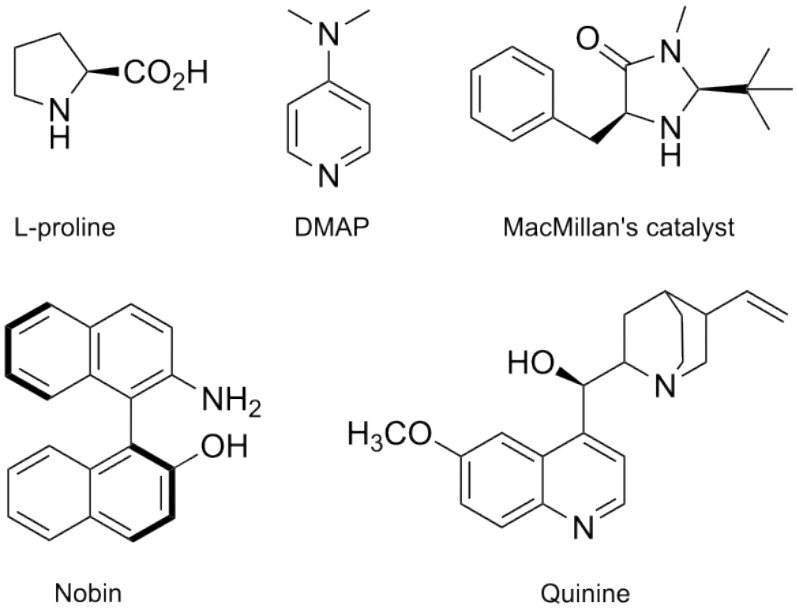

Figure 3.2: Main examples of well-known organocatalysts used in synthetic transformations.

3.1 Non-Covalent Interactions within Organocatalysis: hydrogen bond vs halogen bond

Hydrogen bond (HB) is a non-covalent interaction that is defined by IUPAC[17] as "an attractive interaction between a hydrogen atom from a molecule or a molecular fragment X–H in which X is more electronegative than H, and an atom or a group of atoms in the same or a different molecule, in which there is evidence of bond formation". Organocatalysts that result in the formation of HB complexes are regarded as HB catalysts and have played a predominant role within organocatalysis. HBs are presented in Figure 3.4, where R–H is the HB donor with the hydrogen atom covalently bonded to an R group (more electronegative than hydrogen) and Y is the HB acceptor. HBs are highly flexible with regard to bond length and angle and are characterised to be stronger than van der Waals interactions. HB catalysts are widely known for their strength and their high efficiency to produce multiple chiral centres affording high stereoselectivity.[18–24] Early HB catalysts were mainly based on thiourea derivatives which then further evolved to squaramide-based catalytic scaffolds[25] (Figure 3.3). The successful applications of these HB catalysts led to the development of other non-covalent interactions, most importantly, halogen bonds.

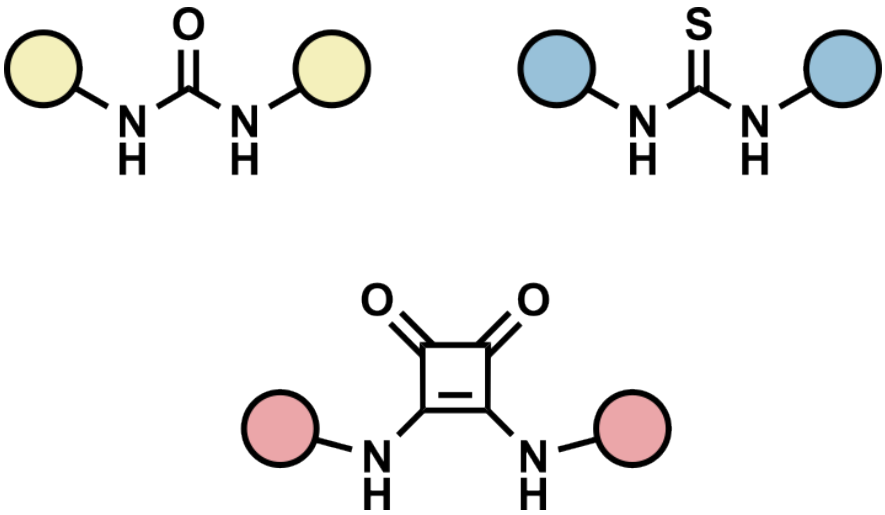

Figure 3.3: Early hydrogen bond-based catalytic scaffolds; urea (top left), thiourea (top right), and squaramide scaffolds (bottom).

Halogen bond (XB) is defined by IUPAC[26] as "a net attractive interaction between an electrophilic region associated with a halogen atom in a molecular entity and a nucleophilic region in another, or the same, molecular entity". Supporting this definition, XB is presented in Figure 3.4, where R–X is the XB donor, X is a halogen atom covalently bonded to an R group (electrophilic region) and Y is the XB acceptor (nucleophilic region). While a group of halogens typically consist of fluorine, chlorine, bromine and iodine with their polarisibility increasing from F $<$ Cl $<$ Br $<$ I, fluorine is not usually considered among the halogens involved in XB due to the atom being less polarisable and can only act as an XB donor when attached to particularly strong electron-withdrawing groups.[27–30]

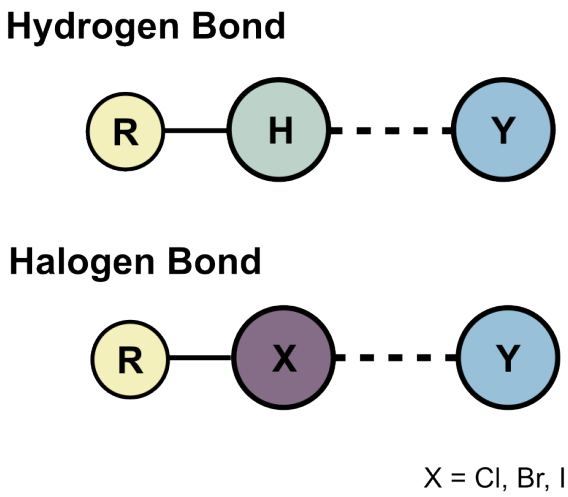

Figure 3.4: Hydrogen bond vs halogen bond interactions.

The first XB complex was synthesised by Colin in 1814.[31] Nevertheless, it took approximately another one and a half centuries to produce pioneering discoveries of charge-transfer interactions, carried out by Mulliken[32] and Hassel[33] which earned them the Chemistry Nobel prize in 1966 and 1969, respectively, for their contributions that lead to significant advancements in the understanding of the interactions that give rise to such complexes. Subsequent computational studies carried out by Politzer *et al.*[34] coined the term 'σ-hole', a concept which represents one of the most accepted explanations for halogen bonding. In this model, the 'σ-hole' describes the halogen atom by an anisotropic distribution of electronic density with a localised field of positive electrostatic potential along the R–X bond, which is depicted in Figure 3.5.

XB has recently emerged as a promising aspect in the field of organocatalysis for their similar features when compared to HBs,[35–37] which are known as one of the most prevalent non-covalent interactions, especially in organocatalysis. Compared to HB, XB presents superior features, making it a more desirable field of research for many scientists. These features include excellent directionality, polarisability, tunability of XB strength through the addition of multiple scaffolds and several halogen atoms that differ in oxidation states leading to diverse solubility and binding energies, and lastly, hydrophobicity, allowing for great efficiency in the design and preparation of self-assembled systems.

XB presents high directionality due to the localisation of the σ-hole along the extension of the R–X bond. Experimental and theoretical investigations have demonstrated that the nucleophile (i.e. the XB acceptor) establishes an interaction with the σ-hole and therefore presents an R-X···Y angle, which is approximately 180°, between the covalent and non-covalent bonds around the halogen atom[38] (Figure 3.5, left).

The strength of the XB interaction can easily be tuned by modifying the

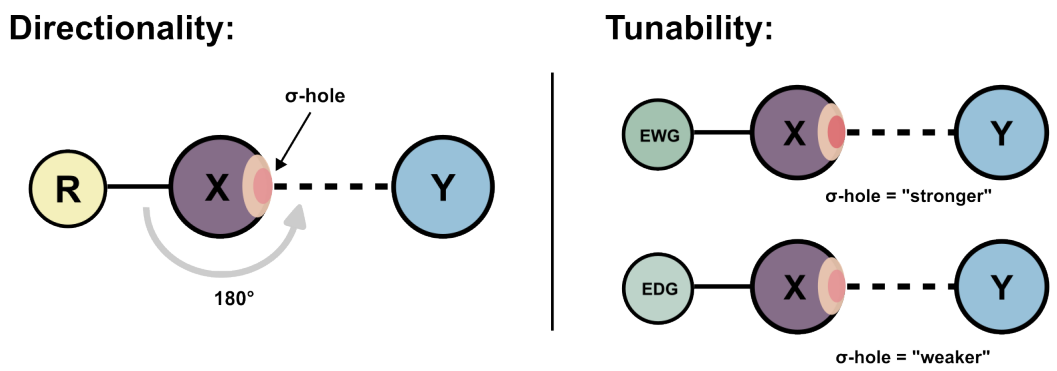

Figure 3.5: Halogen bonding characteristics.

halogen atom or modifying the ability of electron-withdrawing moieties covalently bonded to the halogen atom (Figure 3.5, right). The strength of the XB donor increases from Cl < Br < I, as the electronegativity decreases, leading to an increase in the polarisability of the halogen atom and, therefore, resulting in the increase of the magnitude of the positive sigma hole. The modification of the R-groups attached to the halogen atom affects the electron-donating capabilities and can be suited to increase the strength of the sigma hole, leading to the possibility of stronger XB interactions.

Finally, as hydrogen and halogen atoms reside at polar ends of the periodic table, they differ significantly in orbital size and softness. As a result, the XB catalysts possess lower solvent dependency and have the ability to thrive in apolar solvents, in comparison to HB catalysts. The hydrophobic characteristics of halogen atoms present many benefits and applications in organocatalysis, especially towards drug design where the absorption of a drug and its ability to pass through cell membranes is a critical criterion to consider.[39,40]

The use of XB catalysis within organocatalytic transformations is considered to be a relatively new field. It was only within two decades that synthetic research has been established surrounding the exploration around the modes of activation by XB catalysts (Figure 3.6), in which the majority of these catalysts were achiral and did not produce enantioselectivity. In 2008, Bolm and co-workers[41] were the first group to report an XB interaction to promote the activation of C=N bonds in reducing quinoline derivatives in the presence of perfluoroalkyl iodides. In 2011, the first demonstration of organic halide activation was presented by Huber *et al.*,[42] with strong experimental evidence effectively ruling out the hidden Brønsted acid catalysis as an alternative activation pathway, where it was proposed that cases in which Brønsted acid released from any kind of precursor is responsible for an observed catalytic activity, rather than the precursor itself.[43] Similarly, the first XB-catalysed halide abstraction was established in 2013 by the same group, displaying the success of multiple mono- and multi-dentate XB catalysts in a reaction between 1-chloroisochroman and ketene silyl acetals,[44] ruling out the previous assumption that hidden acid catalysis was the cause of activation in the relative reaction. Furthermore, the aforementioned benchmark reaction was presented to be the first example of an XB-induced C–C bond formation.

However, the mechanistic pathway of halide abstraction remains unknown to this day. Lastly, in 2017, a Michael acceptor activation was established, using molecular iodine as the catalyst, by Breugst and co-workers.[45] The group were able to rule out the competing hidden Brønsted acid catalysis, consequently presenting an approach to distinguish between XB catalysis and Brønsted acid catalysis.

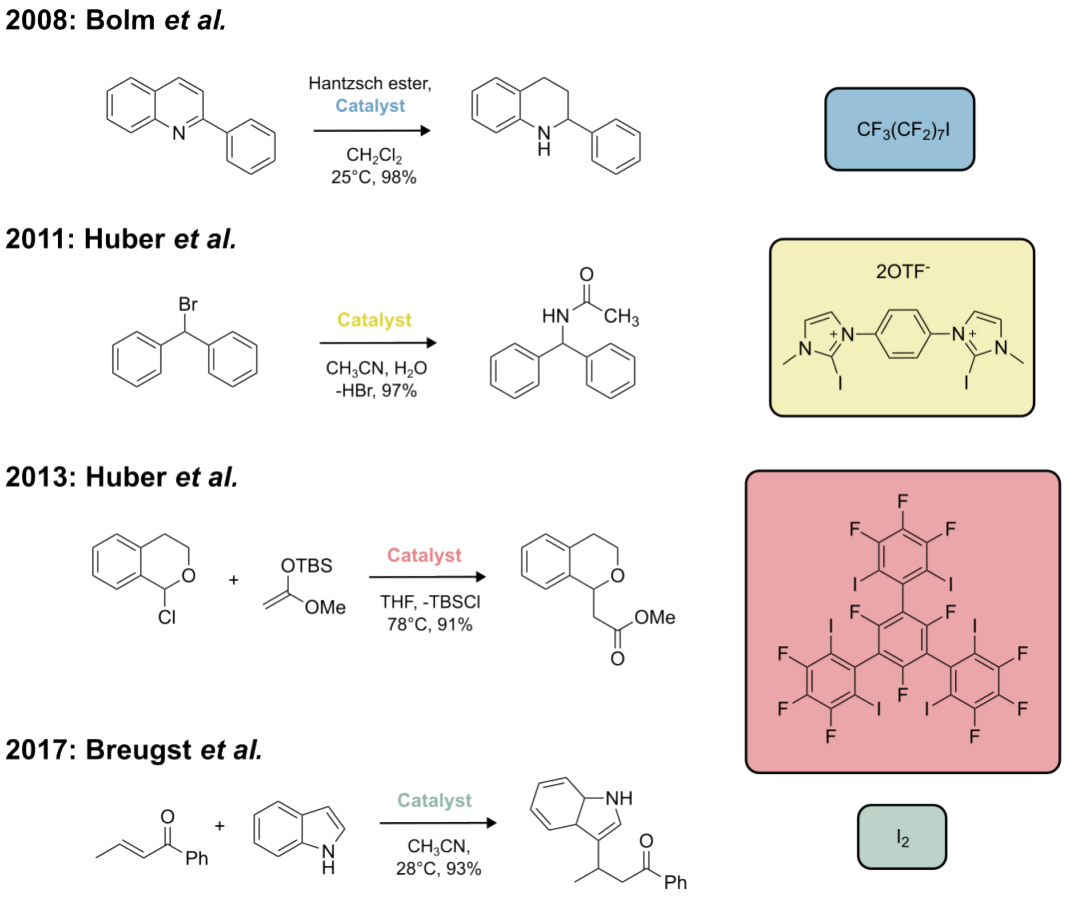

Figure 3.6: Synthetic research on XB-based organocatalysts carried out within the last two decades, displaying the optimal reaction conditions and catalysts used to achieve the highest percentage yield.

3.2 Computational approach

Computational chemistry is a branch of chemistry that uses computer simulations to assist in solving chemical problems. Incorporating computer programs allows the calculation of structures and the analysis of molecular properties. In silico research possesses many advantageous qualities over traditional experimental approaches such as the determination of molecular geometries and the prediction of reaction rates, unknown molecular properties, and mechanistic pathways while presenting an efficient and cost-effective approach towards the synthesis of new compounds. Traditionally, the use of computational methods was perceived as a complementary tool in the validation of synthetic research. However, the continuous development of computing technology has attributed to its evolution from a complimentary aspect to a more synergetic role. While the organocatalytic field of research is just emerging, it has established great potential. For instance, reliable quantum chemical calculations have been able to shed light on the thermodynamics and kinetics of catalytic reactions, have characterised and provided meaningful insights towards transition states which are vital in the understanding of stereoselective properties of XBs and their mode of activation, and finally, have allowed the possibility of designing novel XB catalysts based on theoretical calculations.

Previous research has focused on calculating XB-catalysed transition states and binding complexes which aids in the understanding of XB activation.[46–50] In the early stages of XB catalysis, XB catalysts were primarily neutral compounds. Soon after, charge XB catalysts began to surpass charge-neutral XB catalysts due to their high potency in comparison to the latter.[42,50–53]

Molecular iodine-catalysed reactions have been the subject of the most extensive synthetic and computational studies within XB-catalysed organocatalysis. Breugst *et al.*,[54] carried out a computational study of four different organic reactions catalysed by I_2 (Figure 3.7). These reactions include an intramolecular cyclisation of aminochalcone and three intermolecular Michael addition reactions; pyrrolidine to methyl acrylate, methyl pyrrole to nitrostyrene, and indole to trans-crotonophenone. In comparing the free energy barriers of the catalysed and uncatalysed transition state complexes in each respective reaction, it was found that the reaction barriers of the catalysed complexes lowered the energy barriers by 5.7, 2.4, 1.9, and 7.6 kcal/mol, respectively. Subsequently, a follow-up investigation of the latter XB-catalysed Michael addition reaction of indole to trans-crotonophenone by the same group,[45] helped rule out the Brønsted acid catalysis in favour of the XB catalysis mechanism, as mentioned previously.

In 2016, a neutral in silico-designed tridentate halogen bond catalyst was developed by Wong's group,[55] to catalyse a Diels–Alder addition between cyclopentadiene and buten-2-one. This afforded a more stable free energy barrier in the catalysed reaction by 2.5 kcal/mol. Furthermore, a bidentate cationic catalyst designed by Huber and co,[49] achieved a further 3 kcal/mol stability in the energy barrier of the same reaction, showing the increased potency cationic XB catalysts have over neutrally charged catalysts. While the field of XB catalysis is emerging, the development of XB catalysts has a significantly lower pace in comparison to the design of HB catalysts.

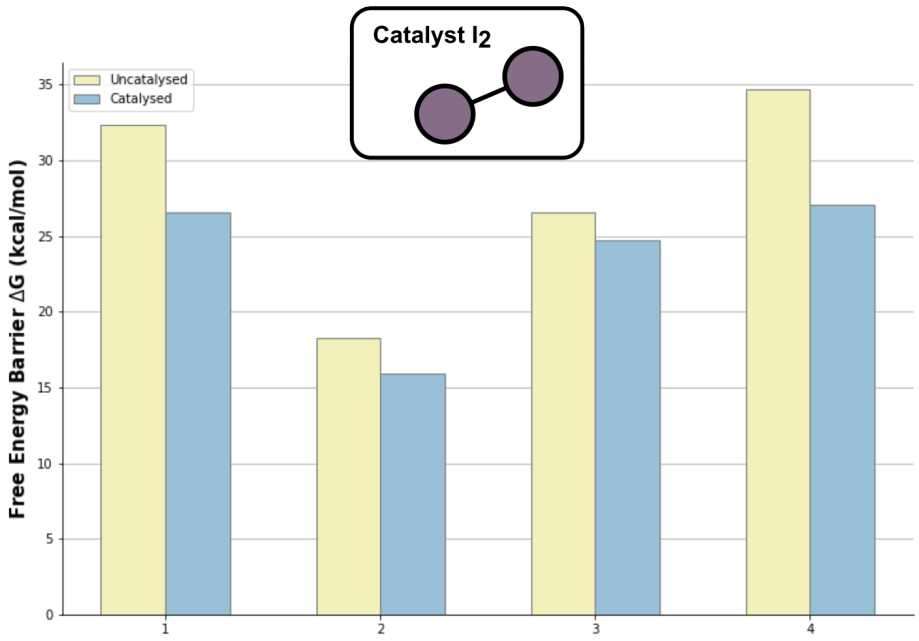

Figure 3.7: Theoretical mechanistic studies carried out on four reactions catalysed by molecular iodine. 1) Cyclisation of aminochalcone. 2) Michael addition of pyrrolidine to methyl acrylate. 3) Michael addition of methyl pyrrole to nitrostyrene. 4) Michael addition of indole to trans-crotonophenone.

3.3 Aims and objectives

At present, from the previous experimental and theoretical studies mentioned, it is clear that there remains to be insufficient research of XB-based catalysts and the nature of the XB interactions towards its applicability in organocatalysis, in comparison to the abundantly researched HB interactions. Furthermore, mechanistic studies in multiple organic transformations that employ XB catalysts continue to be undetermined, either experimentally or theoretically. With the use of computational methods presenting many advantages and having acknowledged the synergy between experimental and computational studies, herein, theoretical investigations have been carried out on HB interactions and XB-based catalysts to further understand these types of non-covalent interactions.

Firstly, an HB-based computational investigation has been carried out in order to study the types of HB binding patterns, shown in Figure 3.8, that can be established within catalytic and biological systems despite its prominence in literature, as there have been no theoretical insights on these patterns themselves.

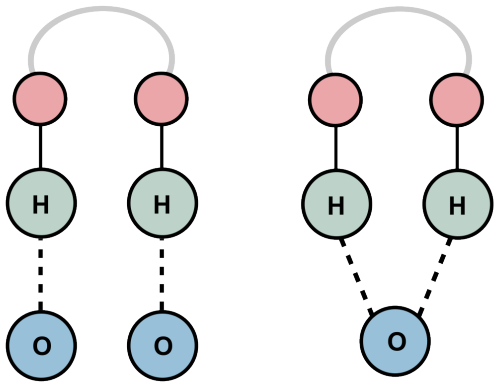

Figure 3.8: Types of hydrogen bond interactions that can be established in biological and catalytic systems; parallel (left) and bifurcated (right).

As HB interactions have been well-established to produce excellent catalytic properties within organocatalysis, the formation of simultaneous HBs has been known to establish cooperative reinforcing effects due to secondary interactions which influence the different types of bond formation and hence, determine the stability of the HB complexes[25,56,57] .

Therefore, in the first part of the manuscript, the exploration of the different types of HB binding modes formed has been studied in both catalytic and biological environments in order to analyse the simultaneous HB formation and the secondary interactions that influence the patterns of the binding modes (Figure 3.8).

In the second part of the project, a theoretical study of the role of XB-based organocatalysis has been presented, for which a halide abstraction and a Michael addition reaction catalysed by XB donors have been investigated.

XB donor catalysts have been well established in facilitating stable carbocation formation through halide abstraction. However, the respective reaction mechanism is still unknown and remains to be unexplored both theoretically and experimentally. There have been two proposed mechanistic pathways (Figure 3.9); pathway 1, where an XB donor interacts with an R–X bond of a leaving group thus facilitating a heterolytic bond cleavage, and pathway 2, where the XB donor binds to the halide anion released during an R–X bond heterolysis.[42,58]

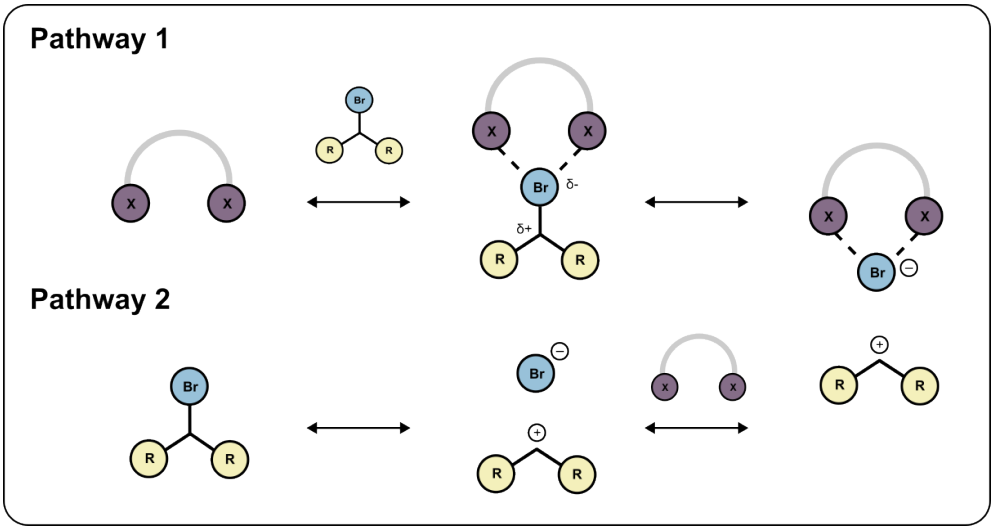

Figure 3.9: Two proposed mechanistic pathways for the halide abstraction reaction.

Following experimental works carried out by Huber *et al.*,[42] where an XB-mediated halide abstraction reaction under the presence of several cationic and neutral XB donors has proven to be a rational benchmark, the above reaction along with its specific reaction conditions was chosen for this computational investigation to shed light on the mechanistic pathway.

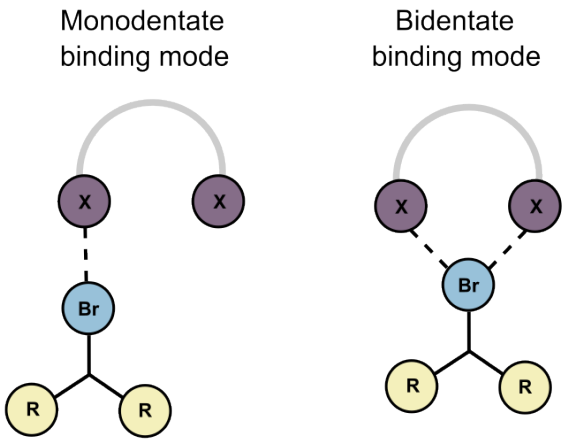

Figure 3.10: Two proposed catalyst-substrate XB binding modes; monodentate (left), and bidentate (right).

Both mono- and multi-dentate XB donors have the potential for activating suitable substrates, having been well described in the literature,[44,50,59] and while the latter is regarded to be systematically more efficient as it tends to bind more strongly to the substrate creating a more stable activated complex, only a handful of multi-dentate XB donors have been examined thus far. The synthesis of mono- and multi-dentate XB donors remains to be a challenging albeit emerging area in organocatalysis with insufficient rational investigations towards the justification of binding modes[60] and therefore has been the driving force of this computational study. This second part of the project imminently focused on revealing the reaction mechanism and determining the binding mode of both catalysts; either a monodentate binding mode consisting of a single parallel XB interaction or a bifurcated binding mode involving two XB interactions (see Figure 3.10).

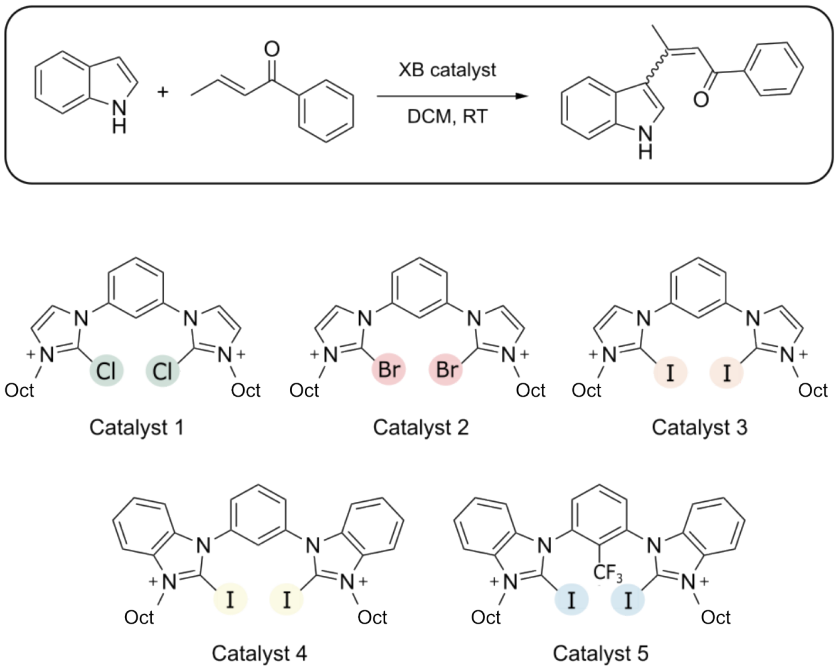

Figure 3.11: Michael addition reaction with trans-crotophenone and an indole, catalysed by five different catalysts.

While the use of XB donors is now on the rise, at present, only a handful of organic reactions employ them as catalysts. The Michael addition reaction catalysed by XB donors, mentioned previously, is one of the few established in the literature. A benchmark reaction carried out by Breugst and coworkers[54] established elemental iodine as an optimal XB catalyst in the Michael addition reaction, however, the possibility of modifying the catalyst in order to improve catalysis is highly limited. Therefore, Gliese *et al.*,[48] built on the aforementioned benchmark reaction, developing multiple XB donors which have been proven to be efficient catalysts in the activation of a carbonyl group (Figure 3.11). Catalysts 1, 2 and 3 were synthetically designed, varying in halogen atom from the least polarisable to the most polarisable, and catalysts 4 and 5 incorporated different scaffolds. The main conclusion of their experimental study entails that

the rate of product conversion within the reaction significantly increases, from chlorine to bromine-based catalysts and more significantly with iodine-based catalysts, demonstrating that the iodine-containing catalysts show greater efficiency in increasing the rate of reaction. Furthermore, great catalytic enhancement was shown within the reaction through the incorporation of structural modifications of the catalysts.

This final part of this project was inspired by the experimental work mentioned above, which aimed to rationalise the experimental findings by exploring the catalyst-substrate binding site. Thereby, obtaining theoretical rationalisations, to be able to generate new catalytic designs that can significantly enhance catalytic properties.

4 Computational theory

4.1 Density Functional Theory

The field of computational chemistry began in the early 20th century and continues to grow exponentially. It has been applied alongside experimental investigations in multiple disciplines within chemistry, however, the limitation of its applicability is related to the status of the computational technology. The combination of the continuous advancement of technology and the development of new quantum methodologies has enabled computational chemists to study chemical systems that were thought to have been impossible in previous years. Density Functional Theory (DFT), is a quantum methodology within computational organic chemistry renowned for its balance between accuracy and computational cost, making it a staple when studying chemical systems.

4.1.1 History

Density Functional Theory is a quantum methodology developed in 1964 by Pierre Hohenberg and Walter Kohn as an alternative to the wavefunction methods used to solve the Schrödinger equation[61] (Equation. 1). This equation assumes that, if photons have both corpuscular and wave behaviour, all the particles should have both behaviours as well.

$$i\hbar\frac{\delta\Psi}{\delta t} = -\frac{\hbar^2}{2m}\left(\frac{\delta^2\Psi}{\delta x^2} + \frac{\delta^2\Psi}{\delta y^2} + \frac{\delta^2\Psi}{\delta z^2}\right) + U(x,y,z)\Psi = \hat{H}\Psi \tag{1}$$

For stationary calculations, the time-dependent Schrödinger equation can be simplified by substituting the Hamiltonian with a version that is independent of time. This can be obtained by rewriting the equation by splitting up the nuclei and electron coordinates(Equation 2).

$$\hat{H}(r_i, R_i)\Psi(x_i, R_i) = E\Psi(x_i, R_i) \tag{2}$$

As the previous mathematical formalism to solve the Schrödinger equation where only hydrogen atom and mono-electronic cations ($He^+, Li^2+, ..$) have an exact solution, Hohenberg and Kohn developed a new formalism, the 'exact density formalism'.[62] It declares that the ground state energy of a system can be obtained from its electronic density, and relates to the wavefunction of the ground state. $\Psi_{(GS)}$, with the electronic density, ρ, in a N-electron system. Obtaining the following equation (Equation. 3) for describing the ground state energy of a system.

$$E_0 = \int ... \int \left[\int [\Psi^*(r, r_2, ..., r_N \hat{H}\Psi(r, r_2, ..., r_N]dr_2...dr_N\right] \tag{3}$$

This new Hamiltonian can be split into multiple parts following the Born-Oppenheimer approximation (Equation. 4). As a result, the nuclear kinetic energy can be neglected and the Hamiltonian can be described as the sum of the electronic kinetic energy, $\hat{T}(r)$, the electron-electron and nucleus-nucleus Coulombic repulsion, $\hat{V}(r)$ and $\hat{V}(R)$ respectively, and the electron-nucleus Coulombic attraction, $\nu(r)$, also known as the external potential.

$$\hat{H}_{el}(r,R) = \hat{T}(r) + \hat{V}(r) + \hat{V}(R) + \nu(r) \tag{4}$$

When this new Hamiltonian is introduced in the ground state energy equation, the first three terms can be combined in the so-called '*functional*' ($F[\rho(r)]$), separated from the external potential (ν), obtaining the following energy expression (Equation. 5).

$$E_0 = \int ... \int F_x[\rho(r)] + \int_{-\infty}^{\infty} \rho(r)\nu(r)dr \tag{5}$$

In contrast with the wavefunction methodology, where it was incapable of solving the equation for multiple electron systems, this new methodology struggles with obtaining the exact electronic density distribution. In such a distribution, the system's energy would be minimized.

To simplify the method and to obtain the functional corresponding to the electronic distribution, Walter Kohn collaborated with Lu Sham to define the electron density as a sum of orbital densities (Equation. 6).[63]

$$F_x[\rho(r)] = \hat{T}[\rho(r)] + \frac{1}{2}\int\int \frac{\rho(r_1)\rho(r_2)}{|r_1 - r_2|}dr_1dr_2 + E_{XC}[\rho(r)] \tag{6}$$

This functional is expressed as the sum of three terms: the electronic kinetic energy, $\hat{T}[\rho(r)]$, remaining changed, the electron-electron interaction in the electronic density and the exchange-correlation energy, $E_{XC}[\rho(r)]$, reflecting the interactions and exchanges between same-spin electrons among the system. The current system is described by a set of orbitals that contains non-interacting electrons, known as Kohn-Sham orbitals, that must satisfy the Schrödinger equation for the system (Equation. 7).

$$\hat{H}^{KS}\Phi_i^{KS}(r_i = \epsilon_i\Phi_i^{KS}(r_i) \tag{7}$$

4.1.2 Functionals and basis sets

The Kohn-Sham theory has resulted in the development of multiple functionals and basis sets under different approximations in order to enhance the level of description of different systems.

The most widely used functional has been B3LYP, a hybrid-functional developed by Becke,[64] due to the fact that it provides a good comparison with previous functionals or other more demanding methods like post-HF methods such as Møller–Plesset or coupled-cluster, in terms of the relationship between computational cost and accuracy.

Despite its popularity, B3LYP presents difficulties in describing non-covalent interactions as it neglects dispersion. Therefore, new functionals were developed that take into account the dispersion aspect, allowing to effectively describe the above interactions. Some examples include M06-2x,[65] ωb97xD[66] and B3LYP-3D,[67,68] for which M06-2X is one of the most popular functionals used.

M06-2X is a hybrid Meta-Generalized Gradient Approximation (meta-GGA) functional. This means that the exchange-correlation energy contribution is cal-

culated as a linear combination of the Hartree-Fok (HF) exchange functional and a certain number of both exchange and correlation density functionals.

To calculate the exchange and correlation energies more accurately, as exact functionals are unknown for these contributions, several approximations have been developed over the years.

Local-Density Approximation (LDA) and Local Spin-Density Approximation (LSDA) are two of the simplest approximations, where the exchange-correlation functional depends only on the (spin-)density at a given coordinate (Equations. 8 and 9).

$$E_{XC}^{LDA}[\rho] = \int \rho[r]\epsilon_{XC}(\rho(r))dr \tag{8}$$

$$E_{XC}^{LSDA}[\rho_\alpha, \rho_\beta] = \int \rho[r]\epsilon_{XC}(\rho_\alpha, \rho_\beta)dr \tag{9}$$

These approximations are highly extended due to the possibility of splitting the exchange-correlation functional linearly in exchange and correlation contributions (Equation. 10).

$$E_{XC}^{LDA/LSDA}[\rho(r)] = E_{X}^{LDA/LSDA}[\rho(r)] + E_{C}^{LDA/LSDA}[\rho(r)] \tag{10}$$

Perdew-Burke-Ernzerhof (PBE) is another approximation which calculates the exchange-correlation functional taking into account the semi-local density at a given point.

M06-2x combines 32 empirically optimised parameters into the exchange-correlation functional with a 54% of HF exchange.

This functional is, amongst all the available 06 families of Minnesota functionals, one of the most suitable options for thermochemistry, kinetics and non-covalent interactions.[69]

In order to solve the Schrödinger equation and obtain the energy of a molecular system it is necessary to use a set of functions that represent the electronic wave-function as algebraic equations instead of differential equations. Among the wide variety of basis sets that have been developed in the past decades, correlation-consistent basis sets and gaussian-type atomic orbitals are the most important, the latter being the most commonly employed for molecular systems.

Correlation-consistent basis sets were developed by Dunning and coworkers[70] and are widely used in combination with post-HF methods since they converge systematically to the complete basis set taking advantage of empirical extrapolations.

The gaussian-type family of basis sets proposed by Pople and coworkers[71,72] is an example of those gaussian-type basis sets and they are also encompassed into split-valence basis sets. Split valence basis sets are defined as a linear combination of individual gaussian functions called primitives (Equation. 11).

$$\eta_\tau^{GTO} = \sum_i^I d_{i\tau}\eta_\alpha^{GTO} \tag{11}$$

The number of primitives used for the core and the valence orbitals are different and can be modified, as well as the possibility of adding polarization functions

or diffuse functions for long-range interaction systems. This makes Pople functions very versatile and adequate for a large variety of systems.

4.2 Techniques for molecular interactions analysis

In addition to energy calculations and geometry optimizations, another very important area of computational organic chemistry is the analysis of non-covalent interactions. These interactions can be studied by analysing topologically the electronic density of the system. There are several methodologies designed for this task, using different approaches and focusing on different aspects of the interaction.

4.2.1 The quantum theory of atoms in molecules

The Quantum Theory of Atoms In Molecules (QTAIM), commonly known as Atoms in Molecules (AIM) is a model used to analyse the electron density distribution function, by obtaining its critical points through derivation. Depending on the values of the Hessian matrix, the second derivative of the density function, at those points several types of critical points are described.

The most important critical points for the analysis of attractive interactions, like non-covalent interactions, are Bond Critical Points (BCPs). These points correspond to points along a bond path at the inter-atomic surface, where the shared electron density reaches a minimum (i.e. saddle points - a minimum in between the atoms involved in the bond/interaction and a maximum in the perpendicular direction).

Besides the numerical values at the bond critical points, AIM also provides molecular graphs of the systems in which the molecules and all the present interactions can be visualised by plotting the critical points and the links between them, obtaining a representation of the systems and the interactions within.

4.2.2 Natural bond orbital

Natural Bond Orbitals (NBO)s are calculated orbitals with maximum electron density commonly used in quantum chemistry to calculate the distribution of electron density in atoms and in the bonds between them. These orbitals are designed to have the highest possible occupancy, providing a description of the system very close to the Lewis structure.

A proper analysis of these orbitals can provide valuable information about the strength of intermolecular interactions, especially in non-covalent interactions where it is possible to measure the stabilization caused by the charge transfer from an occupied orbital in one molecule (usually a LP orbital) to an anti-bonding (σ^*) orbital in the other.

5 Results and Discussion

5.1 Hydrogen bond binding modes

A theoretical study was carried out to investigate the HB binding modes that are established between neighbouring HB donors and HB acceptors with relevance in catalysis and additionally, with relevance to biological systems. The systems chosen are presented in Figure 5.1. Widely known for their ability as HB donors and their potential in catalysing organic reactions; squaramide, thiourea, and guanidinium derivatives were chosen as the three HB donor systems. To analyse the electronic effect on the σ-hole, three different substituents were studied: a hydrogen atom (unsubstituted), an electron-withdrawing (EWG), and an electron donating (EDG) group. The HB acceptors were chosen relating to catalysis; naphthoquinone (onp) and 1,4-naphthoquinone (pnp), and for biological relevance; aspartic acid (asp) and the peptide bond (pep).

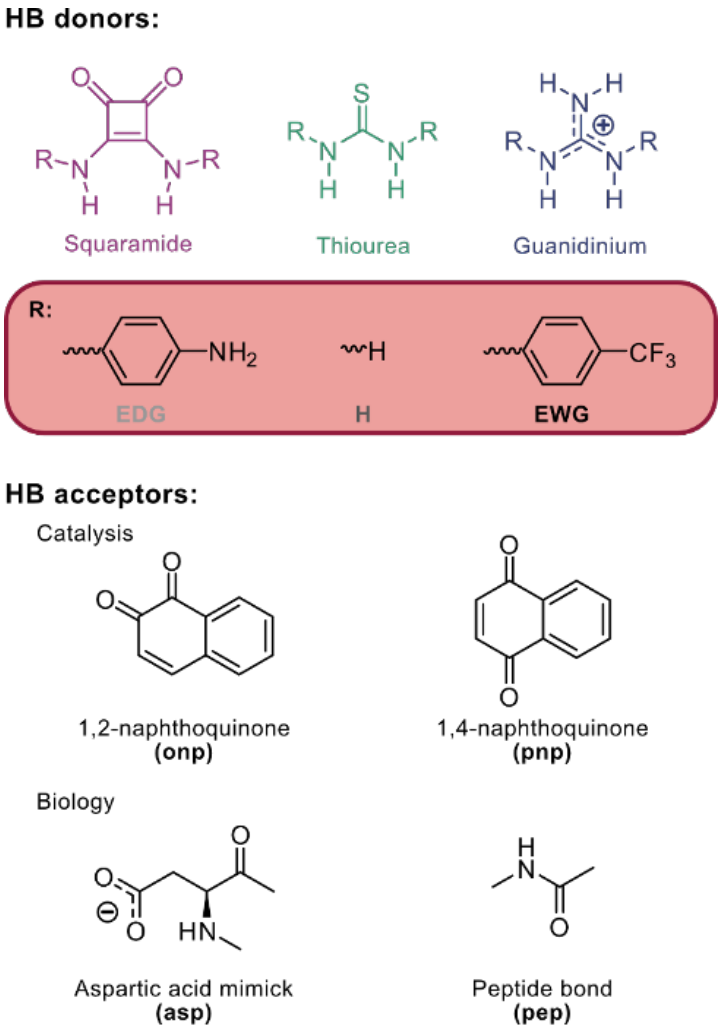

Figure 5.1: Systems chosen for HB donors and HB acceptors within catalytic and biological systems.

5.1.1 Monomers

To analyse how the orientations of the systems influence the HB formation, an analysis on the relative population of the conformations of HB donor systems was carried out in two different solvents; protic (water, H_2O) and non-protic (tetrahydrofuran, THF) (Figure S1). The relative population was estimated for the different conformers; anti-anti (**aa**), anti-syn(**as**), and syn-syn (**ss**), to explore the potential binding modes of the HB donors. A canting of $\sim 6^{\circ}$ of the N-H groups in squaramide has been previously reported[73] relative to thiourea and has been expected to affect the binding ability of squaramide. Evidently, in Figure 5.2, the conformation analysis of squaramide shows a heavily favoured **aa** and **ss** conformation as the molecule is surrounded by a protic solvent, therefore, pi-pi interactions occur between the phenyl rings. Opposingly, when surrounded by a non-protic solvent such as THF, the phenyl rings are more stable and hence favour the **aa** and the **as** conformation. This shows that the conformation is heavily impacted by solvent proticity, having obtained similar results for the thiourea and guanidinium derivatives (Figure S1). However, as the aim of this project was to study the HB formation between the donors and acceptors, only the **aa** conformation was considered.

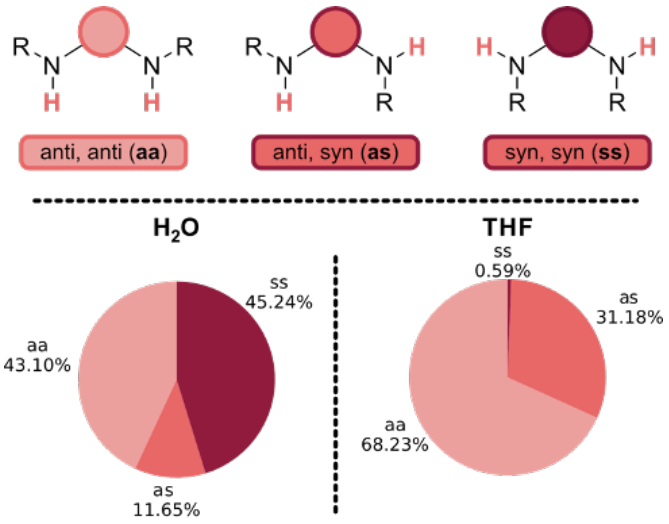

Figure 5.2: The three possible conformations that can be established in the HB donor systems (top figure). Conformation analysis of the EDG-substituted squaramide in H_2O and THF, outlining the population of **aa**, **as** and **ss** conformers (bottom figure), calculated at the M06-2X/6-31+G(d,p) level.

The geometry of the **aa** conformation was further analysed and the following angles were measured; the C-N-H (α), N—N-H (β) angles, and the H-N—N-H dihedral angle (γ). In all HB donor systems, the α-angle values were found to be within 3 - 4° of each other, however, the β-angle for the squaramide systems were found to be $\sim 70^{\circ}$ and thiourea and guanidinium donor systems were almost parallel at around 90°. This indicates that squaramide may not present similar binding patterns as thiourea or guanidinium. A pattern was found for both α and β angles such that $R = EWG \approx EDG < H$, concluding that the size and electronic effects of the substituents have minimal effect for these angles.

Furthermore, the γ angle which is indicative of the planarity of the HB donating system, follows an opposite trend, $Ph - EWG \approx Ph - EDG > H$. It was unexpectedly found that in the squaramide systems, the γ angle is slightly more significant for the EWG substituent than for the EDG analogue, despite the size similarity. Whereas with R=H, the H atoms involved in the potential HB interaction are in the same plane. Therefore, no steric effects seemingly result from the substituents. Additionally, the γ angles observed in systems with R = EWG or EDG are greater than those when unsubstituted in both thiourea and guanidinium systems.

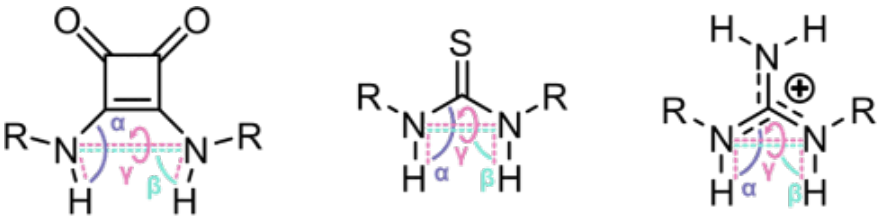

Figure 5.3: The α, β and γ angles that have been measured in the HB donors.

A Molecular Electrostatic Potential (MEP) analysis was carried out for all the HB donor systems under study, to analyse the strength of the potential HB interaction. The MEP is defined as the interaction energy between the charge distribution of a molecule and a unit positive charge. It is used to locate the positively and negatively charged electrostatic potential in the molecule. Each MEP surface has a colour scale that indicates the negative and positive values. The red colour with negative values indicates the minimum electrostatic potential which acts as a nucleophilic region. Oppositely, blue indicates the maximum electrostatic potential acting as an electrophilic region.

It was expected that the strength and binding pattern for each system would be determined by the degree of alignment between the HB donor systems and the corresponding HB acceptors. MEPs were calculated for each system (squaramide, thiourea, and guanidinium with R= H, EDG and EWG) in both solvents and are depicted in Figure S2, Table S2, Figure S3 and Table S3), however, only the squaramide donor system is depicted in Figure 5.4. For each of the nine systems, one MEP maxima value was found, with the exception of the unsubstituted guanidinium and squaramide systems where three and two MEP maxima values, respectively, were obtained due to symmetry. A trend was established between the squaramide (in H_2O only), thiourea (in H_2O and THF), and guanidinium donor systems (in H_2O and THF) where the V_{max} values increased from $R = EDG < H < EWG$. In the squaramide donor systems (in THF), a contrasting trend from the previous was obtained such that $R = H < EDG < EWG$. In general, the most electron-withdrawing substituent produces the greatest V_{max} value and was therefore expected to establish the strongest HB interaction.

A MEP analysis was also carried out for the HB acceptors in both H_2O (Figure 5.5) and in THF (Figure S5). The MEP showed the most negative V_{max} value at the oxygen atom where the HB interactions are expected to take place as the alignment between the maxima of HB donors and the minima in the HB acceptors will result in optimal binding producing the dimers. The asp acceptor shows

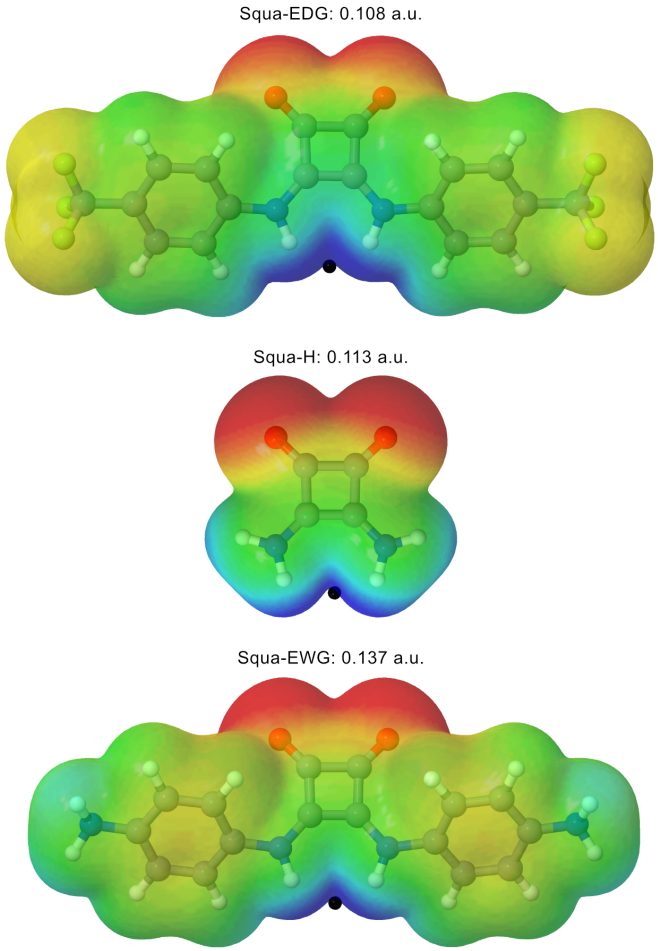

Figure 5.4: Molecular electrostatic potential on the 0.001 a.u. electron density isosurface for EDG-, H- and EWG-substituted squaramide. Colour scheme ranges from red (- 0.100 a.u.) to blue (+ 0.200 a.u.).

the minima over the carboxylate atoms, the pep acceptor presents the minimal values over the carbonyl group, and the naphthoquinones show minima over the corresponding quinone O atoms (i.e. α and β carbonyl groups for onp and α and δ carbonyl groups for pnp).

5.1.2 Dimers

Firstly, an analysis of the preferential binding modes and the associated binding energies was undertaken.

Two binding modes were initially considered; bifurcated and parallel, Figure 5.6. The bifurcated binding mode occurs when the formation of two HB interactions in the shape of a 'V' is produced between the lone pairs on an O atom of an HB acceptor and two N-H atoms on the HB donors. The parallel binding mode is that of two linearly directed HB interactions as a result of an HB formation between two O atoms of the HB acceptor and two N-H atoms of the HB donor. Besides, a third binding mode pattern was established where HB interactions occurred between two vicinal O atoms in the HB acceptor (eg. the onp acceptor) and 2 N-H atoms in the HB donor. This binding pattern was

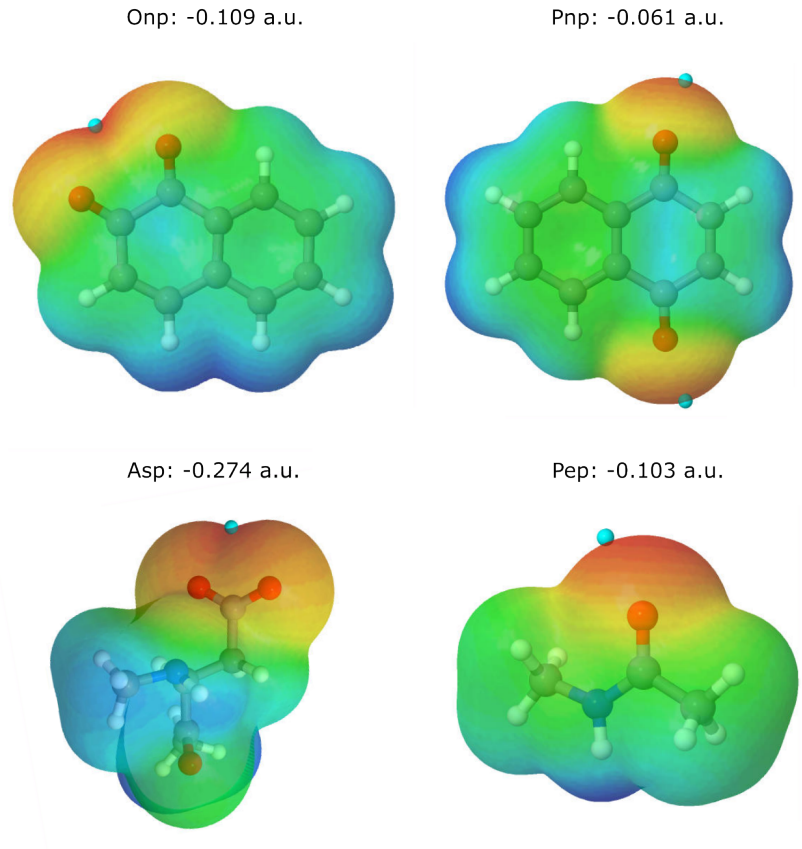

Figure 5.5: Molecular electrostatic potential on the 0.001 a.u. electron density isosurface for all four HB acceptors; onp, pnp, asp and pep. Colour scheme ranges from red (-0.300 a.u.) to blue (+0.100 a.u.).

identified as the zigzag binding mode.

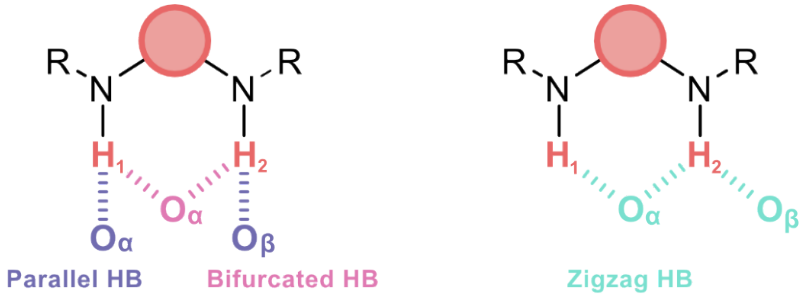

Figure 5.6: HB binding modes under study; parallel (purple), bifurcated (pink), and zigzag (green).

The formation of these zigzag interactions can occur by establishing a 'bifurcated' bond with the alpha C=O ($H_1 \cdot\cdot O_\alpha \cdot\cdot H_2$) and a '3-centred' interaction[74] with the beta C=O ($O_\alpha \cdot\cdot H_2 \cdot\cdot O_\beta$) or vice versa, a 'bifurcated' bonding with

the beta C=O ($H_1 \cdot\cdot O_\alpha \cdot\cdot H_2$) and a '3-centred' interaction with the alpha C=O ($O_\beta \cdot H_2 \cdot\cdot O_\alpha$) (Figure 5.6, QTAIM discussion).

The interaction energies (E_i) for all dimers in both solvents were calculated, considering all possible binding patterns, and are presented in Figure 5.7 and Table S6 and S7. Firstly the E_i values obtained in H_2O have been thoroughly discussed, preceded by an E_i analysis obtained in THF.

In H_2O, the E_i values obtained showed that when the HB donor systems form an interaction with the carboxylate of the asp acceptor, there were two possible binding patterns; the bifurcated and parallel binding modes. This is due to the relative position of the two O atoms of the carboxylate which prevented the zigzag binding to occur. While the E_i difference between the two possible binding modes appeared to be relatively small, the most stable binding mode between both *N,N'*-disubstituted squaramide donor systems and the asp acceptor was found to be the bifurcated binding. Further analysis of the HB bond distance of the two patterns showed that the HB interaction present in the parallel binding mode produced shorter distances than the HB interactions in the bifurcated binding and, accordingly, stronger binding was expected. However, due to the resulting orientation of the amino acid moiety of the asp molecule in the bifurcated binding mode, additional interactions between the phenyl rings of the R substituents (R= EWG/EDG) of the *N,N'*-disubstituted squaramide and the acceptor occurs producing a stabilising effect, (additional discussion in QTAIM section and in Figure Figure S11.1a, b, g, h). Whereas the preferred binding mode of the unsubstituted squaramide was found to be parallel binding as expected, albeit with a small E_i difference, as the above additional interactions are unable to be formed.

Similarly, dimers formed by the unsubstituted and EDG *N,N'*-disubstituted thiourea systems with asp, were seen to preferentially bind through the bifurcated mode even though the parallel binding would facilitate a better orbital overlap between the N-H and the lone pair of the O atoms (Figure 5.7 and Figure S11.2a,b,l,m). However, the parallel binding was found to be more favourable in the HB interactions between the substituted EDG thiourea system and asp, despite having secondary interactions occurring between one of the phenyl groups and the amino acid moiety. It was concluded that the overall interactions in the bifurcated binding mode were not strong enough to compete with shorter and, hence, stronger HB interactions in the parallel mode with additional interactions between one of the methyl group of asp and a phenyl ring of the thiourea (Figure S11.2 f). Furthermore, the strong electron-withdrawing effect over the N-H groups reinforces the HB interactions.

In addition, the preferential binding mode of the three guanidinium systems is parallel binding, regardless of the additional interactions that occur with the R substituents. This was as a result of the better alignment of the N-H groups with the lone pairs in the carboxylate (Figure S11.3) and the positive charge present within the guanidinium systems which further strengthened the HB interactions.[75]

As previously mentioned, the types of HB interactions that can be established with the onp acceptor involve the α or the β carbonyl groups, hence, all three

binding patterns are possible; simultaneous parallel bonds can take place with both α and β carbonyl group or bifurcated and zigzag can be established with either carbonyl group. Upon studying the potential binding modes, it was found that when two zigzag patterns were formed (with either α or β O atom) with all systems, a difference of 0.4 - 6.1 kJ/mol in E_i was noted (Table S6).

According to the Ei, the preferential binding mode of the squaramide and guanidinium systems was found to be the zigzag pattern (Figure 5.7, left and in Figure S11.1c, i, n and S11.3c, i, n). This was observed to be the same for the unsubstituted and the EDG thiourea systems, however, the preferred binding mode for the EWG thiourea was seen to be parallel.

In the case of the pep and pnp acceptor, the only possible binding mode was the bifurcated binding which was observed with all the HB donor systems as only one C=O group is present in the pep and the two C=O groups in pnp are too far in proximity to establish simultaneous HB interactions with the N-H groups. An exception arose with the EWG thiourea system interacting with the pnp acceptor as a pi-pi stacking interaction was established and was unable to form a clear HB pattern (Figure S11.2).

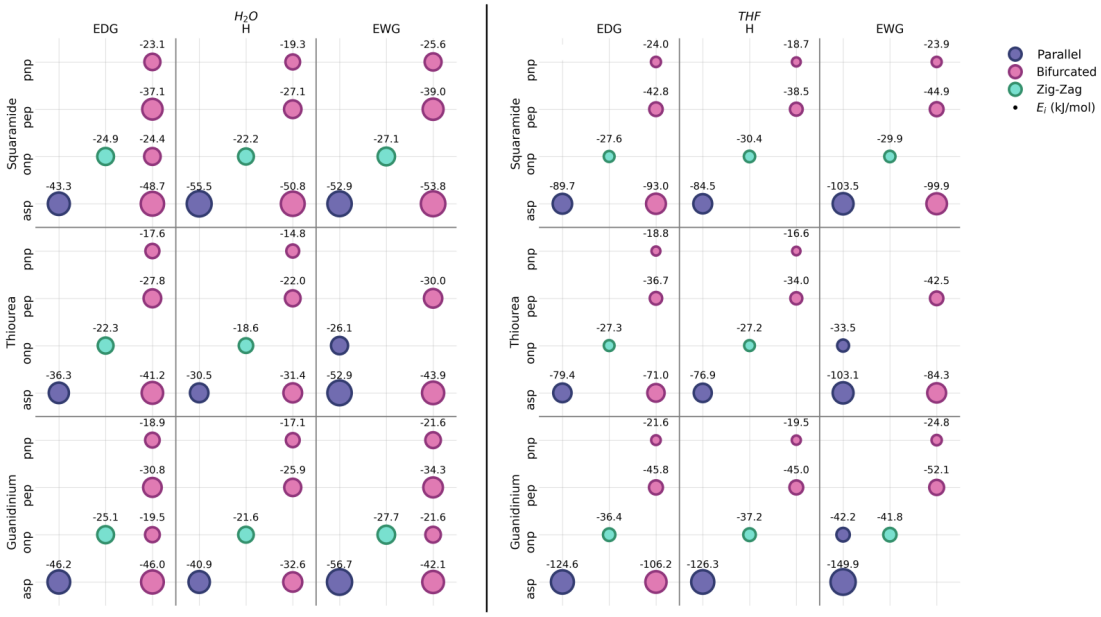

Figure 5.7: The interactions energies (E_i [kJ/mol]) between all three HB donor systems and all the HB acceptors showing the preferential binding mode of each interacting system, in both H_2O (left) and THF (right).

Based on the E_i obtained for the dimers calculated in THF (Figure 5.7, right), a majority of dimers have similar binding patterns to those found in H_2O with a few exceptions. For example, the preferential binding pattern switches from bifurcated (H_2O) to parallel (THF) when EWG squaramide and both unsubstituted and EDG thiourea systems interact with asp. Furthermore, the most favoured binding mode between the EWG guanidinium system and the onp acceptor switches from zigzag (H_2O) to parallel (THF). Unlike in the protic environment above where the Ph rings interact with the asp, in the non-protic one, THF,

the asp molecule rotates away from the Ph rings and no longer establishes the corresponding stabilising secondary interactions [see Figure 5.11, (b)] in QTAIM section) allowing parallel binding to dominate.

In general, there was an increase in E_i for all the dimers due to the decrease in proticity from H_2O to THF resulting in a stronger HB interaction (Figure 5.7 and Table S7). A general trend was observed for most dimers in H_2O where there was an increase in binding energies from $H < EDG < EWG$ which coincides with the MEP analysis for the HB donors (Figure 5.5 and Figure 5.4). However, an exception to the above trend was seen in the binding energies obtained in dimers formed between squaramide and asp. The general trend indicates that the EWG substituent's ability to pull electron density results in an overall stronger HB interaction, coupled with secondary interactions allowing further stabilisation to take place. In THF, however, this general trend is only observed in dimers formed between squaramide and thiourea with asp and pep, thiourea and guanidinium with pnp and, finally, guanidinium with pep; no clear trend was observed in the rest of the complexes studied in THF.

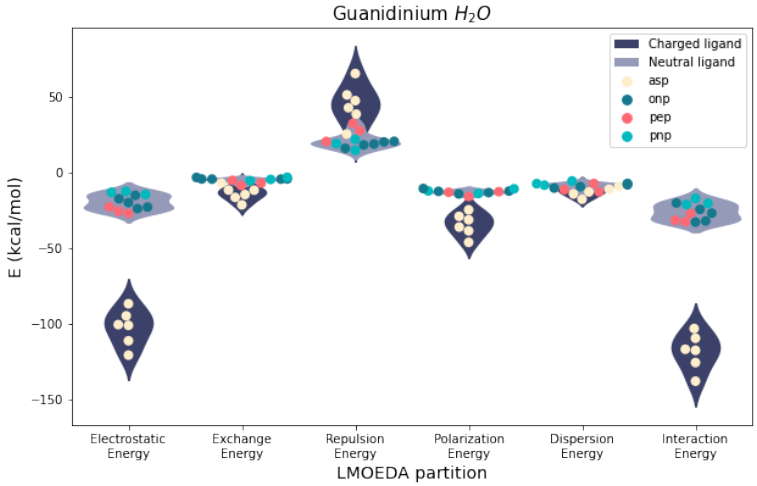

Figure 5.8: LMOEDA energy partition terms for guanidinium complex in H_2O.

A localised molecular orbital energy decomposition analysis (LMOEDA) was carried out to investigate the physical origins of the HB interactions and determine the contribution of the different energy components to the stability of the system. The interaction energies of all the systems studied were found to be dominated by the electrostatic component followed by the polarisation component (Figure 5.8, S7 and S8). This remained to be consistent across all the systems and most evidently in systems involving the asp acceptor. It was found that there was an increase in the dispersion energy component when the systems consist of secondary interactions from the Ph rings and, therefore, rationalising the differing trends found in interaction energies and, later, E(2) NBO energies.

A CSD search was carried out for complexes that present the binding patterns under study between any squaramide, thiourea, and guanidinium systems, and

the carbonyl functionality. For the squaramide derivatives, it was found that 1 structure formed zigzag interactions, 34 structures formed parallel binding and 16 formed bifurcated patterns (Table S8.1). For the thiourea derivatives; 10 zigzag binding, 17 parallel patterns, and 190 forming the bifurcated mode (Table S8.2). Finally, the search for guanidinium derivatives showed 41 complexes with the zigzag pattern, 31 parallel, and 356 structures with bifurcated interactions (Table S8.3). The average HB length (Figure 5.9 and S10) was found to coincide with the calculated bond distances following similar trends with regards to single HBs such that the bond lengths increased from $parallel < bifurcated < zigzag$ (Table S9).

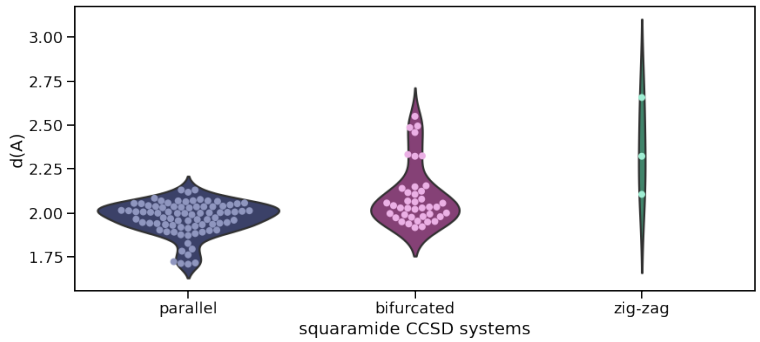

Figure 5.9: HB distances of the squaramide structures extracted from the CCSD search.

In order to validate the methodology employed, a comparison between the experimental distances found in the different crystal structures (CSD) and the computational one was analysed (Figure 5.10). A small sample was optimised in the gas phase and it was found that the molecules presenting more rigid interactions (parallel and zigzag) were in excellent agreement between the experimental and computed HB distances. However, there was a slightly bigger difference within the bifurcated interactions due to the combination of the degree of flexibility within the binding mode and the small size of the monomers involved. Crystal structures and gas-phase structures have comparable HB lengths, but gas-phase structures lack the environmental constraints that constrain crystal structures and further account for the bigger distances within the bifurcated mode.

Although there are small differences, with regard to the three binding modes proposed in this study, these calculations are in agreement with their existence in nature, having been confirmed that they correspond to real systems found in the CCSD, further corroborating the calculations.

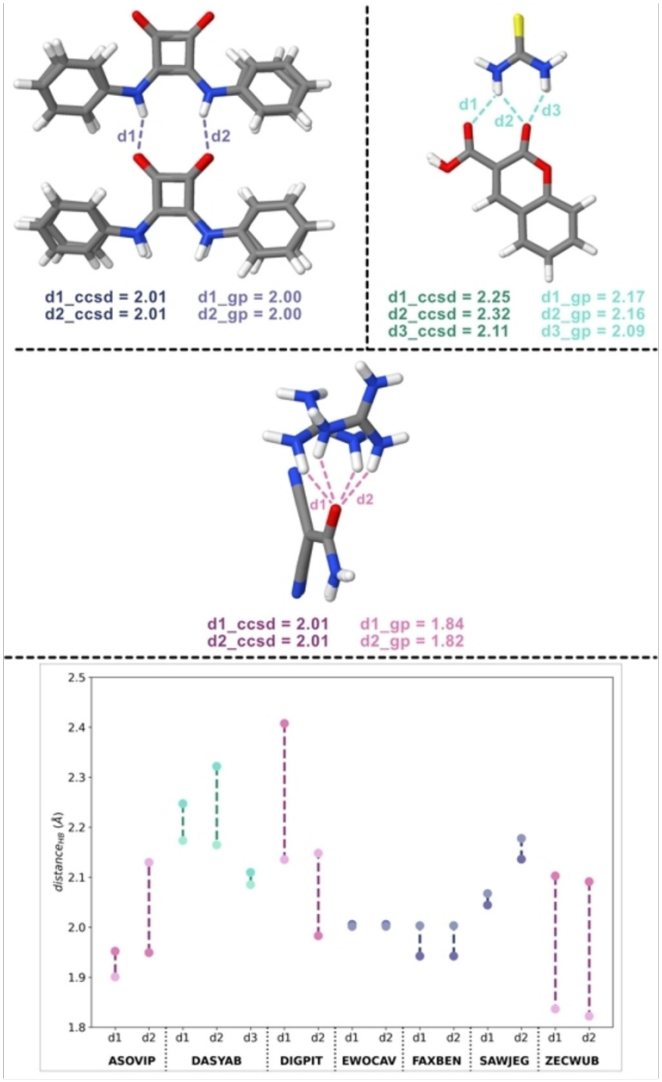

Figure 5.10: Top: Crystal and gas-phase structures. Middle: A comparison of HB distances. Bottom: A comparison graph of hydrogen bond distances between gas-phase and crystal structures.

5.1.3 Characterisation of NCI

In order to analyse and characterise the strength of the HB interactions and the atomic bonds established, a Quantum Theory of Atoms In Molecules (QTAIM) analysis was performed for all the dimers studied (Table S10 and S11). The QTAIM molecular graphs were obtained [Figure 5.11, (a) and in Figure S10 and S11] showing the three possible binding modes that can occur between the HB donor systems and HB acceptors, for this example however, only squaramide systems interacting with pep (bifurcated), asp (parallel) and onp-O_α acceptors (zigzag) are illustrated. Additionally, the molecular graphs obtained evidently show the secondary interactions that have influenced interaction energies and, consequently, the binding modes where the most stable interactions between EWG squaramide and asp in H_2O are shown in comparison to the same systems in THF. In Figure 5.11 (b), the bifurcated binding mode that occurs in the H_2O squaramide systems is the most stable due to the additional interactions

that can be seen between one of the Ph rings in squaramide and the peptide moiety in the asp acceptor. Unlike in THF, where the most stable binding mode (parallel) was formed as a result of asp rotating towards the solvent, was found to produce no additional interaction within the respective systems.

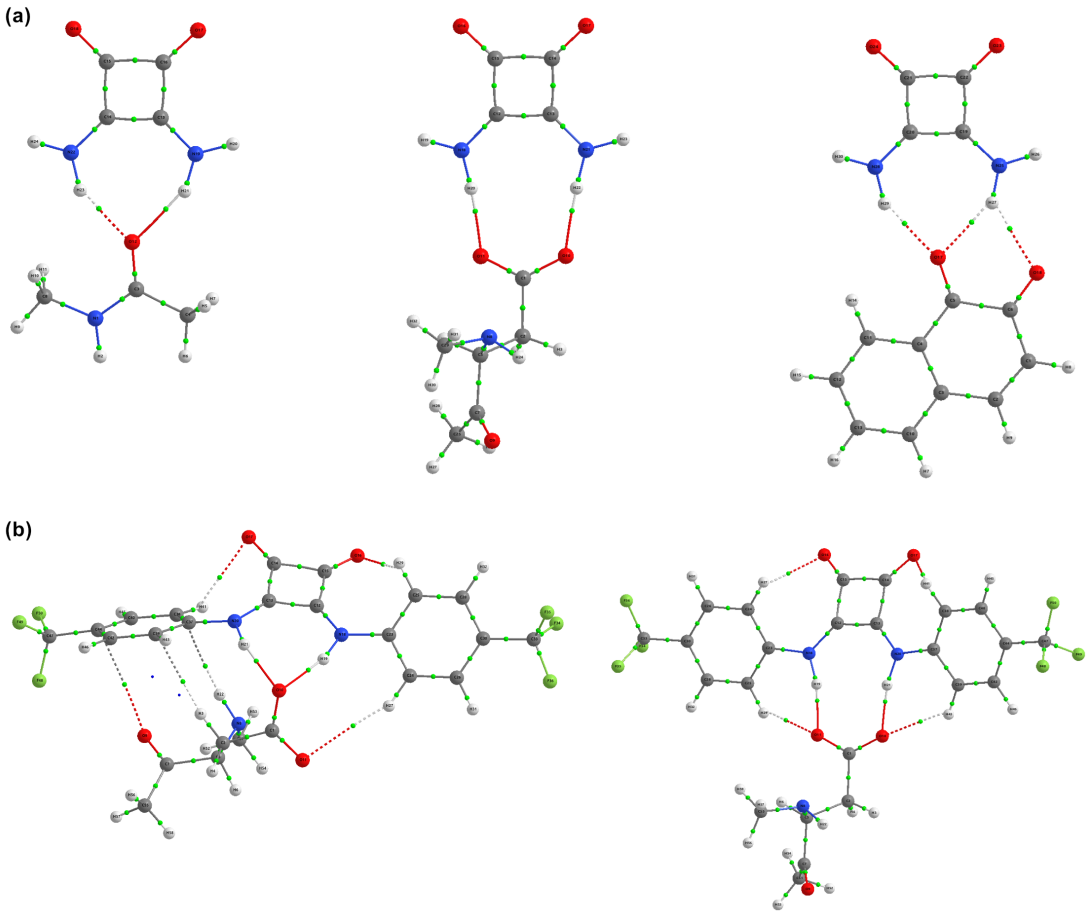

Figure 5.11: a) QTAIM molecular graphs showing the binding patterns established between unsubstituted squaramide and pep, asp and ona-O_α; bifurcated (left), parallel (middle) and zigzag (right). b) Most stable dimer between EWG-substituted squaramide in H_2O (left), producing a bifurcated pattern with secondary interactions, and in THF (right), producing a parallel pattern with no additional interactions.

The electron density at the bond critical points [ρ(BCP)] and the positive Laplacians [$\Delta^2\rho$(BCP)] were obtained for all the dimers and were found to correspond to medium-strong HBs. In H_2O, the dimers which favour the parallel binding mode show the strongest HB interaction with ρ(BCP) values consisting of up to 0.0498 a.u. The dimers exhibiting a preferential zigzag binding present the weakest HB interaction, showing the average ρ(BCP) values of 0.0168 a.u. A similar trend was seen in THF, where the strongest HB interaction was found to be a parallel HB interaction with a ρ(BCP) value of 0.0733 a.u., and the weakest was the zigzag pattern with the average ρ(BCP) value of 0.0176 a.u.

The $\Sigma\rho$(BCP) values of all HB interactions within each binding pattern (two HBs in parallel, two HBs in bifurcated, and three HBs in zigzag) were taken and

analysed. The strongest combination of HBs was found to correspond to the parallel binding mode with an average of the two HBs as 0.0712 a.u. in H_2O and 0.0915 a.u. in THF. Followed by the zigzag interactions where the average of the three HBs was found to be 0.0504 a.u. in water and 0.0519 a.u. in THF. Lastly, the average of the two HBs in bifurcated corresponded to the weakest $\Sigma\rho$(BCP) values of 0.0473 and 0.0459 a.u. in water and THF, respectively. It was concluded that the parallel pattern provides the best and strongest HB donor and acceptor alignment. While zigzag presents the weakest interactions, as stated previously, the combination of three HBs produces a much stronger and better stabilisation than bifurcated.

The ρ(BCP) values of the secondary interactions were also analysed and it was found that the majority of the secondary interactions produced small ρ(BCP) values of ~ 0.01 a.u. Evidently, there were more secondary interactions present in the dimer asp complexes (most abundant with EWG substituents) in which some interactions produced ρ(BCP) values of > 0.01 a.u. The respective secondary interactions were found to be larger in magnitude in THF than in H_2O. While significantly smaller in value, the secondary interactions provide a substantial contribution towards the stability of the dimer complexes.

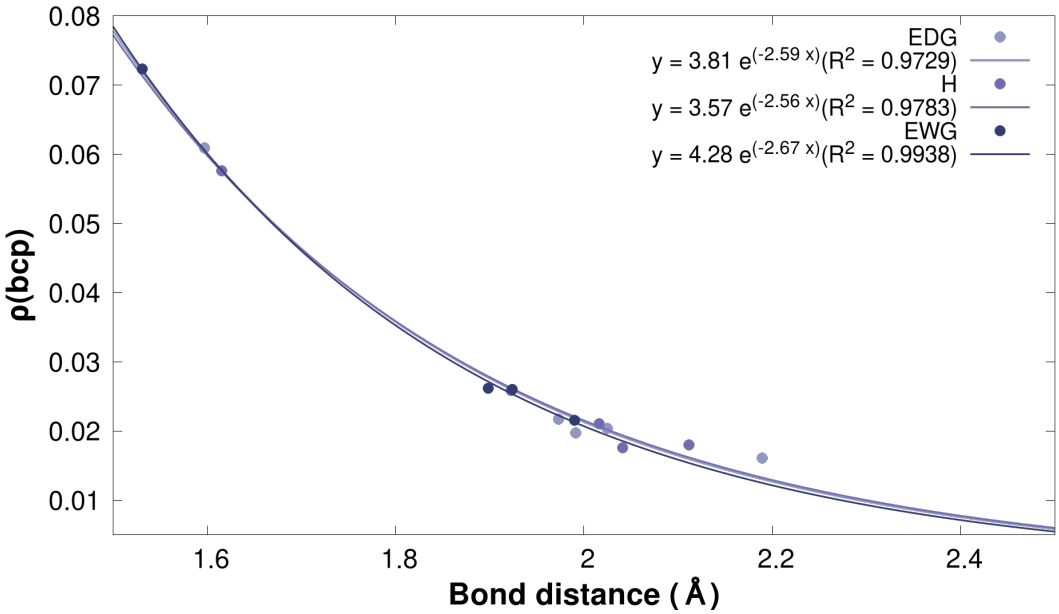

Figure 5.12: Exponential correlation found between (BCP) values and HB distances (Å) in dimers formed between all three guanidinium systems (H-, EDG-, and EWG-substituted) and all HB acceptors in THF.

Good exponential correlations were obtained between the ρ(BCP) values and the intermolecular HB distances in all the systems (Figure 5.12 and in Figures S13 and S14) and have been well described in the literature.[76–78] As expected, it was found that as the HB distances decrease, there is an increase in electron density at BCP indicating that the closer the interaction the stronger the HB. The largest ρ(BCP) values with the shortest bond lengths appeared to correspond to EWG donor systems. The HB interactions formed within the EWG dimers were found to have shorter bond distances than 1.85 Å with an average of 1.93 and

1.85 Å in H_2O and THF, respectively. In unsubstituted dimers, the average bond lengths were found to be 1.99 Å in H_2O and 1.92 Å in THF. Finally, the EDG dimers established an average of 1.99 and 1.96 Å in H_2O and THF, respectively. The bond distances obtained indicate that EWG dimers form the strongest HB interactions, in accordance with the MEPs.

In conclusion, taking into consideration the monomer MEP analysis and the QTAIM analysis, in the case of pep and pnp acceptors where only one O atom is available to bind to the HB donors, it has been observed that only the bifurcated binding mode is possible. Therefore, the acceptor determines the binding pattern. With regards to the asp and onp acceptor, where two O atoms are available to interact with the HB donor (via bifurcated and parallel for asp, or parallel and zigzag for onp), the donor directs which binding mode is more stable.

Lastly, in order to characterise the HBs established, a natural bond orbital (NBO) analysis of the wave functions was performed. The HB interactions between the lone pairs of the O atoms of HB acceptors and the anti-bonding (σ^*) orbitals of the N-H bond of the HB donors and their contributed energy [charge transfer energy E(2)] were calculated (Figure 5.13, in Figures S15 and 16 and in Tables S12 and S13) as well as the sum of all the E(2) which contributed to the HB patterns.

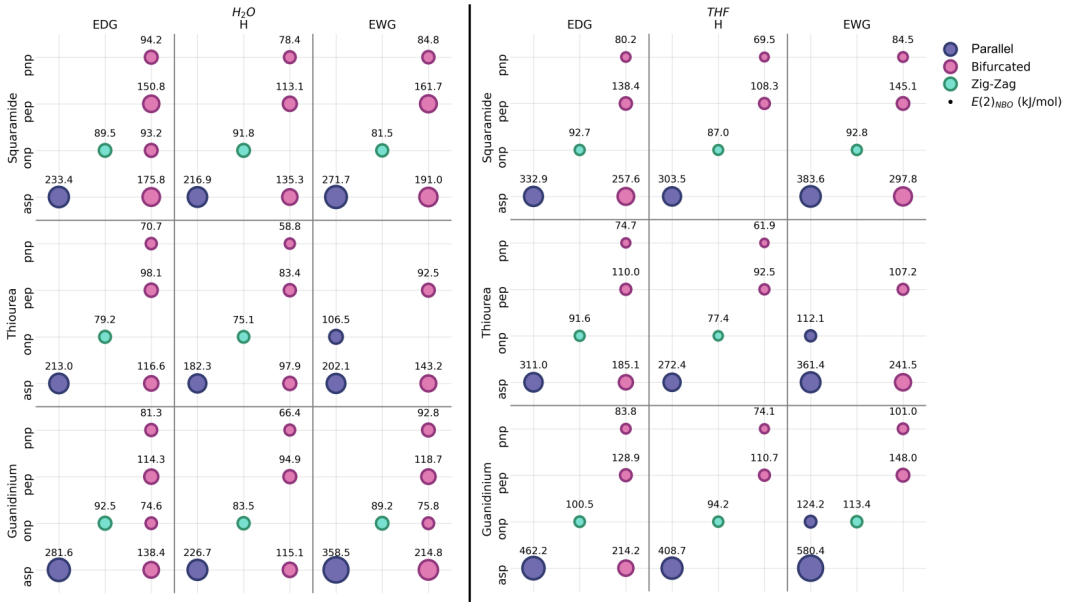

Figure 5.13: NBO energies (E[2] in kJ/mol) between all three HB donor systems and all the HB acceptors, in H_2O and in THF.

The E(2) values of each HB formed within the binding patterns (parallel, bifurcated and zigzag) were compared in each dimer system and guanidinium is presented in Figure 5.14 as an example. In all dimers formed, a general trend was observed for most of the dimers where there is an energy increase from $H < EDG < EWG$, coinciding with the trend found for the interaction energies in both H_2O and THF.

A good agreement was established between the E(2) and E_i values for all

dimers with pep and pnp in both solvents as only one binding mode is possible. However, according to the NBO analysis, the HB interactions within the parallel binding for the *N,N'*-di-substituted squaramide systems (EWG and EDG) with asp are stronger than the HB interactions in bifurcated. This was also seen in the unsubstituted and EDG thiourea systems and are inconsistent with the E_i trend. The NBO trend shows that for all dimers with the asp acceptor, the parallel pattern is more favourable as it presents stronger E(2) values. The NBO analysis for the onp dimers in H_2O show a stabilizing shift in binding mode from zigzag (over O_β) to bifurcated (over O_α) for EDG squaramide, from zigzag (over O_α) to zigzag (over O_β) EWG squaramide, and from zigzag (over O_β) to zigzag (over O_α) for thiourea and guanidinium (Figure 5.13, left). In THF, similar stability shifts are observed for onp where zigzag (over O_α) changes to zigzag (over O_β) with both EWG squaramide and thiourea dimer systems (Figure 5.13, right). The inconsistencies between the E_i and NBO trends emerge from the fact that the E_i values represent the total interaction energy between the HB donor and acceptor which includes secondary interactions. Whereas the E(2) values reflect the stabilization energy resulting from the actual HBs formed.

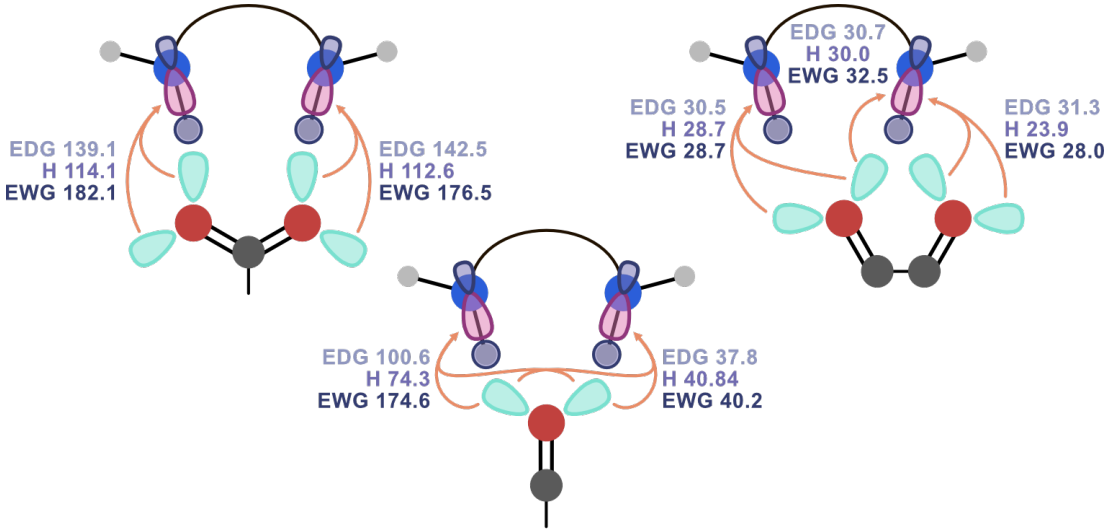

Figure 5.14: NBO values in kJ/mol of each of the guanidinium complexes (H-, EDG- and EWG-substituted) in the different binding patterns established; parallel (left), bifurcated (middle) and zigzag (right).

Furthermore, a slightly poor linear correlation was obtained between E(2) and E_i values in H_2O than in THF. This indicates how the presence of secondary interactions in H_2O influences the binding modes and further reinforcing how the HB donor determines the binding mode formed, in this case, on the basis of the solvent used.

Overall, the NBO values show that for each E(2) contribution in each single HB, the strongest HB interaction formed was within the parallel binding with an average of 112.3 kJ/mol, followed by the bifurcated pattern with an average of 53.2 kJ/mol and finally, the weakest interaction was obtained within the zigzag binding mode with an average of 28.2 kJ/mol, in agreement with the QTAIM analysis.

Additionally, the HB acceptor was established to determine the magnitude of each E(2) contribution within the HB pattern as the asp molecule was seen to obtain the largest E(2) values, showing a range from 182.3 - 358.5 kJ/mol (in H_2O) and 272.4 - 580.4 kJ/mol (in THF), succeeded by pep (83.4 - 161.7 kJ/mol in H_2O, 92.5 - 148.0 kJ/mol in THF), onp (75.1 - 106.5 kJ/mol in H_2O, 77.3 - 124.2 kJ/mol in THF) and finally the pnp dimers with the smallest values (89.2 - 94.2 kJ/mol in H_2O, 61.9 - 101.1 kJ/mol in THF). The asp acceptor was found to have the lowest minimum MEP value, as it consists of a negative charge,[75] in comparison to the other acceptors where the pep and onp acceptor were found to be similar and the pnp was found to have the least negative MEP value (Figure 5.5), thereby justifying the E(2) trend obtained in both solvents.

The AIM analysis together with the MEP analysis indicates that the HB acceptor molecules direct the potential binding mode depending on the O atoms involved in the HB interaction (one O atom for pep and pnp, two geminal O atoms for asp, and two vicinal O atoms for onp). However, depending on the solvent and when the option is available, the HB donors overall establish the most optimal interaction by positioning the NH groups in the best orientation with respect to the HB-accepting atoms.

The results of both AIM and NBO analysis are consistent in terms of HB pattern strength. However, the total E_i does not perfectly coincide with the NBO E(2) values due to the secondary interactions present. Additionally, according to the AIM and NBO, parallel results in the strongest binding, followed by both bifurcated and zigzag interaction.

5.2 Halide abstraction reaction

This thorough computational investigation presents a halide abstraction reaction catalysed by two different catalysts; catalyst A and catalyst B, carried out in acetonitrile as a solvent and as a reactant (Figure 5.15). This reaction was chosen to analyse and understand all the factors that facilitate the reaction, in order to elucidate the halide abstraction mechanism, in which two pathways have been proposed as mentioned in the introduction; pathway 1 or pathway 2 (Figure 3.9). Additionally, this reaction was selected to reveal the preferred catalyst-substrate binding mode. Catalyst A is a dicationic XB donor which has been used experimentally,[42] and it was found to afford the best substrate conversion in the respective reaction (see Figure 5.15, top) in comparison to the other catalysts that have been tested. Catalyst B has been developed by Parrera and co-workers,[60] examining its activity in the same reaction in which they have proposed two binding modes; monodentate and bidentate.

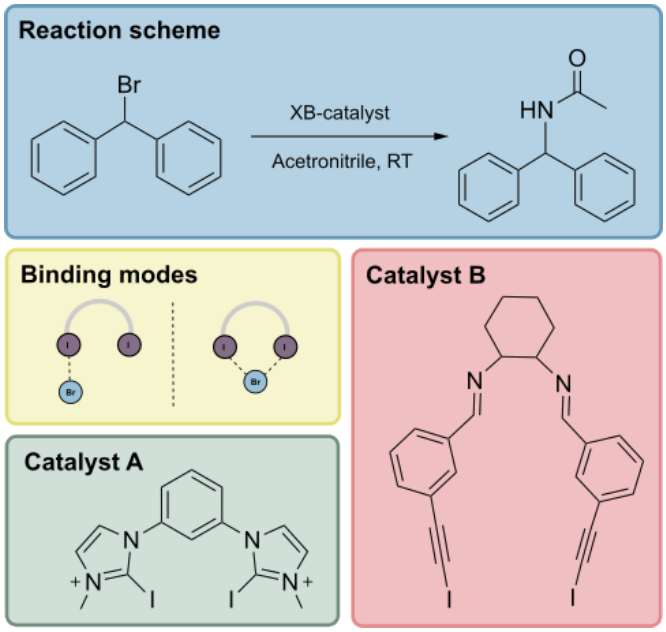

Figure 5.15: Halide abstraction reaction scheme with catalysts A and B and their potential binding modes; monodentate and bidentate.

5.2.1 Catalyst A

In order to study the potential XB interactions established upon complexation between catalyst and substrate, an analysis of the MEP was carried out to compute the electrostatic potential at the surface of the isolated catalysts. This well-known method, which has become customary for effective analysis, predictions in reactivity and for NCIs such as XB,[79–81] characterises the positive and negative regions, V_{max} and V_{min} respectively, within the molecule allowing us to quantify the σ-hole present and predict the potential XB strength. The MEP was calculated for catalyst A (Figure 5.16). Two V_{max} values were found to be 0.265 a.u. and 0.266 a.u. and are both located approximately 180° from the two iodine atoms present, as expected.[38] The magnitude and position of these

values are indicative of the presence of σ-holes directly at the end of the iodine atoms. In theory, since the catalyst is symmetrical, it was anticipated that both values would be identical, while there is a small difference obtained of 0.001 a.u., it was not expected to affect the binding mode. The orientation of the σ-holes indicates that both iodine atoms are capable of forming an XB interaction, most likely through a bidentate bonding mode, where one iodine atom is only slightly stronger than the other. This agrees with the symmetry of the catalyst conveying that no side (left or right) of the catalyst is favoured as one iodine atom is not significantly more influenced to produce a greater σ-hole value and therefore form a stronger XB interaction.

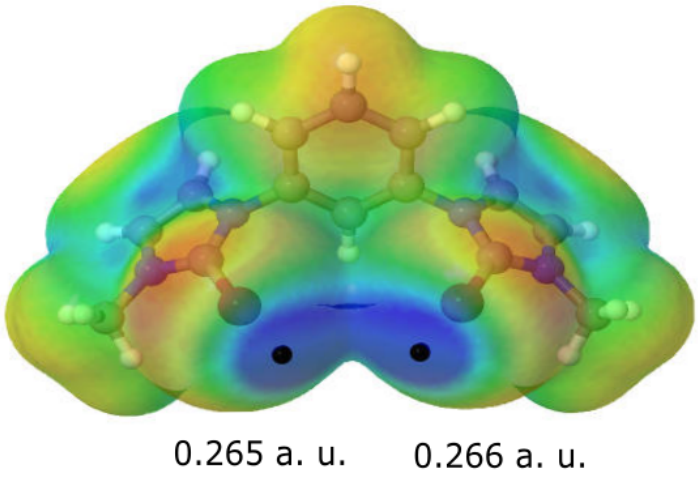

Figure 5.16: Molecular electrostatic potential on the 0.001 a.u. electron density isosurface calculated for catalyst A; Colour scheme ranges from red (0.180 a.u.) to blue (0.250 a.u.).

The free energy profile was obtained for the reaction studied under the presence of catalyst A (Figure 5.17). Both pathway 1 and pathway 2 were investigated and only a transition state of the catalyst-substrate complex corresponding to pathway 1 was found. Therefore, it was established that the halide abstraction proceeds via pathway 1, considered to be a step-wise mechanism, where an XB donor interacts with an R–X bond of a leaving group, facilitating a heterolytic bond cleavage. Starting from the entrance channel (**EC**), a catalyst-substrate complex (cat-complex) transition state (**TS1**) is initially formed where an XB interaction occurs between two iodine atoms of the catalyst and the bromine atom of the benzhydryl bromide substrate, resulting in the cleavage of the C–Br bond. Subsequently, a carbocation intermediate structure (**INT**) is formed followed by the formation of another transition state structure (**TS2**) where the acetonitrile molecule attacks the carbocation resulting in the formation of a catalyst-substrate product (**PROD**). All the structures can be found in Figure A.1. It was found that the energy barrier for **TS1** was far greater than **TS2** at 27.5 and 7.7 kcal/mol, respectively, meaning that the **TS1** requires higher activation energies than **TS2**.

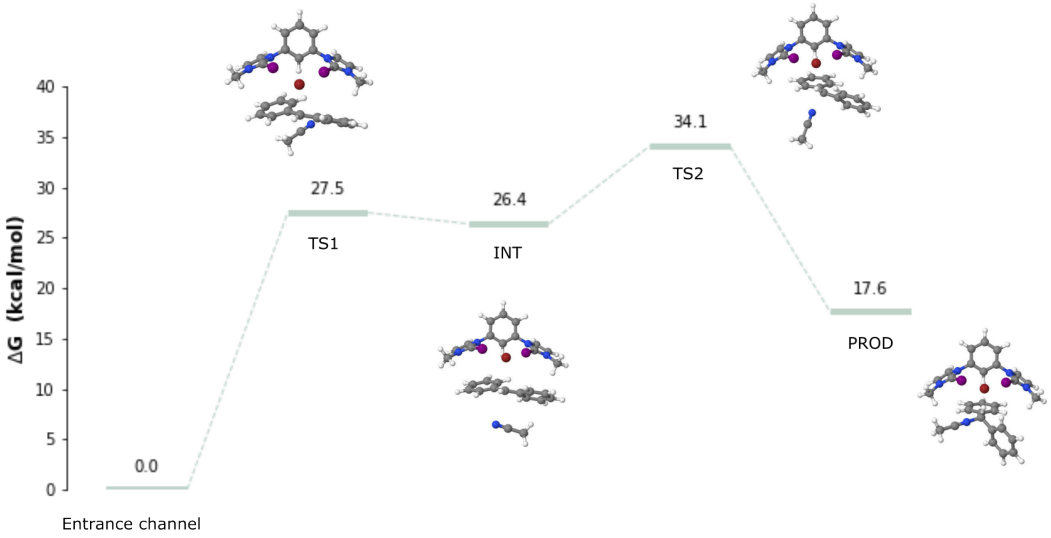

Figure 5.17: Free energy profile of catalyst A in kcal/mol.

It should be noted that as the final step of the reaction was not computed, the **PROD** structure is not very energetically stable, as seen in Figure 5.17. Therefore, the free energy profile presents a reversible reaction in this computational study.

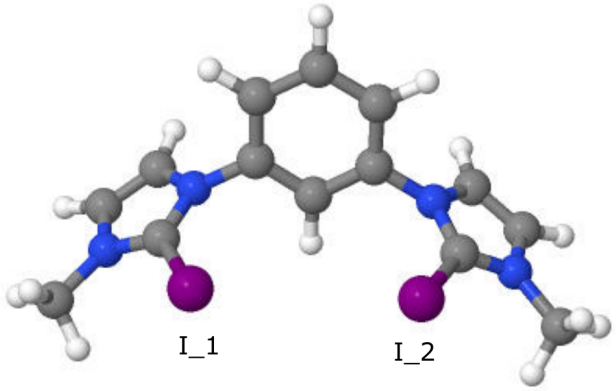

Figure 5.18: Catalyst A isolated monomer; I_1 represents the left iodine and I_2 represents the right iodine.

Table 5.1: Bond distances measured for the cat-complex A; **TS1**, **INT**, **TS2** and **PROD** structures.

Bonds	**TS1 (Å)**	**INT (Å)**	**TS2 (Å)**	**PROD (Å)**
I_1-Br	3.32	3.20	3.18	3.20
I_2-Br	3.24	3.19	3.18	3.19
C-Br	2.88	3.36	4.31	3.98
C-N	5.04	3.18	2.12	1.44

The I–Br, C–Br, and C–N distances of each structure were analysed (Table 5.1), where the I–Br bond length indicates the XB interaction (I_1 represents the left iodine and I_2 represents the right iodine, see Figure 5.18), the C–Br distance indicates the leaving anion and substrate bond, and the C–N distance indicates the N-terminal of the acetonitrile bonding to the carbocation. As the reaction progresses from **EC** to **PROD**, both I–Br bond distances remain at $\sim$ 3.2 Å, demonstrating an XB interaction, as expected. The C–Br bond distance becomes elongated from **TS1** on-wards as the bromine atom cleaves from the substrate, breaking the C–Br bond. Finally, the C–N bond does not form until the acetonitrile N-terminus attacks the carbocation, producing the **TS2** structure and therefore forming a C–N bond of 2.12 Å and in the **PROD** structure formed, a C–N bond distance of 1.44 Å.

Upon further analysis of both I–Br bond distances along the energy profile, it was seen that both I_1 and I_2 bond distances in the **TS1** structure only differ by 0.08 Å suggesting that one iodine forms a slightly stronger XB interaction, but it was not expected to significantly influence the binding mode.

In order to analyse and characterise the strength of the XB interactions and the atomic bonds established, a QTAIM analysis was performed. The electron density (ρ) at BCP and the Laplacian values were obtained, illustrated in Table 5.2 and Table A.1, respectively, where the ρ(BCP) value is related to the strength of the bond and the Laplacian of the density at the BCP ($\nabla^2\rho$) represents the nature of the interaction.

Table 5.2: The electron density values found at each BCP of the I–Br bond (I_1 and I_2) in all the cat-complex A structures, calculated at the ωb97xD/def2SVP computational level (solvent = acetonitrile, SMD model and T = 273K).

Cat-complex A	**I_1 (a.u.)**	**I_2 (a.u.)**	**ρ(BCP) (a.u.)**
TS1	0.017	0.020	0.037
INT	0.021	0.022	0.043
TS2	0.022	0.023	0.045
PROD	0.022	0.022	0.044

There were two ρ(BCP) values obtained for each cat-complex structure and were found to range from 0.017 - 0.023 a.u (Figure 5.24 and Table A.1). The values of BCP $\nabla^2\rho$ were found to be positive for all the BCPs which is direct evidence of the closed shell nature of the interactions investigated, ranging from 0.042 - 0.05 a.u. QTAIM molecular graphs were obtained for all the cat-complex structures and are shown in Figure A.2. The **TS1** structure (Figure 5.20), in particular, showed that both iodine atoms form a bond with the bromine atom. Additionally, along the bonds between both I–Br, a BCP with the density values of 0.017 and 0.020 a.u. indicates that two strong XB interactions were formed. This reinforces the result found in the free energy profile, confirming that the halide abstraction proceeds via pathway 1 step-wise mechanism and that catalyst A forms a bidentate XB interaction.

A very good correlation was found, with $r^2 = 0.9589$, between the ρ(BCP) values and the corresponding I-Br distances (in Å), shown in Figure 5.19. As

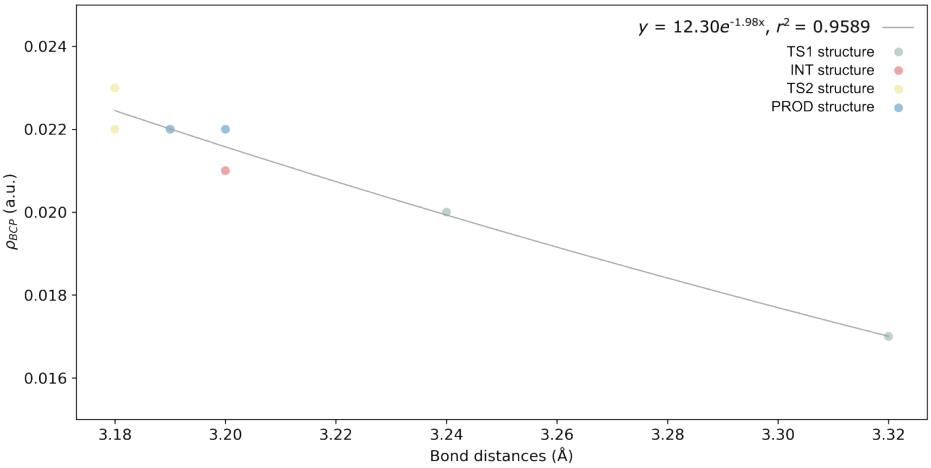

Figure 5.19: Exponential relationship of ρ(BCP)values and the bond distances (Å) in all the cat-complex structures in the reaction.

expected, there is an increase in electron density at the BCP as the I–Br distance decreases, meaning that as the reaction proceeds, the XB interaction gets stronger. The relatively weaker electron densities found at longer bond distances represent the I–Br interaction in the **TS1** structure, where the bond XB is starting to form. The greater electron densities found at shorter bond distances represent the I–Br interaction in the **TS2** and **PROD** structures, where the XB is more stabilised and well-established.

Additionally, according to the QTAIM molecular graphs of **TS1**, it was found that while both iodine atoms show the ability to form an XB interaction, there appear to be secondary interactions which anchor the substrate to the catalyst contributing towards the strength of the XB formed, see Figure 5.20. I_1 was found to form two additional interactions (I-C and I-I) and I_2 formed three additional interactions (I-C, I-H, and I-I)(Table A.2).

Finally, an NBO analysis was performed to identify and characterise the intermolecular charge transfer upon complexation. When studying non-covalent interactions, the stabilization due to the charge transfer between a lone pair and an empty anti-bonding orbital is considered one of the most important contributions to the energy. The charge transfer occurs from a lone pair of the bromide to an empty anti-bonding orbital (σ^*) of the iodine atom. For each NBO calculation, the second-order perturbation energies [E(2)] in kJ/mol were evaluated as well as the total energy that represents the sum of all the E(2) contributions to the XB interaction observed. All the calculated E(2) values were obtained for each of the I_1–Br and I_2–Br interactions and are depicted in Table 5.3. The total E(2) contribution in each cat-complex was also computed and is displayed in Table 5.4. The NBO values were found to correspond to strong XB interactions, with the sum of all the E(2) contributions ranging from 135 - 188 kJ/mol, coinciding with the AIM analysis above. It can be observed that the general trend of the perturbation energies found for I_1 and I_2 in the **TS1** structure, as well

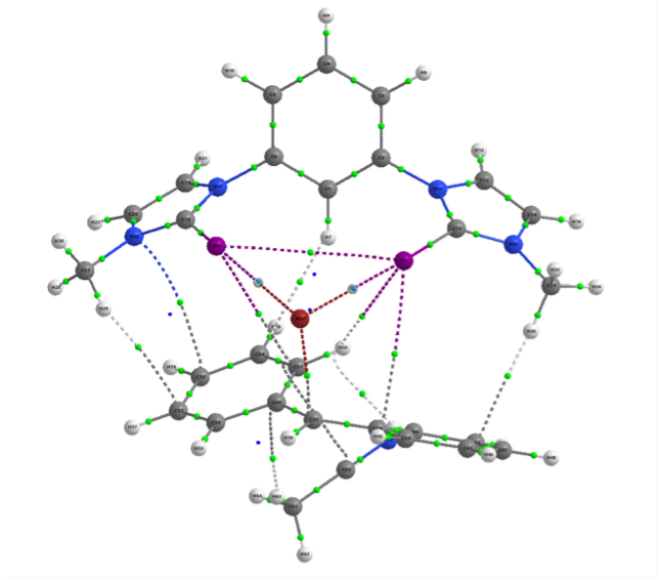

Figure 5.20: A QTAIM molecular graph of the cat-complex A, **TS1** structure.

as the other structures, are in agreement with the general trend with the AIM analysis results (Table A.7).

Table 5.3: Perturbation energies E(2) for each I–Br bond (I_1 and I_2) in the cat-complex A structures, calculated at the ωb97xD/def2SVP computational level (solvent = acetonitrile, SMD model and T = 273K).

Cat-complex A	**Orb(1)**	**Orb(2)**	**I_1 E(2)(kJ/mol)**	**I_2 E(2)(kJ/mol)**
TS1	LP_{Br}	σ^*_{C-I}	58.7	76.9
INT	LP_{Br}	σ^*_{C-I}	89.2	104.9
TS2	LP_{Br}	σ^*_{C-I}	98.7	97.5
PROD	LP_{Br}	σ^*_{C-I}	93.5	94.6

Table 5.4: Total perturbation energies E(2) for cat-complex A, calculated at the ωb97xD/def2SVP computational level (solvent = acetonitrile, SMD model and T = 273K).

Cat-complex A	**Total E(2) (kJ/mol)**
TS1	135.6
INT	194.1
TS2	196.2
PROD	188.1

5.2.2 Catalyst B

An MEP was also calculated for catalyst B, see Figure 5.21. Similar to catalyst A, two V_{max} values were obtained (0.055 a.u. and 0.057 a.u.) differing slightly

by 0.002 a.u, despite the catalysts' symmetry, and were located approximately 180° from the two iodine atoms present. Furthermore, the magnitude of both values were observed to be significantly lower in comparison the the MEP values of catalyst A isolated. This indicates that while a σ-hole associated with each of the iodine atoms involved is found, the predicted strength of the XB interaction to occur will be weaker than catalyst A. Additionally, as catalyst B is symmetrical with similar MEP values, in theory, the bidentate binding mode could occur. However, due to the structural orientation of both iodine atoms, in which the σ-holes point out in opposite directions, this indicates that a monodentate binding mode will most likely occur in this case.

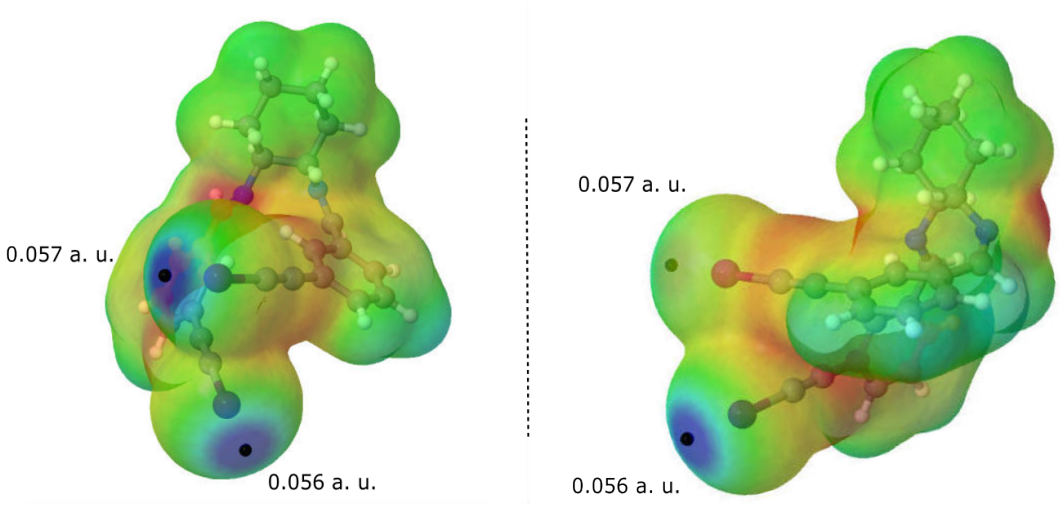

Figure 5.21: Molecular electrostatic potential on the 0.001 a.u. electron density isosurface calculated for catalyst B (Left: front view, right: side view); Colour scheme ranges from red (-0.050 a.u.) to blue (0.060 a.u.).

Further investigations were carried out for the mentioned reaction under the presence of catalyst B to reveal the characteristics and nature of such interactions. The free energy profile was obtained for catalyst-substrate complex (cat-complex) B and is displayed in Figure 5.22. It was found to be similar to catalyst A, confirming the step-wise mechanism; where the reaction profile proceeds through a **TS1** structure, establishing an XB interaction and facilitating the C–Br bond cleavage to generate a carbocation intermediate, **INT** structure. This is followed by a **TS2** structure resulting from the acetonitrile attacking the carbocation intermediate producing a cat-substrate product, **PROD** structure. All the structures can be found in Figure A.3.

As previously mentioned, the binding modes proposed for catalyst B in the literature[60] were monodentate and bidentate. Evidently, the resulting XB interaction was not strong enough to compete with the structural nature of the catalyst due to its high degree of flexibility, hindering its ability to form the bidentate binding mode, thus, only the monodentate binding mode was observed. The transition state structure can be seen in Figure 5.23.

Accounting for the orientation of the σ-holes and the magnitude of the V_{max} value found in the MEP analysis, catalyst B, with best interest, was strongly

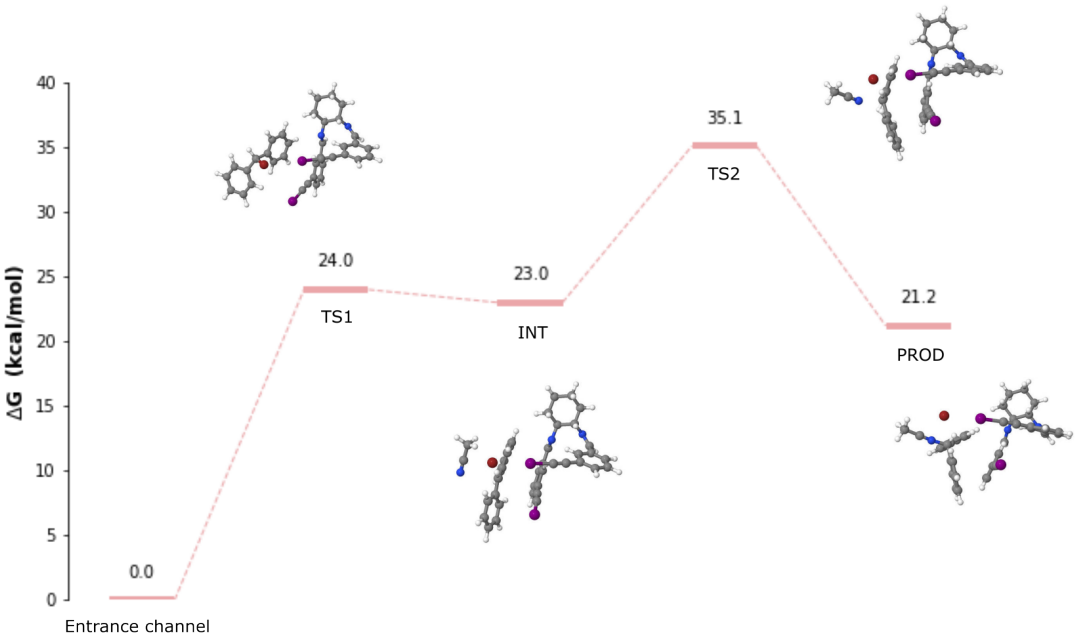

Figure 5.22: Free energy profile of catalyst B in kcal/mol.

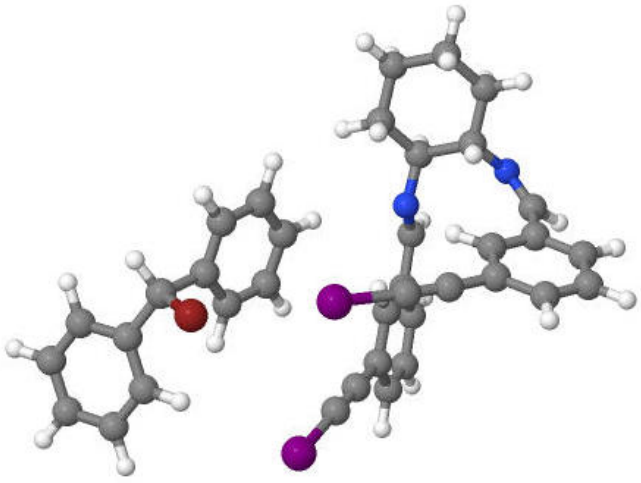

Figure 5.23: Cat-complex B, **TS1** structure.

discouraged for future use as an efficient catalyst as weak XB interactions were expected to form due to the small σ-hole value found.

Similar to catalyst A, an AIM analysis was performed and QTAIM molecular graphs were obtained (Table 5.5 and Figure A.4, respectively) to characterise the different non-covalent interactions upon complexation. The ρ(BCP) values were found to range from 0.023 - 0.024 a.u. and the $\nabla^2\rho$ were found to be positive which again is direct evidence of the closed shell nature of the interactions under study. In contrast to catalyst A, only one I–Br bond was formed in **TS1** structure with the ρ(BCP) value of 0.024, solidifying the monodentate formation. The molecular graphs for **TS1**, depicted in Figure 5.24, show additional interactions between the

phenyl ring of the substrate and the phenyl rings of the catalyst. Therefore, upon XB formation, the catalyst anchors the substrate to favour one side, rationalising why the bidentate binding mode is impossible to achieve.

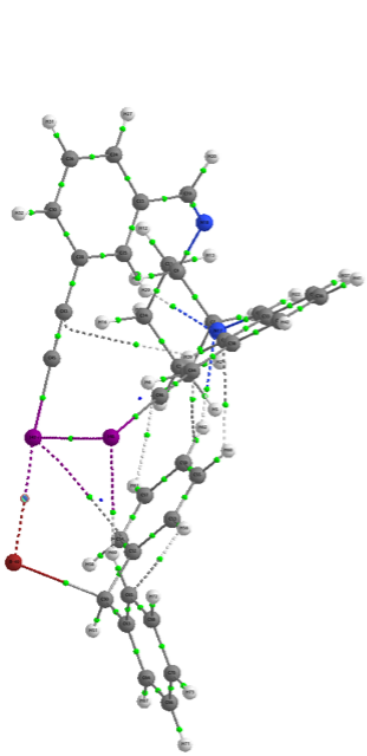

Figure 5.24: A QTAIM molecular graph of the cat-complex B, **TS1** structure.

The ρ(BCP) values of the two I–Br interactions present in cat-complex A and the ρ(BCP) values of the singular I–Br interaction formed by cat-complex B were taken into consideration. As BCP is related to the strength of the bond,[82] it can be concluded that the XB formed in the monodentate binding mode in catalyst B (Table 5.5), is far weaker than the XB formed in the bidentate binding mode of catalyst A (Table 5.2). The ρ(BCP) values differed by $\sim$ 0.02 a.u., supporting the MEP analysis and the results found in the free energy profile where weak XB interactions were predicted.

Table 5.5: The ρ(BCP) and $\nabla^2\rho$ values of all the cat-complex B structures, calculated at the ωb97xD/def2SVP computational level (solvent = acetonitrile, SMD model and T = 273K).

Cat-complex B	**ρ(BCP) (a.u.)**	**$\nabla^2\rho$ (a.u.)**
TS1	0.024	0.052
INT	0.023	0.052
TS2	0.023	0.052
PROD	0.023	0.063

An NBO analysis was obtained and is displayed in Table 5.6. The NBO analysis was as expected, showing that for each structure in the reaction profile, the E(2)

values were obtained for only one of the iodine atoms, which is in agreement with the conclusion from the free energy profile and the AIM results, signifying that only one iodine forms an XB interaction.

The NBO analysis of both catalysts, A and B, were compared, similar to the AIM analysis. It was found that the total E(2) values for cat-complex A (Table 5.3) are twice in magnitude than cat-complex B (Table 5.6), further confirming that the catalyst A forms a significantly stronger XB interaction than catalyst B, also corroborating with the AIM results.

Table 5.6: Perturbation energies E(2) values for cat-complex B, calculated at the ωb97xD/def2SVP computational level (solvent = acetonitrile, SMD model and T = 273K).

Cat-complex B	**Orb(1)**	**Orb(2)**	**E(2)(kJ/mol)**
TS1	LP_{Br}	σ^*_{C-I}	86.5
INT	LP_{Br}	σ^*_{C-I}	98.7
TS2	LP_{Br}	σ^*_{C-I}	99.5
PROD	LP_{Br}	σ^*_{C-I}	103.0

In conclusion, from the theoretical study of the halide abstraction, pathway 2, where the XB donor binds to the halide anion released during an R-X bond heterolysis, has now been effectively ruled out in favour of pathway 1, where an XB donor interacts with an R–X bond of a leaving group thereby producing a heterolytic bond cleavage. Additionally, Catalyst A was observed to only have a strong preference in the bidentate binding mode and catalyst B, while very difficult to achieve, only has a preference for the monodentate binding mode. This was seen in both the AIM and NBO results where it was found that catalyst A produced two strong XB interactions while catalyst B produced one weak XB interaction.

5.3 Michael addition

In this section, a theoretical study of the first step of the Michael addition, C–C coupling, between an indole and a trans-crotonophenone was undertaken. Dichloromethane (DCM) was used as the solvent and five different catalysts (**1** to **5**) were tested. This reaction was chosen to rationalise the XB interactions and gain knowledge of what stabilises the reaction states, with the goal to design potential catalysts with greater efficiency (Figure 5.25). Catalysts **1**, **2** and **3** were designed, varying in the halogen donor atom starting from the least to the most polarisable (X= Cl, Br, I, respectively), in order to analyse the XB donor effect. Catalysts **4** and **5** were designed, varying in molecular structure while the XB donor atom (X= I) remains unchanged, in order to investigate the substituent effect. It should be noted that the octyl substituents present in the experimentally designed catalysts have been replaced by a methyl group for simplification in theoretical calculations.

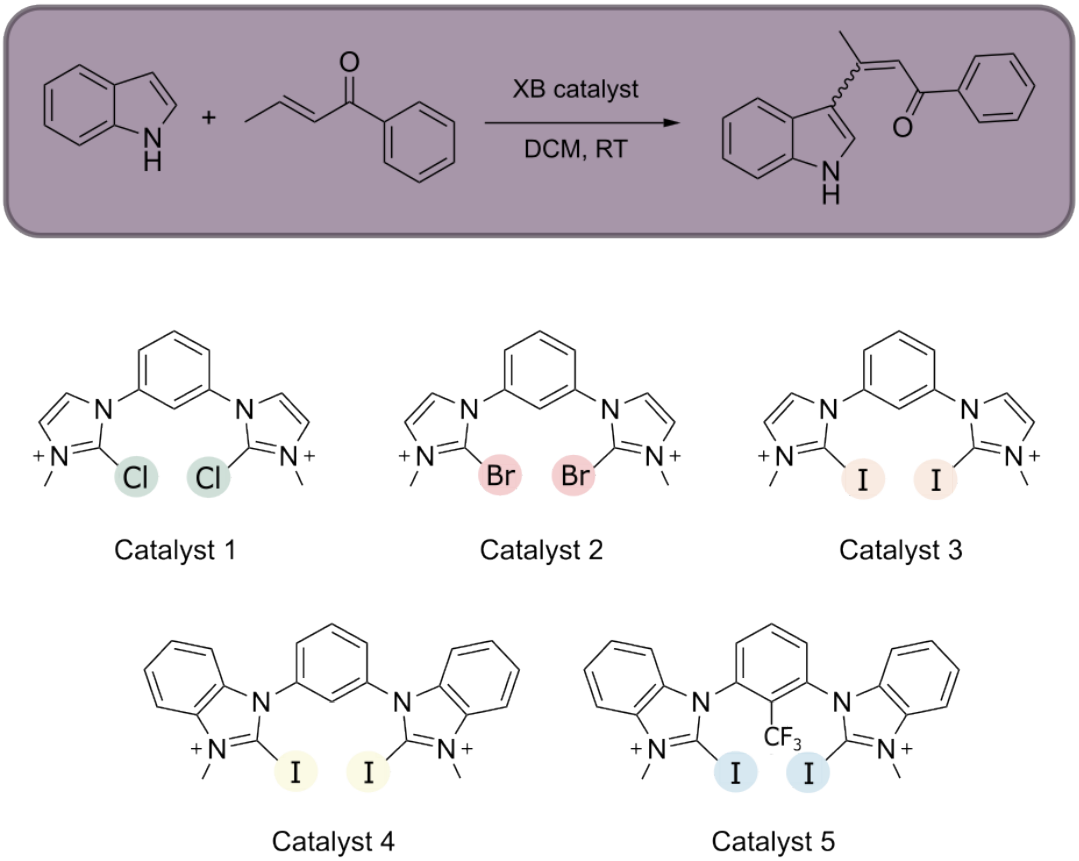

Figure 5.25: Michael addition reaction scheme with five different catalysts. Catalysts **1** to **3**, varying in halogen atom, and catalysts **4** and **5**, varying in the catalytic scaffold.

5.3.1 Structural and energetic analysis

Firstly, the MEP was calculated for catalyst **1** to catalyst **5** in order to identify and quantify the σ-holes where the XB interactions are most likely to occur. For each of the five catalyst monomers, two V_{max} values were found.

Catalysts **1** to **3** have been grouped together for a more meaningful comparative analysis. The following trend was observed where the V_{max} increased from catalyst **1** < **2** < **3** (Figure 5.26). This indicates that the magnitude of the σ-hole increases, predicting an increasing XB strength, starting with catalyst **1** being the weakest to catalyst **3** being the strongest. This outcome was expected since larger halogen donor atoms possess lower electronegativity values and are more polarizable going down the halogen group. The magnitude of V_{max} value for catalysts **1** and **2** were very similar, differing in 0.003 a.u., whereas the strength of the σ-hole increases significantly with catalyst **3**, by approximately 0.04 a.u. (Figure 5.26). Evidently, catalyst **3** is expected to produce the greatest XB formation than catalysts **1** and **2**. This coincides with the experimental values[48] as an increase in the rate of conversion is seen from catalysts **1** to **3**. It is important to note, that while catalyst **3** is symmetrical and, in theory, should have produced identical MEP values similar to catalyst **1** and **2**, a small difference of 0.004 a.u. was obtained which is not expected to affect the strength of XB.

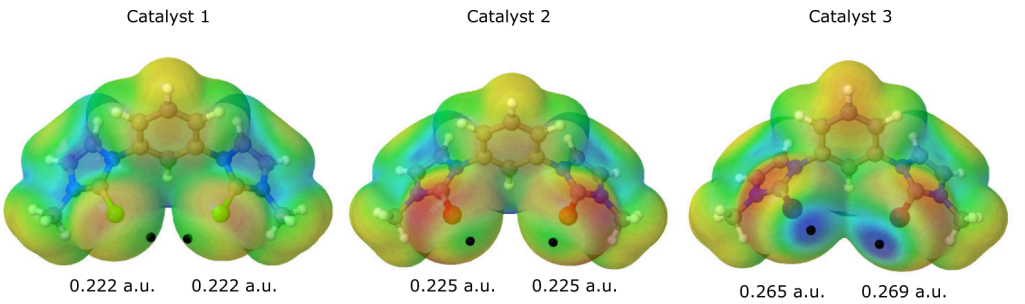

Figure 5.26: Molecular electrostatic potential on the 0.001 a.u. electron density isosurface calculated for catalysts **1** to **3**; Colour scheme range from red to blue (0.180 - 0.260 a.u.).

Furthermore, a comparison of the MEP values for catalysts **3**, **4** and **5** was carried out to analyse, if any, the influence of the structural differences each catalyst has on the σ-hole. The following trend was observed where the V_{max} increased from catalyst **5** < **3** < **4** (Figure 5.27) where catalyst **4**, theoretically, would form the strongest XB interaction and catalyst **5** would form the weakest XB interaction. This was not in agreement with the experimental values where it was established that catalyst **5** produced the highest rate of conversion, followed by **4** and then **3**, and was therefore expected to have the most positive V_{max}. However, as this was not the case, this phenomenon has been further explored in later sections. Once again, it was noted that while catalyst **5** is symmetrical, a small difference of 0.001 a.u. was obtained.

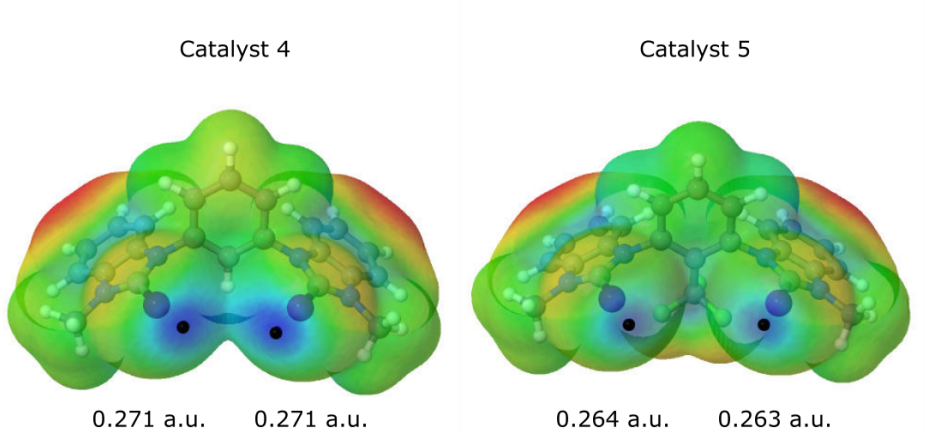

Figure 5.27: Molecular electrostatic potential on the 0.001 a.u. electron density isosurface calculated for catalysts **4** and **5**; Colour scheme range from red to blue (0.1845 - 0.270 a.u.).

The dihedral angle (α) and the X–X distance of each catalyst were measured and are depicted in Figure 5.28 and Table A.24. In comparing catalysts **1** to **3**, there was no obvious trend found, indicating that the size of the halogen atom does not influence the orientation. For catalysts **3** to **5**, while the α-angle for both catalysts **3** and **4** remained at around 70-80°, producing similar I–I distance at $\sim$ 4.7 Å, catalyst **5** obtained an α angle close to 100° which produced an I–I distance of 5.6 Å. This indicates that due to the structural orientation of both iodine atoms in catalyst **5**, as a result of the CF_3 in the para position promoting an increase in distance between the two iodine atoms relative to catalysts **3** and **4**, catalyst **5** is predicted to produce a slightly weaker interaction than **3** and **4**. This was due to proximity of the I atoms making it relatively harder to establish a simultaneous XB. Therefore, due to the placement of the CF_3 substituent which produces a steric hindrance, catalyst **5** is expected to incur an energetic penalty.

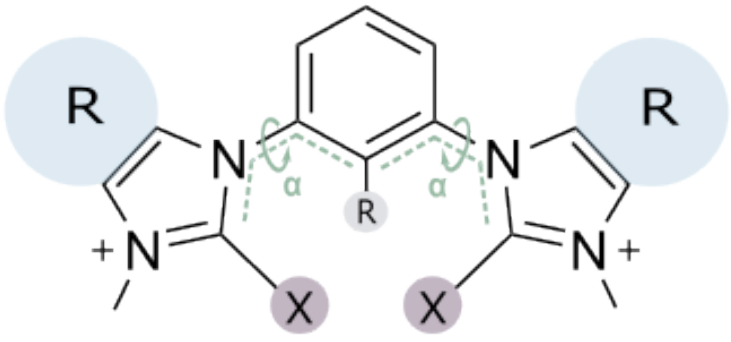

Figure 5.28: The α angles that have been measured in the catalyst monomers **1** to **5**.

Free energy profiles of the reaction were obtained under the presence of all the catalysts under study, in order to visualise the magnitude of the activation energy corresponding to each catalyst. Once again, cat-complex **1** to **3** and cat-complex **3** to **5** have been grouped together for ease of comparison (Figure 5.29 and Figure 5.31, respectively). In accordance with the experimental results and the MEP values, a trend was obtained for cat-complex **1** to **3**, such that the transition state structure (cat-ts) **1** had the highest activation energy, followed by **2**, and further cat-ts **3** which had the lowest energy barrier. The cat-ts structures can be seen in Figure A.5. The products (cat-prod) obtained also followed the same trend. Furthermore, an analysis of the respective halogen bond distances was carried out where it was found that the I–O bond length increases from cat-ts **1** < **2** < **3**, inline with the above trend. This is expected as the halogen atom increases in size and therefore increases the length of the XB. It should be noted that the energy profiles obtained in this reaction are reversible as only the first step of this reaction was studied.

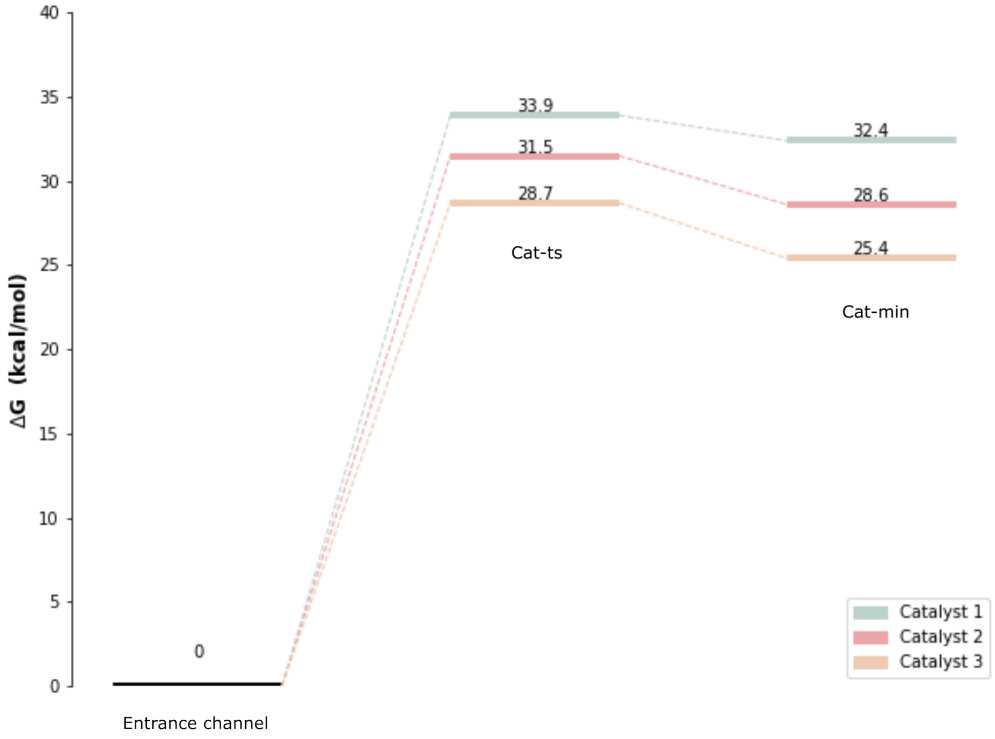

Figure 5.29: Free energy profile for cat-complex **1** to **3** in kcal/mol.

In Figure 5.31, while it was found that the activation energies for all three cat-ts **3** to **5** only differ by 0.5 - 1.3 kcal/mol, a trend was found where the activation energy increases from **4** < **3** < **5**. This indicates that catalyst **5** produces the least stable ts complex while **4** produces the most stable ts complex. This is in correspondence to the trend found in both MEP analysis and the prediction from the α angles measured. However, as already mentioned, this does not correspond with the experimental observation of catalyst **5** being the best catalyst established

to produce the highest and fastest conversion.

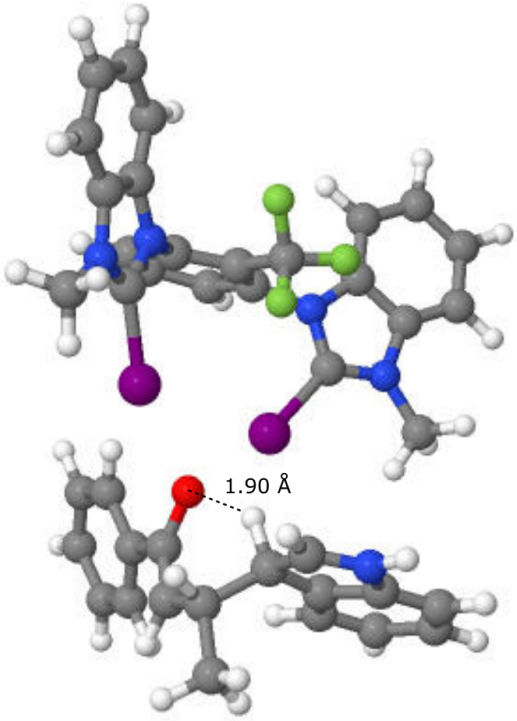

Figure 5.30: Cat-prod **5** complex, showing the O...H distance.

The succeeding step in the energy profile would be the H transfer. Therefore, the O...H distances of cat-prod **3** to **5** were subsequently measured and, interestingly, the O...H distance in catalyst **5** was found to be less than 1.90 Å (as seen in Figure 5.30) where the others produced far greater distances of 2.12 - 2.41 Å. This indicates that catalyst **5** has a greater potential to facilitate an H transfer more easily. Therefore, it was concluded that because this study mainly focused on exploring the C–C bond activation, that the preceding proton transfer step may be the cause of the rapid conversion found in the literature.

A comparative analysis was carried out between the activation energies for cat-ts **3**, **4** and **5**; which were also compared to the un-catalysed ts and cat-ts $\mathbf{I}_2$ (Figure 5.32), as catalyst $\mathbf{I}_2$ was seen to exhibit great efficiency in catalysing the relevant Michael addition reaction in literature.[54] Cat-ts **4** was seen to have the most stable activation energy and, therefore, while the energy difference between catalysts **4** and I_2 is minimal by 0.02 kcal/mol, catalyst **4** was concluded to be the slightly better catalyst. Additionally, catalyst **4** was observed to lower the activation energy more efficiently when compared to the un-catalysed reaction by 0.8 kcal/mol. Overall, it was determined that catalysts **3** to **5** are good catalysts and are comparable to catalyst $\mathbf{I}_2$ as the difference in activation energies in catalysts **3** to **5** and catalyst $\mathbf{I}_2$ are minuscule. However, the structural modifications applied to these catalysts, in hopes to pursue better catalytic activity, seems to be inadequate in the C–C coupling step, despite the fact. While catalysts **3** to **5** were designed to present advantages over the simple diatomic catalyst $\mathbf{I}_2$ in terms of tunability, accounting for the small energetic difference between them, it was

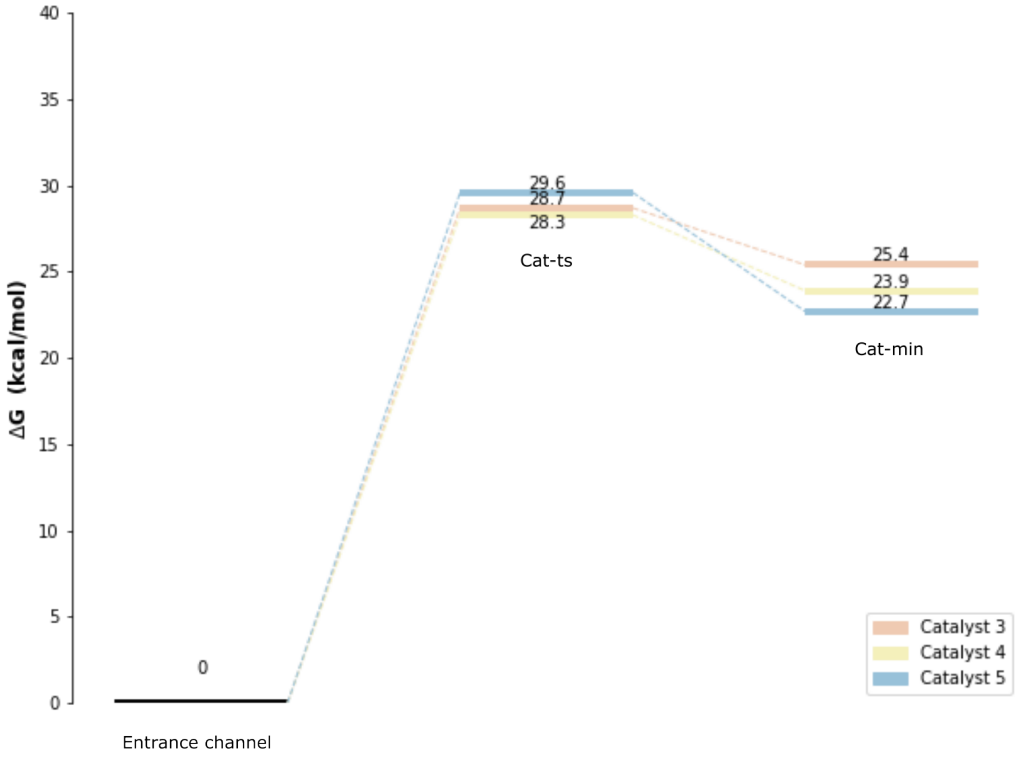

Figure 5.31: Free energy profile for cat-complex **3** to **5** in kcal/mol.

deduced that the structural modification applied to catalysts **3**, **4** and **5**, does not produce a significant difference in the C–C bond activation but it may do so in the proceeding step of the Michael addition reaction.

5.3.2 Characterisation of NCI

A QTAIM analysis was carried out for all the catalysts and the ρ(BCP) and Laplacians values were obtained (Table 5.7). The Laplacians were found to be positive values indicative of the XB interactions present (Table A.23). A trend regarding the values of the density associated to the BCPs was seen, such that **1** < **2** < **3** (Table 5.7), in agreement with the previous MEPs and activation energies. As the magnitude corresponds to the strength of the XB, according to the AIM results, catalyst **1** produces the weakest XB interaction, followed by catalyst **2**, and catalyst **3** was found to form the strongest XB interaction. A trend was obtained for catalysts **3** to **5** where **3** < **4** < **5**, and was found to be in agreement with experimental values, however, the trend does not coincide with the previous trends in the MEP and activation energies. Catalyst **5** shows the strongest XB, while catalyst **4** shows medium strength and catalyst **3** shows the weakest XB.

Upon further analysis of the QTAIM molecular graphs for catalysts **1** to **5** (Figure A.6), there is a web of interactions present in catalysts **1** to **3**, where one of

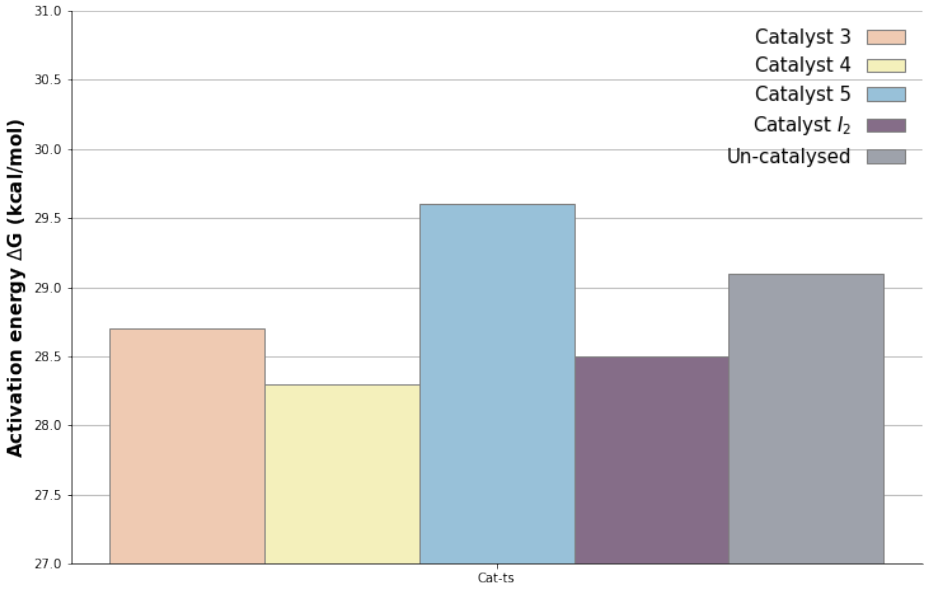

Figure 5.32: Activation energies for cat-ts **3** to **5**, $\mathbf{I}_2$ and the un-catalysed transition state structure, in kcal/mol.

Table 5.7: The ρ(BCP) values for cat-ts **1** to **5**, calculated at the ωb97xD/def2SVP computational level (solvent = DCM, SMD model and T = 273K).

Complex	**ρ(BCP) (a.u.)**
cat-ts 1	0.036
cat-ts 2	0.042
cat-ts 3	0.043
cat-ts 4	0.046
cat-ts 5	0.050

the I atoms form an interaction with one or more of the H atoms in the substrate, and in catalyst **4**, where both iodine atoms form additional interactions with the H atoms of the substrate and within the catalyst. Furthermore, catalyst **5** shows an abundance of these 'webs of interactions' that are not as pronounced in the others, as seen in Figure 5.33 (right). The web of interactions in catalyst **5** consists of both I atoms forming an additional interaction with the H atom of the substrate and, additionally, with the F atom within the catalyst. These contribute to a more stabilising effect which is evident in the BCP obtained. This accounts for the inconsistency in the trend when compared to the ones obtained in the MEP results and activation energies. Additionally, the CF_3 group forms additional interactions within the catalyst itself, reducing its flexibility. Furthermore, while the CF_3 group was expected to reinforce the σ-holes by drawing electron density away from the iodine atoms of the catalyst, instead, the CF_3 substituent forms additional interactions with the nitrogen atom in both sides of the catalyst, hindering the

strength of the σ-hole, as seen in the MEP analysis. This explains why the activation energy of catalyst **5** is higher than catalyst **3** and **4**.

The ρ(BCP) of the individual halogen atoms of each catalyst involved in the XB were obtained. It was observed that one halogen atom formed a slightly stronger XB interaction than the other, despite the similarity in XB lengths. This was due to the geometry of the substrate as it interacts with the catalyst resulting in one halogen atom closer in proximity to the lone pair of the O atom than the other.

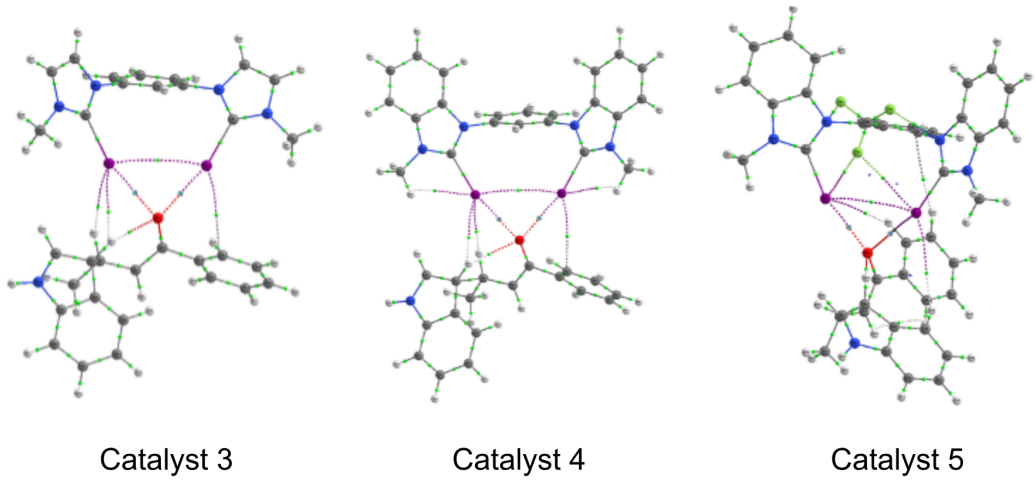

Figure 5.33: QTAIM molecular graphs for catalysts **3** (left), **4** (middle) and **5** (right).

Finally, an NBO analysis was performed for all catalysts and the perturbation energies were obtained (Table A.25). A trend can be observed in the total E(2) contribution, such that the E(2) energies increase from **1** < **2** < **3** and further a trend where **3** < **4** < **5** (Table 5.8). The trend obtained for catalysts **1** to **3** is in agreement with the previous results in the QTAIM analysis and activation energies. Similarly, despite the trend for catalysts **3** to **5** not corresponding with the trend in the MEP analysis and the activation energies, the overall trend does coincide with QTAIM results and experimental values.

Table 5.8: Total perturbation energies E(2) for cat-ts **1** to **5**, calculated at the ωb97xD/def2SVP computational level (solvent = DCM, SMD model and T = 273K).

Complex	**Orb(1)**	**Orb(2)**	**E(2)(kJ/mol)**
Cat-ts 1	LP_O	σ^*_{C-Cl}	20.8
Cat-ts 2	LP_O	σ^*_{C-Br}	63.8
Cat-ts 3	LP_O	σ^*_{C-I}	95.6
Cat-ts 4	LP_O	σ^*_{C-I}	104.0
Cat-ts 5	LP_O	σ^*_{C-I}	121.5

Upon further analysis of the individual halogen atoms and the respective XB formation, an observation was made such that the strongest XB formed was

produced by the opposite halogen atom as seen in the QTAIM analysis. Once again, due to the geometry of the substrate as it interacts with the catalyst, the halogen atom (opposite to the above mentioned in QTAIM) that produces the strongest interaction appears to be further away from the O atom. This strong interaction results from a more effective alignment formed with the lone pair of the O atom and therefore facilitates a better charge transfer.

5.4 Improvement of XB-catalyst design

As previously mentioned, the structural modifications applied to catalysts **3**, **4** and **5** were found to be anti-climactic in the C–C bond activation. As these catalysts were found to significantly increase the rate of reaction experimentally, a redesign based on the previous catalysts was undertaken (Figure 5.34) to improve the catalytic activity in the first step of the reaction and produce more optimal XB-catalysts. The placement of the CF_3 substituent in catalyst **5** was considered to be problematic as it hindered the flexibility of the phenyl rings within the catalyst. Although the specific placement of the CF_3 substituent in the ortho position was seen to be highly beneficial in experimental studies,[48] by moving the substituent to the meta position, it was anticipated that the resulting flexibility of the catalyst would compensate. Consequently, CF_3 was placed in the meta position, now called catalyst **6**.

Furthermore, the goal was to produce a bigger σ-hole from what was present in order to establish greater XB formation. Considering the CF_3 placement in catalyst **5** that proved to be detrimental in producing a relatively strong σ-hole, the distance of CF_3 in the ortho position was regarded to be too far in length and was unable to conjugate with the other rings. Placing the CF_3 substituent in close proximity to the σ-hole, forming catalyst **7**, was considered to be far more beneficial and was expected to produce a σ-hole bigger in magnitude resulting in the formation of a stronger XB interaction.

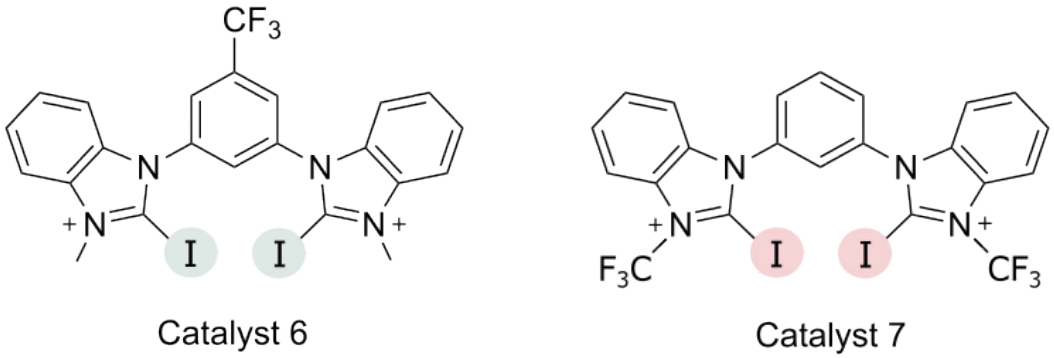

Figure 5.34: Two new theoretical catalytic designs; catalysts **6** (left) and **7** (right).

5.4.1 Structural and energetic analysis

Firstly, an analysis of the MEP was carried out for both catalysts, **6** and **7**. The V_{max} for both catalysts were obtained and are illustrated in Figure 5.35. Similar to the MEP values obtained in the previous catalysts, two σ-holes were found for each I atom, where one iodine produces a slightly stronger V_{max} than the other despite the symmetry of both catalysts which would, in theory, produce identical MEP values. However only small differences of 0.003 and 0.002 a.u. were calculated for catalyst **6** and **7**, respectively, and is therefore not anticipated to affect the strength of the XB interaction. Both calculated σ-holes of each respective

catalyst, were seen to be significantly greater than the σ-holes in catalysts **3**, **4** and **5**. Therefore, it was anticipated that both catalysts **6** and **7** are expected to form much stronger XBs than the latter, with catalyst **7** expected to form a stronger XB as it produced a more positive σ-hole value than catalyst **6**.

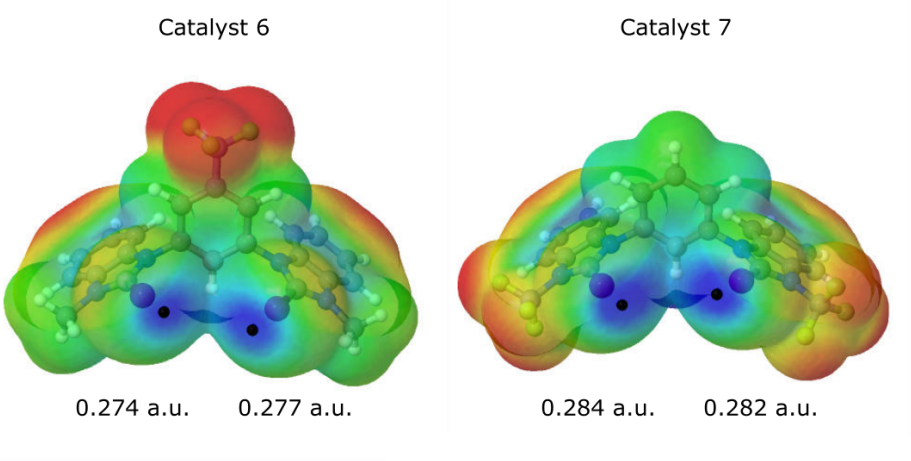

Figure 5.35: Molecular electrostatic potential on the 0.001 a.u. electron density isosurface calculated for catalysts **6** and **7**; Colour scheme range from red to blue (0.145 - 0.270 a.u.).

The activation energies were obtained for both cat-complex **6** and **7** and was compared to cat-complex **3** to **5** (Figure 5.36). The cat-ts structures of each catalyst can be found in Figure A.8. It was found that there was a notable difference between the energy barriers for cat-ts **6** in comparison to cat-ts **3**, **4** and **5**, differing in 2.3, 1.9, and 3.2 kcal/mol, respectively, and more significantly with cat-ts **7**, differing by 3.6, 3.2 and 4.5 kcal/mol. The structural modification of catalysts **6** and **7** resulted in a more stable transition state complex and, therefore, is anticipated to better catalyse the Michael addition reaction, experimentally.

Most importantly, catalysts **6** and **7** were observed to theoretically lower the activation energy when compared to the un-catalysed reaction by 2.7 and 4 kcal/mol, respectively.

The O...H bond distance was measured for cat-prod **6** and **7** in order to compare with the O...H distances obtained for cat-prod **3** to **5**. As previously mentioned, cat-prod **5** produced the shortest O...H distance with a length of 1.90 Å, in comparison to the other catalysts, ranging from 2.12 - 2.41 Å, predicting an easier proton transfer. The O...H distance of cat-prod **6** and **7** were 1.90 and 2.01 Å, respectively, which is similar in distance to cat-prod **5**. This shows that the addition of the CF_3 substituent in the scaffolds, regarding catalysts **5**, **6** and **7**, appear to be beneficial for the subsequent proton transfer step. Therefore, catalysts **6** and **7** are anticipated to readily facilitate the H transfer step of the global Michael addition reaction.

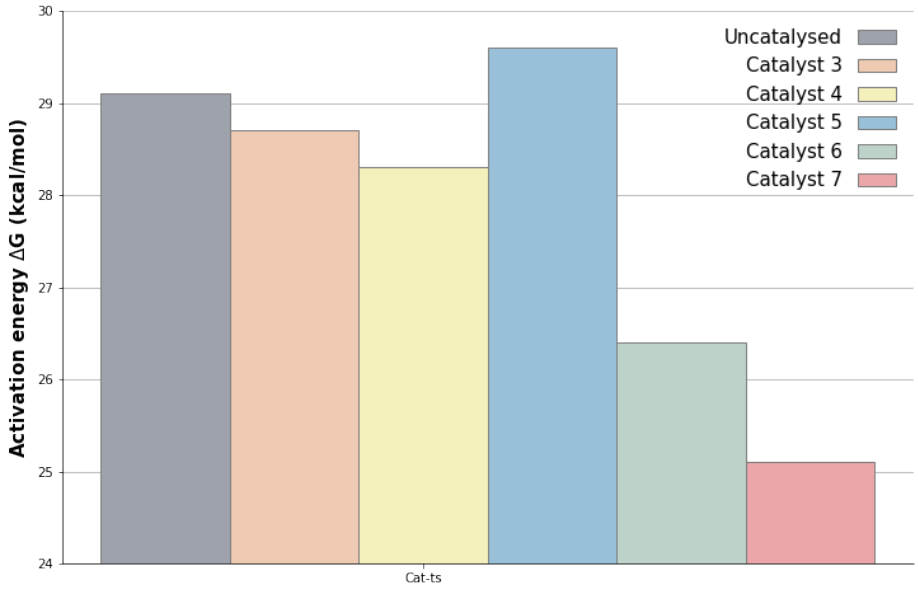

Figure 5.36: A comparison of the activation energies (kcal/mol) in the presence of different catalysts and in the un-catalysed reaction.

5.4.2 Characterisation of NCI

A QTAIM analysis was carried out for cat-complex **6** and **7** which were then compared to the previous catalysts, varying in scaffolds (cat-complex **3** to **5**). The electron density found at different BCPs was obtained (Table 5.9 and Table A.31) and the following trend achieved (**6** < **7**) was found to be consistent with the MEP and activation energy trend. A comparative analysis was performed for catalysts **3** to **7** producing an average correlation between ρ(BCP) and bond distances with an r^2 value of 0.9113 (Figure 5.37). The QTAIM molecular graphs were analysed and a similar web of interactions, seen in catalyst **5** (Figure 5.33, right), was present in both catalysts (Figure 5.38). Additionally, a new weak pi-pi interaction was established between the phenyl ring (centre) of catalyst **7** and the phenyl ring of the substrate which was established to contribute to stabilising the energy barrier of the transition state structure.

Table 5.9: The (BCP) values for cat-ts **6** and **7**, calculated at the ωb97xD/def2SVP computational level (solvent = DCM, SMD model and T = 273K).

Complex	**ρ(BCP) (a.u.)**
cat-ts 6	0.0510
cat-ts 7	0.0538

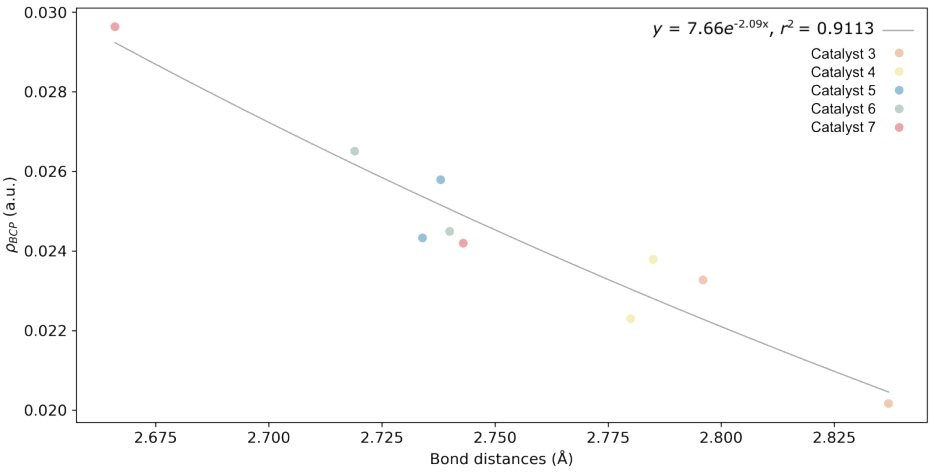

Figure 5.37: Exponential correlation found between (BCP) values and XB distances (Å) in cat-ts **3** to **7**.

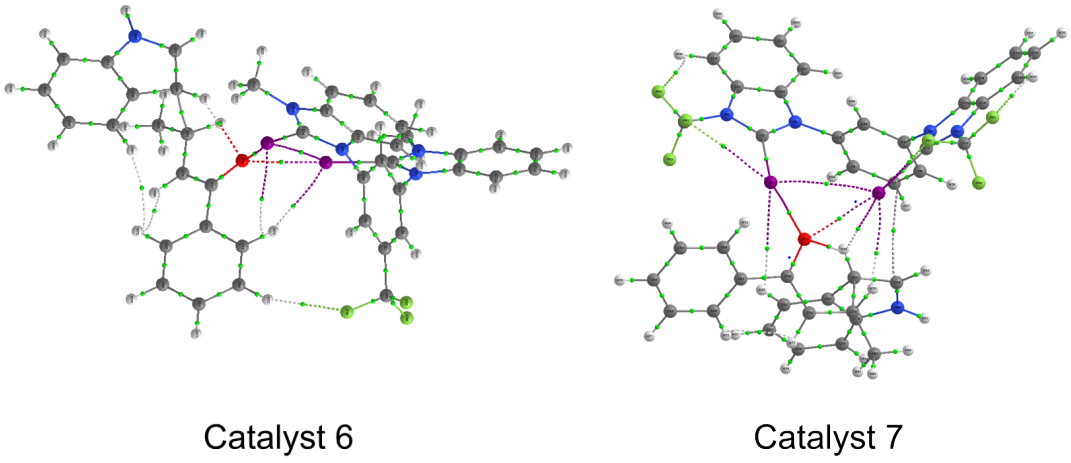

Figure 5.38: QTAIM molecular graphs for cat **6** to **7**

Finally, an NBO analysis was performed for catalysts **6** and **7**. The second-order perturbation energies were collected (Table 5.10 and Table A.32) and it was found that the E(2) for catalysts **6** and **7**, in comparison to catalysts **3** to **5**, corresponded to the trends obtained in MEPs, activation energies and the QTAIM results. The E(2) values for catalysts **6** and **7** were found to be more stable than catalysts **3** to **5** at 125.8 and 127.7 kJ/mol, respectively.

Table 5.10: Perturbation energies E(2) for cat-ts **6** and **7**, calculated at the ωb97xD/def2SVP computational level (solvent = DCM, SMD model and T = 273K).

Complex	**Orb(1)**	**Orb(2)**	**Total E(2)(kJ/mol)**
Cat-ts 6	LP_O	σ^*_{C-I}	125.8
Cat-ts7	LP_O	σ^*_{C-I}	127.7

In summary, the two new catalysts **6** and **7** (designed based on the previous theoretical study) were successful in lowering the activation energy of the C–C coupling step and, therefore, are predicted to synthetically produce higher rates of conversion in the Michael addition reaction between a trans-crotophenone and an indole.

6 Conclusions

In summary, the theoretical studies carried out in this project have proven to produce great insight into various chemical reactions and have allowed the analysis of chemical properties which would not have been possible in synthetic research.

A new zigzag HB pattern was established when studying the HB interactions. The formation of the three binding modes was found to occur synthetically and the HB acceptors direct the type of bonding mode formed for each of the systems due to the number and position of the O atoms involved in the HB interactions. However, HB donors have the ability to position themselves in the best orientation to achieve optimal interaction depending on the solvent and when the options are available. Additionally, it was concluded that interaction energies are dominated by the electrostatic component, followed by the polarisation component for all the complexes presented in the project. Finally, the strength of each binding mode was quantified. It was established that the parallel binding produces the strongest HB interactions, followed by the bifurcated and the zigzag pattern.

Besides, the first reported theoretical investigation of the halide abstraction mechanism to date was presented, having no previous experimental evidence to support the mechanisms proposed. The reaction mechanism was revealed to proceed via pathway 1, a step-wise mechanism. A first transition state structure is formed where a halogen bond interaction is established between the iodine XB donor and the Br atom of the substrate. The transition state produces the formation of a carbocation intermediate structure through the cleavage of the C-Br bond which is then followed by an acetonitrile N-terminal attacking the carbocation to form a catalyst-substrate product. This was the first reported theoretical investigation of the reaction mechanism to date. Upon analysis of the two chosen catalysts within the halide abstraction, it was found that catalyst A had a strong preference to bind via a bidentate mode as the catalyst produced a strong σ-hole as seen in the MEP analysis and both iodine atoms were in the optimal orientation for a bidentate mode to occur, in contrast to catalyst B, where the preferential bind mode was found to be monodentate as the σ-hole appeared to be significantly weaker in combination with both iodine atoms orientated away from each other and therefore, only the monodentate binding can occur.

Lastly, in the Michael addition reaction under the presence of XB catalysts, it was found that the more polarisable the halogen atom is the stronger the XB strength, as seen with the theoretical calculations of catalysts 1 to 3, validating experimental results. However, in the analysis of the different catalytic scaffolds applied to the catalysts, the structural modification of each catalyst was established to have an insignificant influence on the XB strength, in the C-C coupling step, in comparison to the molecular iodine as previously expected from experimental results. Based on the catalyst which was anticipated to be the optimal catalyst affording anti-climactic results in comparison to the other catalysts, the design of two new catalytic scaffolds was produced. These catalysts were observed to successfully improve the C-C coupling activation energies in silico. This was achieved by varying the placement of the CF_3 substituent, as the previous substituent position was found to be unfavourable, resulting in a much stronger σ-hole value as seen with the previous catalyst.

7 Computational details

In the first part of this project where hydrogen bond interactions were studied, all structures of the complexes were optimised at the M06-2X/6-31+G(d,p) computational level[83,84] The harmonic vibrational frequencies were computed at the same level used for the geometry optimisations to confirm that the stationary points are local minima. The calculations were performed using the Gaussian 16 software.[85] Single point energies were computed using M062X/6-311++G(3df,2p). Interaction energies (E_i) were calculated as the difference of the energy of the optimised complex minus the energy of each optimised monomer. Solvent effects (H_2O and THF) were included in the optimised structures by the solvation model based on the density (SMD) approach implemented in Gaussian 16[86] The molecular electrostatic potential (MEP) of the isolated monomers was calculated on the electron density isosurface of 0.001 a.u..[87] These calculations were carried out with the Gaussian 16 software and the results were analysed using Multiwfn,[88] and plotted using Jmol.[89] The quantum theory of atoms in molecules (QTAIM) methodology[87] was used to analyse the electron density of the systems with the AIMAll program.[90] The natural bond orbital (NBO) method[91] was employed to evaluate atomic charges using the NBO-7 program.

An energy decomposition analysis based on the localised molecular orbital energy decomposition analysis (LMOEDA)[92] scheme has been carried out at the M06-2X/6-31+G(d,p) computational level. The interaction energy is obtained as a sum of different energetic terms, as shown in 12:

$$E_{int} = E_{elec} + E_{exc} + E_{rep} + E_{pol} + E_{disp} \tag{12}$$

where E_{elec} is the electrostatic term describing the classical Coulombic interaction of the occupied orbitals of one monomer with those of the other. The E_{exc} and E_{rep} terms are the exchange and repulsive components associated with the Pauli exclusion principle, and E_{pol} and E_{disp} correspond to polarization and dispersion terms, respectively. These calculations were carried out using the GAMESS program (version 2018-R2).[93]

The structures in the halide abstraction and Michael addition reaction were optimised at the ωb97xD/def2SVP computational level.[94] Harmonic vibrational frequencies were also computed at the same level as the geometry optimisations. Calculations were performed using the Gaussian 09 software.[85] Single point energies were computed at the ωb97xD/def2TZVP. Solvent effects (acetonitrile in the halide abstraction and DCM in the Michael addition reaction) were included in the optimised structures by the SMD approach in Gaussian 09.[73] The MEPs of the isolated monomers were calculated on the electron density isosurface of 0.001 a.u.[95] with the Gaussian 09 software and were analysed using the same methods and programs as previously mentioned above; Multiwfn,[88] Jmol,[89] QTAIM,[90] and NBO.[91]

References

(1) J.-M. Paris, in *Comprehensive Chirality*, ed. E. M. Carreira and H. Yamamoto, Elsevier, Amsterdam, 2012, pp. 30–53.

(2) W. H Brooks, W. C Guida and K. G Daniel, *Current topics in medicinal chemistry*, 2011, **11**, 760–770.

(3) J. H. Kim and A. R. Scialli, *Toxicological Sciences*, 2011, **122**, 1–6.

(4) A. E. KELLIE and E. R. SMITH, *Nature*, 1956, **178**, 323–323.

(5) U. Eder, G. Sauer and R. Wiechert, *Angewandte Chemie International Edition in English*, 1971, **10**, 496–497.

(6) Z. G. Hajos and D. R. Parrish, *The Journal of Organic Chemistry*, 1974, **39**, 1615–1621.

(7) Q.-L. Zhou, *Angewandte Chemie International Edition*, 2016, **55**, 5352–5353.

(8) L. S. Hegedus, *Journal of the American Chemical Society*, 2009, **131**, 17995–17997.

(9) J. Zhou and B. List, *Journal of the American Chemical Society*, 2007, **129**, 7498–7499.

(10) J. W. Yang, M. T. Hechavarria Fonseca, N. Vignola and B. List, *Angewandte Chemie International Edition*, 2005, **44**, 108–110.

(11) S. Hoffmann, A. M. Seayad and B. List, *Angewandte Chemie International Edition*, 2005, **44**, 7424–7427.

(12) S. G. Ouellet, A. M. Walji and D. W. C. Macmillan, *Accounts of Chemical Research*, 2007, **40**, PMID: 18085748, 1327–1339.

(13) D. A. Nicewicz and D. W. C. MacMillan, *Science*, 2008, **322**, 77–80.

(14) J. B. Tuttle, S. G. Ouellet and D. W. C. MacMillan, *Journal of the American Chemical Society*, 2006, **128**, 12662–12663.

(15) M. Marigo, T. Schulte, J. Franzén and K. A. Jørgensen, *Journal of the American Chemical Society*, 2005, **127**, 15710–15711.

(16) S. Lee and D. W. MacMillan, *Tetrahedron*, 2006, **62**, Tetrahedron Young Investigator Award, 11413–11424.

(17) E. Arunan, G. R. Desiraju, R. A. Klein, J. Sadlej, S. Scheiner, I. Alkorta, D. C. Clary, R. H. Crabtree, J. J. Dannenberg, P. Hobza et al., *Pure and applied chemistry*, 2011, **83**, 1637–1641.

(18) A. G. Doyle and E. N. Jacobsen, *Chemical Reviews*, 2007, **107**, 5713–5743.

(19) S. J. Connon, *Chemical communications*, 2008, 2499–2510.

(20) Z. Zhang and P. R. Schreiner, *Chemical Society Reviews*, 2009, **38**, 1187–1198.

(21) W.-Y. Siau and J. Wang, *Catalysis Science & Technology*, 2011, **1**, 1298–1310.

(22) O. V. Serdyuk, C. M. Heckel and S. B. Tsogoeva, *Organic & biomolecular chemistry*, 2013, **11**, 7051–7071.

(23) T. J. Auvil, A. G. Schafer and A. E. Mattson, *European Journal of Organic Chemistry*, 2014, **2014**, 2633–2646.

(24) P. Chauhan, S. Mahajan, U. Kaya, D. Hack and D. Enders, *Advanced Synthesis & Catalysis*, 2015, **357**, 253–281.

(25) J. Alemán, A. Parra, H. Jiang and K. A. Jørgensen, *Chemistry – A European Journal*, 2011, **17**, 6890–6899.

(26) G. R. Desiraju, P. S. Ho, L. Kloo, A. C. Legon, R. Marquardt, P. Metrangolo, P. Politzer, G. Resnati and K. Rissanen, *Pure and Applied Chemistry*, 2013, **85**, 1711–1713.

(27) P. Cardillo, E. Corradi, A. Lunghi, S. V. Meille, M. T. Messina, P. Metrangolo and G. Resnati, *Tetrahedron*, 2000, **56**, 5535–5550.

(28) P. Metrangolo, J. S. Murray, T. Pilati, P. Politzer, G. Resnati and G. Terraneo, *Crystal growth & design*, 2011, **11**, 4238–4246.

(29) M. Cametti, B. Crousse, P. Metrangolo, R. Milani and G. Resnati, *Chemical Society Reviews*, 2012, **41**, 31–42.

(30) M. S. Pavan, K. D. Prasad and T. G. Row, *Chemical Communications*, 2013, **49**, 7558–7560.

(31) J. J. Colin and H. Gaultier de Claubry, *Annales de Chimie*, 1814, **90**, 87–100.

(32) R. S. Mulliken, R. S. Mulliken and W. B. Person, *Molecular complexes: a lecture and reprint volume*, Wiley-Interscience, 1969.

(33) L. Turunen, J. H. Hansen and M. Erdélyi, *The Chemical Record*, 2021, **21**, 1252–1257.

(34) T. Clark, M. Hennemann, J. S. Murray and P. Politzer, *Journal of Molecular Modeling*, 2007, **13**, 291–296.

(35) O. Hassel, *Science*, 1970, **170**, 497–502.

(36) P. Politzer, J. S. Murray and T. Clark, *Physical Chemistry Chemical Physics*, 2013, **15**, 11178–11189.

(37) R. S. Mulliken, *Journal of the American Chemical Society*, 1950, **72**, 600–608.

(38) P. Politzer, J. S. Murray and T. Clark, *Physical Chemistry Chemical Physics*, 2010, **12**, 7748–7757.

(39) A. Vargas Jentzsch and S. Matile, *Journal of the American Chemical Society*, 2013, **135**, 5302–5303.

(40) A. V. Jentzsch, D. Emery, J. Mareda, S. K. Nayak, P. Metrangolo, G. Resnati, N. Sakai and S. Matile, *Nature Communications*, 2012, **3**, 905.

(41) A. Bruckmann, M. Pena and C. Bolm, *Synlett*, 2008, **2008**, 900–902.

(42) S. M. Walter, F. Kniep, E. Herdtweck and S. M. Huber, *Angewandte Chemie International Edition*, 2011, **50**, 7187–7191.

(43) T. T. Dang, F. Boeck and L. Hintermann, *The Journal of organic chemistry*, 2011, **76**, 9353–9361.

(44) F. Kniep, S. H. Jungbauer, Q. Zhang, S. M. Walter, S. Schindler, I. Schnapperelle, E. Herdtweck and S. M. Huber, *Angewandte Chemie International Edition*, 2013, **52**, 7028–7032.

(45) D. von der Heiden, S. Bozkus, M. Klussmann and M. Breugst, *The Journal of Organic Chemistry*, 2017, **82**, PMID: 28349682, 4037–4043.

(46) X. Li and G. Zou, *Chemical Communications*, 2015, **51**, 5089–5092.

(47) A. Dreger, P. Wonner, E. Engelage, S. M. Walter, R. Stoll and S. M. Huber, *Chemical Communications*, 2019, **55**, 8262–8265.

(48) J.-P. Gliese, S. H. Jungbauer and S. M. Huber, *Chemical Communications*, 2017, **53**, 12052–12055.

(49) S. H. Jungbauer, S. M. Walter, S. Schindler, L. Rout, F. Kniep and S. M. Huber, *Chemical Communications*, 2014, **50**, 6281–6284.

(50) S. H. Jungbauer and S. M. Huber, *Journal of the American Chemical Society*, 2015, **137**, PMID: 26329271, 12110–12120.

(51) W. He, Y.-C. Ge and C.-H. Tan, *Organic letters*, 2014, **16**, 3244–3247.

(52) R. A. Squitieri, K. P. Fitzpatrick, A. A. Jaworski and K. A. Scheidt, *Chemistry – A European Journal*, 2019, **25**, 10069–10073.

(53) A. Dreger, E. Engelage, B. Mallick, P. D. Beer and S. M. Huber, *Chemical Communications*, 2018, **54**, 4013–4016.

(54) M. Breugst, E. Detmar and D. von der Heiden, *ACS Catalysis*, 2016, **6**, 3203–3212.

(55) C. W. Kee and M. W. Wong, *The Journal of Organic Chemistry*, 2016, **81**, 7459–7470.

(56) A. S. Mahadevi and G. N. Sastry, *Chemical reviews*, 2016, **116**, 2775–2825.

(57) S.-i. Kawahara, K. Taira and T. Uchimaru, *Chemical physics*, 2003, **290**, 79–83.

(58) D. Bulfield and S. M. Huber, *Chemistry – A European Journal*, 2016, **22**, 14434–14450.

(59) P. Metrangolo, G. Resnati, T. Pilati and S. Biella, *Halogen bonding: fundamentals and applications*, 2008, 105–136.

(60) M. D. Perera and C. B. Aakeröy, *New Journal of Chemistry*, 2019, **43**, 8311–8314.

(61) E. Schrödinger, *Annalen der Physik*, 1926, **384**, 489–527.

(62) P. Hohenberg and W. Kohn, *Physical Review*, 1964, **136**, B864–B871.

(63) W. Kohn and L. J. Sham, *Physical Review*, 1965, **140**, A1133–A1138.

(64) A. D. Becke, *The Journal of Chemical Physics*, 1993, **98**, 1372–1377.

(65) Y. Zhao and D. G. Truhlar, *Theoretical Chemistry Accounts*, 2007, **120**, 215–241.

(66) J.-D. Chai and M. Head-Gordon, *The Journal of chemical physics*, 2008, **128**, 084106.

(67) S. Grimme, *Journal of computational chemistry*, 2004, **25**, 1463–1473.

(68) S. Grimme, *Journal of computational chemistry*, 2006, **27**, 1787–1799.

(69) N. Mardirossian and M. Head-Gordon, *Molecular Physics*, 2017, **115**, 2315–2372.

(70) T. H. Dunning Jr, *The Journal of chemical physics*, 1989, **90**, 1007–1023.

(71) P. C. Hariharan and J. A. Pople, *Theoretica Chimica Acta*, 1973, **28**, 213–222.

(72) M. J. Frisch, J. A. Pople and J. S. Binkley, *The Journal of Chemical Physics*, 1984, **80**, 3265–3269.

(73) J. P. Malerich, K. Hagihara and V. H. Rawal, *Journal of the American Chemical Society*, 2008, **130**, PMID: 18847268, 14416–14417.

(74) I. Rozas, I. Alkorta and J. Elguero, *The Journal of Physical Chemistry A*, 1998, **102**, 9925–9932.

(75) I. Alkorta and J. Elguero, *The Journal of Physical Chemistry*, 1996, **100**, 19367–19370.

(76) I. Alkorta, I. Rozas and J. Elguero, *Structural Chemistry*, 1998, **9**, 243–247.

(77) E. Espinosa, I. Alkorta, I. Rozas, J. Elguero and E. Molins, *Chemical Physics Letters*, 2001, **336**, 457–461.

(78) E. Espinosa, I. Alkorta, J. Elguero and E. Molins, *The Journal of Chemical Physics*, 2002, **117**, 5529–5542.

(79) P. Politzer, P. R. Laurence and K. Jayasuriya, *Environ Health Perspect*, 1985, **61**, 191–202.

(80) P. Politzer, J. S. Murray and Z. Peralta-Inga, *International Journal of Quantum Chemistry*, 2001, **85**, 676–684.

(81) T. Brinck, P. Jin, Y. Ma, J. S. Murray and P. Politzer, *Journal of Molecular Modeling*, 2003, **9**, 77–83.

(82) R. F. W. Bader, *Chemical Reviews*, 1991, **91**, 893–928.

(83) Y. Zhao and D. G. Truhlar, *Theoretical Chemistry Accounts*, 2008, **120**, 215–241.

(84) R. Ditchfield, W. J. Hehre and J. A. Pople, *The Journal of Chemical Physics*, 1971, **54**, 724–728.

(85) R. A. Gaussian09, *Inc., Wallingford CT*, 2009, **121**, 150–166.

(86) A. V. Marenich, C. J. Cramer and D. G. Truhlar, *The Journal of Physical Chemistry B*, 2009, **113**, PMID: 19366259, 6378–6396.

(87) R. F. W. Bader, M. T. Carroll, J. R. Cheeseman and C. Chang, *Journal of the American Chemical Society*, 1987, **109**, 7968–7979.

(88) T. Lu and F. Chen, *Journal of Computational Chemistry*, 2012, **33**, 580–592.

(89) Jmol development team, *Jmol*, version 14.6.4, 2016.

(90) T. A. Keith, *AIMAll, ATK Gristmill Software*, version 19.10.12, 2011.

(91) A. E. Reed, L. A. Curtiss and F. Weinhold, *Chemical Reviews*, 1988, **88**, 899–926.

(92) P. Su and H. Li, *The Journal of Chemical Physics*, 2009, **131**, 014102.

(93) M. W. Schmidt, K. K. Baldridge, J. A. Boatz, S. T. Elbert, M. S. Gordon, J. H. Jensen, S. Koseki, N. Matsunaga, K. A. Nguyen, S. Su, T. L. Windus, M. Dupuis and J. A. Montgomery Jr, *Journal of Computational Chemistry*, 1993, **14**, 1347–1363.

(94) J.-D. Chai and M. Head-Gordon, *Physical Chemistry Chemical Physics*, 2008, **10**, 6615–6620.

(95) R. F. W. Bader, *Accounts of Chemical Research*, 1985, **18**, 9–15.

(96) M. R. Garcia, I. Iribarren, I. Rozas and C. Trujillo, *Cover Profile: Simultaneous Hydrogen Bonds with Different Binding Modes: The Acceptor "Rules" but the Donor "Chooses"*, 2023.

(97) M. R. Garcia, I. Iribarren, I. Rozas and C. Trujillo, *Front Cover: Simultaneous Hydrogen Bonds with Different Binding Modes: The Acceptor "Rules" but the Donor "Chooses"*, 2023.

(98) M. R. Garcia, I. Iribarren, I. Rozas and C. Trujillo, *Chemistry–A European Journal*, 2023, **29**, e202203577.

(99) N. Melnyk, M. R. Garcia, I. Iribarren and C. Trujillo, *Tetrahedron Chem*, 2023, 100035.

(100) I. Iribarren, M. R. Garcia and C. Trujillo, *WIREs Computational Molecular Science*, 2022, **12**, e1616.

A Supporting information

The supporting information for the hydrogen bond binding mode section can be found in this link: `https://zenodo.org/record/7569240`.

ace-mono-def
Imaginary frequencies=0
SCF energy=-132.6146851
C 0 0 -1.176696
H 0 1.03419 -1.547733
H -0.895635 -0.517095 -1.547733
H 0.895635 -0.517095 -1.547733
C 0 0 0.277626
N 0 0 1.433946

benz-mono-def
Imaginary frequencies=0
SCF energy=-3075.4081875
C -1.316218 -0.95361 1.021969
C -2.448599 -1.683532 1.376991
C -3.505299 -1.826266 0.475116
C -3.422467 -1.233532 -0.784239
C -2.290143 -0.499952 -1.138111
C -1.227469 -0.351787 -0.239637
H -0.495235 -0.854448 1.736016
H -2.505553 -2.147561 2.364426
H -4.391448 -2.401086 0.754736
H -4.241833 -1.342813 -1.49866
H -2.229357 -0.035636 -2.126123
C -0.017969 0.45139 -0.660925
H -0.069983 0.616426 -1.743208
C 1.31107 -0.192341 -0.330185
C 1.977477 -0.018942 0.887323
C 1.858532 -1.060949 -1.283497
C 3.164765 -0.703142 1.147113
H 1.576159 0.667074 1.636362
C 3.04441 -1.746173 -1.02333
H 1.347759 -1.202325 -2.239968
C 3.701323 -1.569561 0.194675
H 3.674638 -0.553782 2.101752
H 3.457842 -2.418384 -1.778965
H 4.633939 -2.100908 0.398457
Br -0.163811 2.288681 0.072445

catA-mono-def
Imaginary frequencies=0
SCF energy=-1355.4008678

C -0.008486 1.485655 -0.233605
C 1.187362 1.761884 0.420654
C 1.211853 2.312491 1.699499
C 0.007818 2.589608 2.342425
C -1.204249 2.308402 1.716487
C -1.196254 1.757899 0.437473
H -0.014415 1.062744 -1.239314
H 2.168167 2.514884 2.184847
H 0.01416 3.020225 3.344731
H -2.154333 2.508016 2.215056
N 2.426343 1.479281 -0.243868
C 3.236412 2.427209 -0.835281
C 2.996511 0.267722 -0.383901
C 4.308482 1.76608 -1.342598
H 2.969855 3.48036 -0.842206
H 5.177167 2.127431 -1.886178
N -2.443525 1.475155 -0.211148
C -3.002278 0.26093 -0.373793
C -3.27216 2.428006 -0.768038
C -4.34277 1.767431 -1.278935
H -3.017157 3.483939 -0.752166
H -5.221868 2.132052 -1.803231
C 5.076691 -0.626668 -1.426871
H 4.577319 -1.34677 -2.087532
H 5.917598 -0.164169 -1.953498
H 5.440798 -1.134126 -0.524578
C -5.084496 -0.630985 -1.414955
H -5.920244 -0.168027 -1.949437
H -4.575261 -1.346003 -2.073457
H -5.457584 -1.144148 -0.519486
N 4.141922 0.428667 -1.054402
N -4.157194 0.425374 -1.026974
I 2.24776 -1.509879 0.343107
I -2.231979 -1.52672 0.303871

catA-int1
Imaginary frequencies=0
SCF energy=-4563.4262953
C -2.305797 1.575417 -1.010229
C -2.07121 2.910099 -0.689591
C -3.032296 3.682771 -0.040718
C -4.252409 3.107599 0.303694
C -4.498742 1.766892 0.021249
C -3.521893 1.015764 -0.628922
H -1.553478 0.980564 -1.529069
H -2.818115 4.726468 0.19644
H -5.01047 3.704618 0.812842

H -5.441345 1.296525 0.306606
N -0.816924 3.519771 -1.022696
C -0.668472 4.548551 -1.933025
C 0.375584 3.262759 -0.447283
C 0.639639 4.909927 -1.90622
H -1.507316 4.922594 -2.51342
H 1.18166 5.66938 -2.463103
N -3.793441 -0.366312 -0.90202
C -3.325887 -1.421189 -0.203351
C -4.667584 -0.814403 -1.872992
C -4.720454 -2.165416 -1.757674
H -5.167227 -0.128676 -2.551469
H -5.279432 -2.908452 -2.319785
C 2.680848 4.173923 -0.635027
H 2.791504 4.418508 0.429068
H 3.163009 3.211293 -0.845927
H 3.142386 4.958141 -1.24363
C -3.717412 -3.886999 -0.240982
H -4.482333 -4.105781 0.515758
H -3.828796 -4.571118 -1.089363
H -2.720332 -4.005019 0.196998
N 1.267747 4.103131 -0.981281
N -3.88304 -2.521814 -0.720781
I 0.745315 1.773043 0.981396
I -1.840633 -1.305702 1.267411
C 2.258298 -1.841726 -0.066367
H 2.43368 -2.516191 0.776839
Br 0.90588 -0.819732 2.840171
C 3.226169 -0.813345 -0.246236
C 4.046981 -0.481468 0.860475
C 3.445004 -0.162308 -1.485858
C 5.003915 0.513281 0.749044
H 3.883654 -0.990485 1.812139
C 4.42317 0.812981 -1.593833
H 2.89308 -0.468746 -2.374554
C 5.189688 1.160644 -0.476847
H 5.616565 0.783696 1.610698
H 4.603488 1.299024 -2.554062
H 5.954993 1.934883 -0.56778
C 1.134049 -2.15421 -0.877039
C 0.609741 -3.46783 -0.778927
C 0.501794 -1.222749 -1.740071
C -0.450243 -3.859739 -1.579847
H 1.074859 -4.175834 -0.089795
C -0.58125 -1.615103 -2.510079
H 0.828371 -0.182735 -1.757765
C -1.043922 -2.934015 -2.44372

H -0.832338 -4.880103 -1.523246
H -1.079845 -0.893753 -3.159917
H -1.894784 -3.237492 -3.058638
N 4.04424 -4.242042 -1.132243
C 4.926455 -3.527357 -1.353437
C 6.022917 -2.61178 -1.621526
H 5.880288 -2.139221 -2.602912
H 6.049092 -1.835544 -0.842979
H 6.975117 -3.159933 -1.61757

catA-prod
Imaginary frequencies=0
SCF energy=-4563.4545667
C 1.953135 1.697947 0.523322
C 1.648972 2.994618 0.123806
C 2.591276 3.794496 -0.517516
C 3.862163 3.278115 -0.764787
C 4.185341 1.976728 -0.38485
C 3.223194 1.200234 0.256093
H 1.212557 1.087162 1.036099
H 2.329795 4.810222 -0.819313
H 4.607757 3.895316 -1.26841
H 5.175801 1.562917 -0.5819
N 0.347637 3.51716 0.418643
C 0.101517 4.514751 1.341803
C -0.823295 3.085612 -0.090462
C -1.245289 4.677164 1.393027
H 0.907722 5.004102 1.881028
H -1.861583 5.346841 1.986386
N 3.54845 -0.125532 0.692471
C 3.027988 -1.276416 0.223154
C 4.421142 -0.409367 1.724919
C 4.416503 -1.757628 1.88194
H 4.95311 0.376871 2.253239
H 4.954064 -2.396788 2.576853
C -3.226817 3.613586 0.264056
H -3.521733 2.582361 0.500579
H -3.767488 4.308988 0.914259
H -3.456581 3.834486 -0.786073
C 3.221027 -3.687561 0.800932
H 3.883856 -4.261777 1.456699
H 2.175981 -3.858519 1.093549
H 3.372853 -3.999108 -0.239816
N -1.79905 3.780668 0.503668
N 3.546165 -2.275126 0.946089
I -1.058369 1.537015 -1.482661
I 1.573553 -1.438716 -1.276857

C -1.575827 -1.524165 0.863789
H -1.322906 -1.159577 -0.147461
Br -1.060429 -1.224495 -3.07792
C -3.087237 -1.47269 1.021415
C -3.879017 -1.17657 -0.089965
C -3.683747 -1.719255 2.261972
C -5.266803 -1.109471 0.043512
H -3.406637 -1.005463 -1.061915
C -5.069092 -1.65811 2.389888
H -3.062853 -1.95268 3.131022
C -5.861351 -1.347684 1.281733
H -5.883366 -0.870478 -0.825933
H -5.534333 -1.847841 3.35971
H -6.947323 -1.292006 1.386919
C -0.787104 -0.722449 1.892427
C 0.391236 -1.198506 2.473365
C -1.239959 0.562218 2.217857
C 1.101254 -0.404949 3.376778
H 0.772915 -2.193119 2.233024
C -0.527414 1.353387 3.116316
H -2.158153 0.948063 1.769381
C 0.645128 0.871258 3.70119
H 2.01804 -0.793562 3.825339
H -0.89189 2.354707 3.356402
H 1.203892 1.492372 4.404453
C -0.833329 -3.993737 0.775306
C -0.422145 -5.366771 0.68455
H 0.026302 -5.665608 1.64238
H -1.306734 -5.983758 0.469764
H 0.311687 -5.458736 -0.12903
N -1.149373 -2.895263 0.846418

catA-ts1
Imaginary frequencies=1
SCF energy=-4563.4252927
C 1.346211 2.217739 0.983632
C 0.575588 3.347715 0.720047
C 1.123496 4.480408 0.121485
C 2.470863 4.484872 -0.228936
C 3.255662 3.35831 -0.000391
C 2.683402 2.237456 0.597287
H 0.913512 1.336423 1.4597
H 0.491675 5.348909 -0.072697
H 2.908516 5.367428 -0.697578
H 4.308266 3.33875 -0.288362
N -0.814159 3.371406 1.074496
C -1.350457 4.187917 2.051349

C -1.81139 2.693482 0.47075
C -2.69318 3.989775 2.035132
H -0.723925 4.829175 2.664996
H -3.486238 4.424956 2.637006
N 3.510248 1.084369 0.810579
C 3.547243 -0.020347 0.039128
C 4.478172 0.984214 1.790284
C 5.10214 -0.206967 1.604014
H 4.629649 1.770254 2.524669
H 5.917336 -0.677637 2.146547
C -4.286301 2.575382 0.700014
H -5.017795 3.11547 1.309562
H -4.480443 2.763692 -0.36335
H -4.354675 1.499758 0.90624
C 4.929708 -2.092925 -0.044011
H 5.534982 -2.613955 0.705138
H 4.046337 -2.695311 -0.286858
H 5.52405 -1.922225 -0.951199
N -2.958178 3.062605 1.050006
N 4.511723 -0.81463 0.516285
I -1.57059 1.262604 -1.029755
I 2.197201 -0.469003 -1.473515
C -1.466881 -2.750348 -0.522397
H -1.411298 -3.499787 -1.314777
Br -0.71001 -1.26575 -2.869075
C -2.779281 -2.222977 -0.263901
C -3.74199 -2.291402 -1.299074
C -3.170506 -1.710123 0.993571
C -5.024489 -1.80761 -1.10263
H -3.449182 -2.69587 -2.270003
C -4.465186 -1.248469 1.190305
H -2.482679 -1.718266 1.837385
C -5.386135 -1.279455 0.14192
H -5.753403 -1.844288 -1.914207
H -4.758916 -0.869189 2.170849
H -6.39972 -0.903009 0.297912
C -0.300908 -2.655748 0.310598
C 0.644914 -3.702768 0.213232
C -0.048179 -1.591466 1.206731
C 1.759746 -3.724439 1.038526
H 0.476898 -4.508286 -0.50521
C 1.082128 -1.608402 2.012079
H -0.717161 -0.731655 1.240811
C 1.975857 -2.67977 1.941963
H 2.471565 -4.5493 0.974293
H 1.272344 -0.779951 2.697189
H 2.860608 -2.691126 2.583079

C -1.33871 -2.638641 4.199269
C -0.78145 -3.959362 3.960778
H -1.460219 -4.725793 4.359715
H -0.655976 -4.112702 2.879306
H 0.195908 -4.046983 4.454482
N -1.784001 -1.584516 4.368892

catA-ts2
Imaginary frequencies=1
SCF energy=-4563.4193747
C 1.936837 -1.612968 -0.793851
C 1.515521 -2.919998 -0.576476
C 2.390978 -3.89373 -0.104402
C 3.714546 -3.543332 0.157627
C 4.155202 -2.236021 -0.040797
C 3.257786 -1.282258 -0.515498
H 1.243569 -0.86555 -1.172509
H 2.03629 -4.913066 0.057289
H 4.41053 -4.296766 0.529654
H 5.188659 -1.955716 0.169893
N 0.154763 -3.256618 -0.875342
C -0.247001 -4.033362 -1.944834
C -0.933382 -2.816319 -0.213389
C -1.604805 -4.049975 -1.927247
H 0.470097 -4.488736 -2.622068
H -2.319932 -4.533372 -2.587067
N 3.705304 0.055777 -0.767456
C 3.292771 1.177498 -0.142225
C 4.6206 0.39198 -1.746343
C 4.754944 1.74212 -1.710047
H 5.08068 -0.360881 -2.38025
H 5.366385 2.413314 -2.306694
C -3.395612 -3.026673 -0.485154
H -3.553965 -1.945319 -0.380361
H -4.038653 -3.415071 -1.281654
H -3.632484 -3.530047 0.461149
C 3.756175 3.611222 -0.356793
H 4.429244 4.206392 -0.982576
H 2.717813 3.917654 -0.538441
H 4.008418 3.759099 0.700769
N -2.009622 -3.28679 -0.852396
N 3.923897 2.208721 -0.714165
I -0.919548 -1.508322 1.421341
I 1.867619 1.271629 1.395217
C -1.818822 1.44259 -0.747535
H -1.326415 1.838008 0.146484
Br -0.618852 0.991068 3.362615

C -3.184378 1.010306 -0.561268
C -3.66286 0.903877 0.759705
C -4.038183 0.701567 -1.640224
C -4.945206 0.42513 0.997267
H -3.005 1.167581 1.593792
C -5.325893 0.248319 -1.394532
H -3.700855 0.853304 -2.66696
C -5.772511 0.094851 -0.077865
H -5.30614 0.316242 2.021629
H -5.990759 0.015869 -2.22836
H -6.783889 -0.273132 0.109598
C -0.922297 0.987769 -1.802375
C 0.287717 1.680453 -2.013462
C -1.185876 -0.175877 -2.549625
C 1.184955 1.248602 -2.979039
H 0.499817 2.578927 -1.430252
C -0.272337 -0.61414 -3.505153
H -2.082663 -0.765677 -2.357866
C 0.903302 0.10121 -3.729311
H 2.114757 1.797306 -3.143927
H -0.479349 -1.524659 -4.070347
H 1.616534 -0.244528 -4.480671
C -2.495834 4.507367 -1.641942
C -2.941881 5.82573 -2.042946
H -2.390918 6.585238 -1.471556
H -2.753236 5.962626 -3.116494
H -4.017612 5.92238 -1.841754
N -2.136571 3.458952 -1.323953

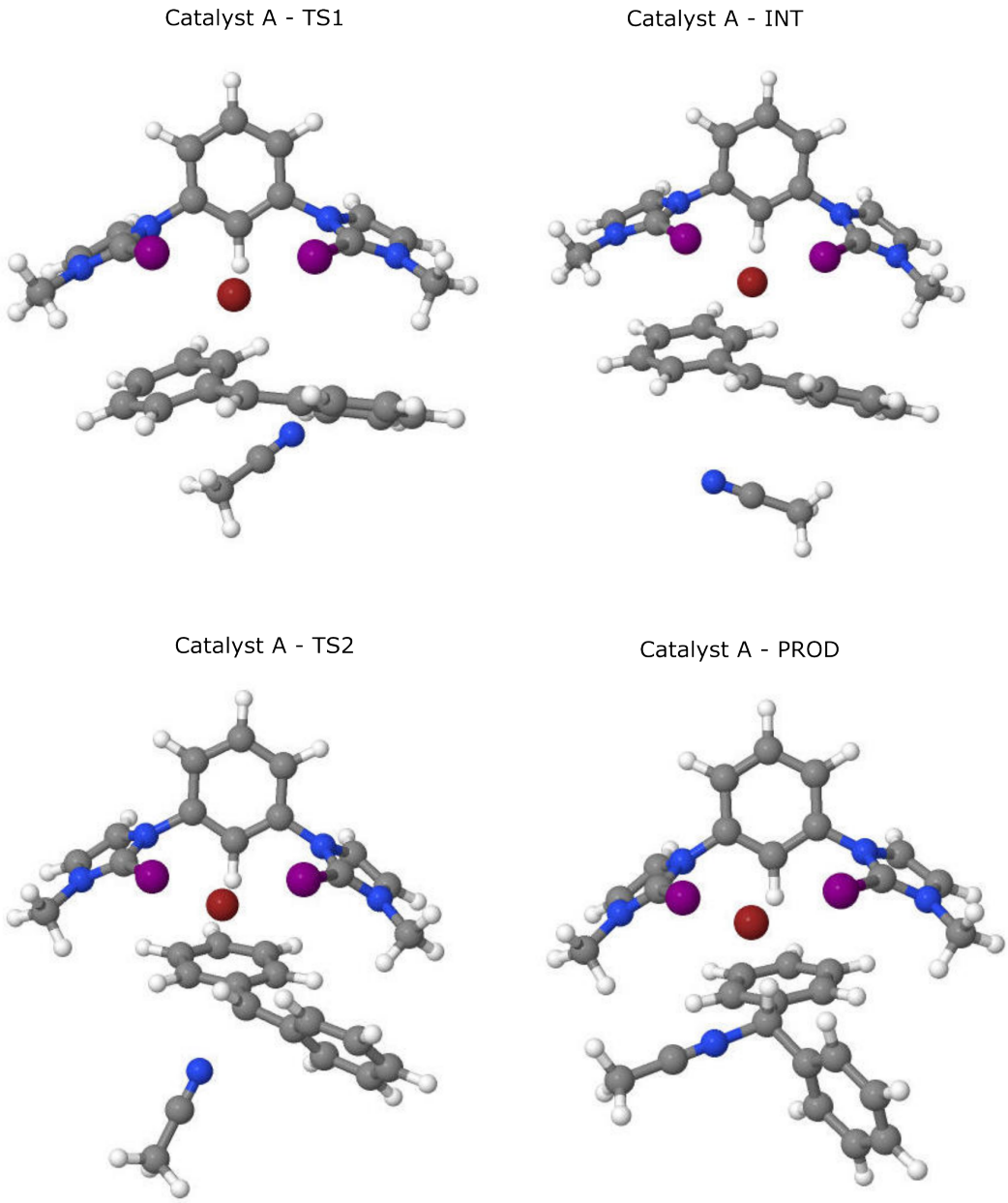

Figure A.1: Halide abstraction: catalyst A, cat-complex structures.

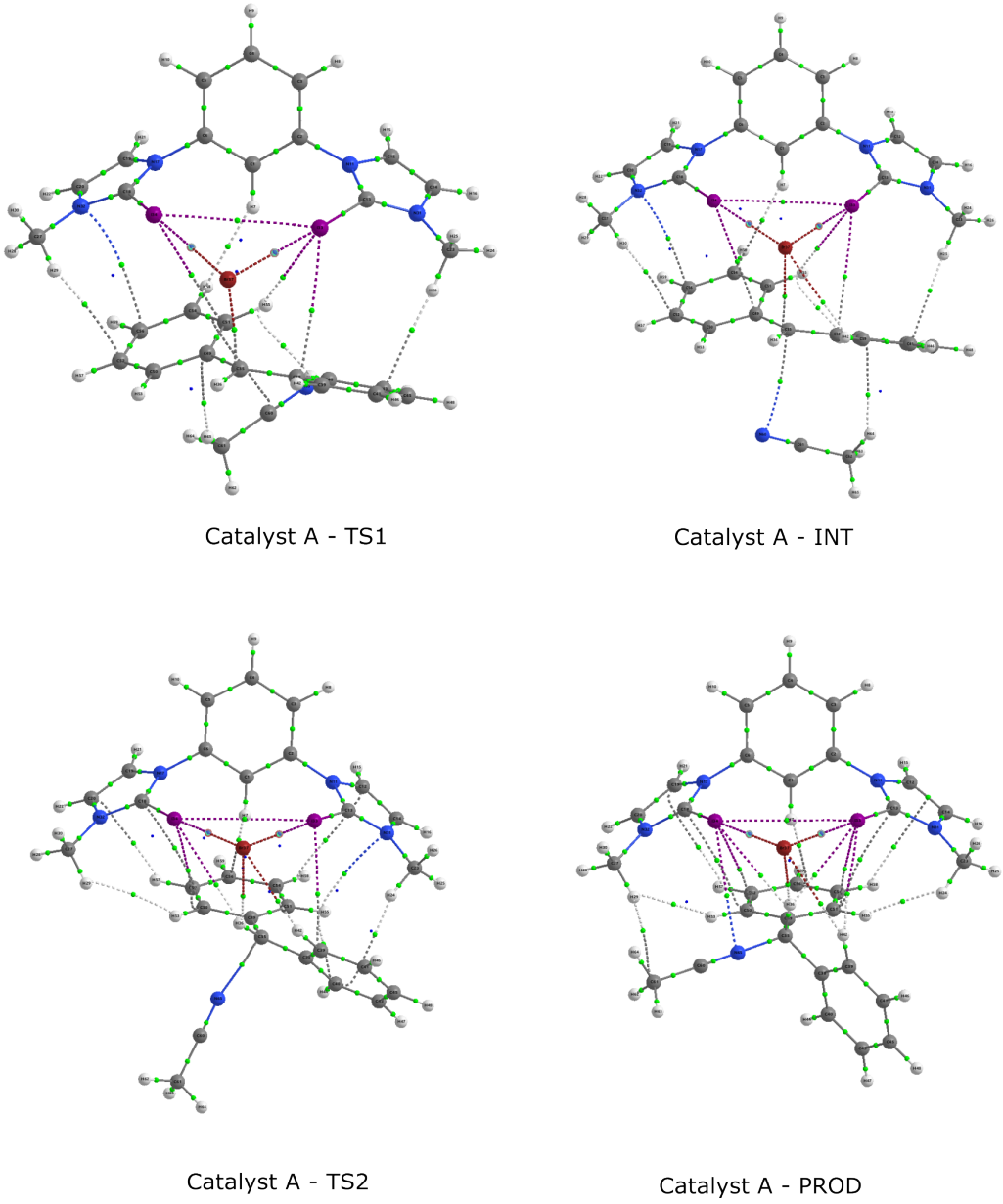

Figure A.2: Halide abstraction: catalyst A, QTAIM molecular graphs of the cat-complex structures showing the I–O electron density at BCP.

Table A.1: The ρ(BCP) and $\nabla^2\rho$ values of all the cat-complex A structures, calculated at the ωb97xD/def2SVP computational level (solvent = acetonitrile, SMD model and T = 273K).

Cat-complex A	**ρ(BCP) (a.u.)**	**$\nabla^2\rho$ (a.u.)**
TS1	0.017	0.042
	0.020	0.047
INT	0.021	0.049
	0.022	0.049
TS2	0.022	0.050
	0.023	0.050
PROD	0.022	0.049
	0.022	0.050

Table A.2: The ρ(BCP) (a.u.) and the $\nabla^2\rho$ (a.u.) calculated for the TS1 structure of catalyst A.

Atoms	**ρ(BCP) (a.u.)**	**$\nabla^2\rho$ (a.u.)**
H26 - C43	0.006	0.018
I33 - C38	0.006	0.015
H44 - H55	0.012	0.052
C51 - C60	0.005	0.015
C49 - H63	0.005	0.016
H44 - N65	0.008	0.022
I33 - H55	0.007	0.020
C35 - Br37	0.023	0.049
H7 - H58	0.004	0.016
I34 - C51	0.007	0.019
N32 - C56	0.005	0.013
H29 - C52	0.006	0.017
I33 - Br37	0.020	0.047
I34 - Br37	0.017	0.042
I33 - I34	0.005	0.014
I33 - C38	0.006	0.015
I33 - H55	0.007	0.020

Table A.3: The ρ(BCP) (a.u.) and the $\nabla^2\rho$ (a.u.) calculated for the INT structure of catalyst A.

Atoms	**ρ(BCP) (a.u.)**	**$\nabla^2\rho$ (a.u.)**
C35 - N60	0.006	0.020
C39 - H64	0.005	0.016
H30 - C52	0.005	0.018
N32 - C56	0.005	0.016
I34 - C49	0.006	0.017
H7 - C54	0.004	0.016
C35 - Br37	0.010	0.028
H44 - H55	0.011	0.049
I33 - H55	0.005	0.015
Br37 - H42	0.006	0.020
I33 - C38	0.006	0.014
H25 - C43	0.006	0.017
I34 - Br37	0.021	0.049
I33 - Br37	0.022	0.049
I33 - I34	0.007	0.018

Table A.4: The ρ(BCP) (a.u.) and the $\nabla^2\rho$ (a.u.) calculated for the TS2 structure of catalyst A.

Atoms	**ρ(BCP) (a.u.)**	**$\nabla^2\rho$ (a.u.)**
C35 - N65	0.050	0.114
H24 - C40	0.005	0.016
I33 - C39	0.006	0.017
C40 - H55	0.011	0.045
Br37 - H42	0.008	0.019
H36 - Br37	0.004	0.011
I34 - H36	0.004	0.011
H29 - H53	0.002	0.009
C20 - H57	0.004	0.014
C18 - C50	0.004	0.012
I34 - C50	0.006	0.017
H7 - C56	0.007	0.025
C12 - H58	0.003	0.009
N31 - H55	0.005	0.016
I33 - Br37	0.023	0.050
I34 - Br37	0.022	0.050
I33 - I34	0.008	0.021

Table A.5: The ρ(BCP) (a.u.) and the $\nabla^2\rho$ (a.u.) calculated for the PROD structure of catalyst A.

Atoms	**ρ(BCP) (a.u.)**	**$\nabla^2\rho$ (a.u.)**
H29 - C61	0.003	0.013
I34 - N65	0.005	0.015
Br37 - H42	0.007	0.016
I33 - H42	0.004	0.012
H36 - Br37	0.009	0.021
I33 - H36	0.008	0.024
I34 - H36	0.007	0.023
C19 - H57	0.004	0.011
H29 - H53	0.004	0.016
C18 - C50	0.005	0.014
I34 - C50	0.005	0.012
H7 - C56	0.008	0.026
H24 - H55	0.004	0.015
C14 - H58	0.005	0.013
C13 - C51	0.005	0.015
I33 - C51	0.005	0.015
I33 - Br37	0.022	0.050
I34 - Br37	0.022	0.049
I33 - I34	0.007	0.020

Table A.6: The ρ(BCP) (a.u.) and the $\nabla^2\rho$ (a.u.) calculated for the PROD structure of catalyst A.

Atoms	**ρ(BCP) (a.u.)**	**$\nabla^2\rho$ (a.u.)**

Table A.7: Perturbation energies E(2) of the LP_{Br} to σ^*_{C-I} in the cat-complex A structures, calculated at the ωb97xD/def2SVP computational level (solvent = acetonitrile, SMD model and T = 273K).

Cat-complex A	**Orb(1)**	**Orb(2)**	**Total E(2)(kJ/mol)**
TS1	LP_{Br37}	$\sigma^*_{C_{13}-I_{33}}$	76.94
	LP_{Br37}	$\sigma^*_{C_{13}-I_{34}}$	58.74
INT	LP_{Br37}	$\sigma^*_{C_{13}-I_{33}}$	104.89
	LP_{Br37}	$\sigma^*_{C_{13}-I_{34}}$	89.24
TS2	LP_{Br37}	$\sigma^*_{C_{13}-I_{33}}$	97.49
	LP_{Br37}	$\sigma^*_{C_{13}-I_{34}}$	98.66
PROD	LP_{Br37}	$\sigma^*_{C_{13}-I_{33}}$	94.64
	LP_{Br37}	$\sigma^*_{C_{13}-I_{34}}$	93.51

catB-mono-def
Imaginary frequencies=0
SCF energy=-1630.4464212
C -5.762913 -1.586972 -2.040214
H -6.56464 -0.871437 -2.293365
H -5.790469 -2.37781 -2.805844
C -4.415114 -0.871675 -2.084745
H -4.251501 -0.407197 -3.070036
H -3.598586 -1.598877 -1.933192
C -4.305216 0.212893 -1.008456
H -5.086563 0.980209 -1.187822
C -4.564126 -0.385211 0.392883
H -3.78137 -1.140922 0.585435
C -5.923151 -1.094454 0.421699
H -6.07246 -1.528267 1.423183
H -6.714112 -0.337932 0.278839
C -6.027188 -2.171425 -0.654401
H -7.021431 -2.643228 -0.616401
H -5.290275 -2.967481 -0.448402
N -2.983174 0.795979 -1.041974
N -4.592115 0.680255 1.374013
C -3.732147 0.828429 2.297814
H -3.930994 1.642841 3.014736
C -2.852549 2.035669 -1.273935
H -3.724558 2.683607 -1.484529
C -2.485683 0.070461 2.610018
C -2.148423 -0.130289 3.956949
C -1.606141 -0.375862 1.620391
C -0.974197 -0.797215 4.301551
H -2.815808 0.238381 4.740548
C -0.412327 -1.028846 1.961805
H -1.83245 -0.187029 0.569495
C -0.101536 -1.246965 3.313016
H -0.730232 -0.958745 5.353676
H 0.825494 -1.757078 3.582209
C -1.538733 2.714578 -1.249725
C -1.466015 4.082471 -1.53923
C -0.372506 2.024121 -0.89946
C -0.244763 4.753064 -1.477074
H -2.376115 4.624577 -1.809674
C 0.85119 2.698024 -0.808086
H -0.420119 0.955942 -0.682275
C 0.910145 4.071954 -1.107114
H -0.194463 5.819484 -1.706414
H 1.864349 4.598111 -1.038342
C 0.463766 -1.450503 0.903886
C 2.026981 1.995969 -0.372468

C 1.156376 -1.778603 -0.039745
C 3.008096 1.407306 0.037511
I 2.25298 -2.305651 -1.630077
I 4.60797 0.438438 0.755108

catB-int
Imaginary frequencies=0
SCF energy=-4838.4675945
C -5.871316 3.303378 -1.592215
H -6.423846 3.922151 -0.863681
H -5.586053 3.970097 -2.42093
C -4.618209 2.738948 -0.927808
H -3.995605 3.550354 -0.518382
H -4.001937 2.206524 -1.672824
C -4.958071 1.76366 0.202431
H -5.534412 2.299981 0.984371
C -5.861191 0.622284 -0.321144
H -5.299869 0.078079 -1.10182
C -7.121219 1.209879 -0.967758
H -7.743907 0.382177 -1.342424
H -7.706847 1.723505 -0.185828
C -6.781485 2.183464 -2.092771
H -7.707055 2.601186 -2.518884
H -6.274992 1.63861 -2.908807
N -3.741662 1.20395 0.745372
N -6.271594 -0.217206 0.78577
C -5.922655 -1.430827 0.931805
H -6.37793 -1.962522 1.784328
C -3.538401 1.263248 1.99593
H -4.247463 1.77079 2.676987
C -5.003691 -2.28947 0.129493
C -5.335677 -3.641148 -0.047497
C -3.791589 -1.81865 -0.382034
C -4.488887 -4.489524 -0.758475
H -6.26675 -4.028828 0.374668
C -2.924169 -2.673057 -1.080086
H -3.498455 -0.780798 -0.214177
C -3.285013 -4.015078 -1.275572
H -4.762743 -5.536928 -0.902165
H -2.616858 -4.683185 -1.82269
C -2.358178 0.649791 2.638771
C -2.17338 0.806767 4.017316
C -1.428683 -0.088981 1.897604
C -1.071009 0.235689 4.651643
H -2.899322 1.384719 4.595132
C -0.330615 -0.679813 2.53244
H -1.561696 -0.206877 0.820918

C -0.152481 -0.50733 3.918588
H -0.928671 0.367796 5.726057
H 0.706581 -0.966939 4.41157
C -1.683122 -2.135491 -1.566224
C 0.612492 -1.464428 1.787421
C -0.656296 -1.598173 -1.940964
C 1.439015 -2.134196 1.200116
I 1.004266 -0.533582 -2.473379
I 2.852145 -3.216051 0.28634
Br 3.492008 1.347313 -3.006007
C 2.592556 1.432814 0.568709
C 3.576119 0.694199 1.27446
C 3.445932 0.23624 2.61149
C 4.749083 0.366823 0.543592
C 4.46938 -0.485742 3.196972
H 2.521374 0.399889 3.162902
C 5.780003 -0.332692 1.15026
H 4.824072 0.684335 -0.501342
C 5.638823 -0.756783 2.473797
H 4.36052 -0.856141 4.217663
H 6.688422 -0.566986 0.592831
H 6.44355 -1.323785 2.947731
C 1.441686 2.13665 1.010395
C 1.186996 2.521872 2.35279
C 0.514625 2.512053 0.00237
C 0.031017 3.214021 2.665437
H 1.923768 2.331741 3.13196
C -0.654699 3.177316 0.330216
H 0.728982 2.254306 -1.03696
C -0.895576 3.523931 1.661767
H -0.156463 3.522983 3.69488
H -1.375556 3.437901 -0.445925
H -1.812002 4.058968 1.922001
H 2.761388 1.467689 -0.520281
C 3.878824 4.358419 -0.164182
N 4.516469 4.045421 0.749225
C 3.066024 4.720692 -1.312318
H 2.036623 4.925287 -0.985992
H 3.479653 5.618243 -1.792732
H 3.069183 3.880618 -2.028022

catB-prod
Imaginary frequencies=0
SCF energy=-4838.4895014
C -5.892195 3.164904 -2.342687
H -6.515402 3.848075 -1.739458
H -5.574495 3.728282 -3.233922

C -4.668523 2.748748 -1.530135
H -4.102225 3.633183 -1.197521
H -3.987379 2.147209 -2.156652
C -5.05228 1.919321 -0.30045
H -5.693416 2.534509 0.364021
C -5.879826 0.684278 -0.71945
H -5.247822 0.063526 -1.379362
C -7.11096 1.123179 -1.52071
H -7.676927 0.225781 -1.816852
H -7.767162 1.713346 -0.857869
C -6.724729 1.949084 -2.744612
H -7.631017 2.263739 -3.285265
H -6.141088 1.321193 -3.440314
N -3.852711 1.490613 0.383
N -6.335931 -0.014663 0.463948
C -5.957943 -1.182052 0.794513
H -6.449279 -1.612397 1.683385
C -3.664858 1.837471 1.588683
H -4.382695 2.484679 2.127269
C -4.963947 -2.108898 0.178783
C -5.238767 -3.48439 0.2092
C -3.741599 -1.674651 -0.343156
C -4.323549 -4.400652 -0.305038
H -6.178619 -3.837936 0.641716
C -2.803232 -2.594133 -0.836473
H -3.49587 -0.611264 -0.330771
C -3.106634 -3.96506 -0.824408
H -4.552419 -5.468388 -0.286133
H -2.380163 -4.684332 -1.208135
C -2.472229 1.418115 2.354926
C -2.177287 2.044759 3.570689
C -1.625155 0.412658 1.878622
C -1.043261 1.677564 4.295042
H -2.838772 2.829478 3.946958
C -0.502573 0.017957 2.615095
H -1.841056 -0.073795 0.927579
C -0.210141 0.665218 3.829163
H -0.813333 2.176899 5.238507
H 0.666939 0.363061 4.403857
C -1.537767 -2.113969 -1.320586
C 0.309385 -1.064747 2.132638
C -0.467288 -1.674787 -1.701542
C 0.941144 -2.014304 1.712171
I 1.340028 -0.904497 -2.276155
I 1.89137 -3.642251 1.034817
Br 4.146724 0.359866 -2.983724
C 2.8581 1.956451 0.142354

C 3.32419 1.0475 1.275784
C 3.037663 1.313165 2.615114
C 4.065967 -0.090453 0.934123
C 3.491561 0.443409 3.608586
H 2.451855 2.191699 2.891679
C 4.522909 -0.950479 1.9289
H 4.28209 -0.292629 -0.120923
C 4.232585 -0.686869 3.269199
H 3.261344 0.653033 4.655678
H 5.098966 -1.837681 1.656443
H 4.583103 -1.366958 4.048983
C 1.753319 2.938369 0.464041
C 2.012681 4.152698 1.107215
C 0.441415 2.600005 0.125031
C 0.963634 5.018393 1.411914
H 3.038 4.424236 1.37305
C -0.605095 3.470781 0.424381
H 0.239234 1.65144 -0.3793
C -0.34696 4.678643 1.071445
H 1.171381 5.965093 1.915708
H -1.625309 3.19907 0.146521
H -1.167595 5.359965 1.307772
H 2.537589 1.315967 -0.69634
C 4.905664 3.007017 -1.00415
N 3.99952 2.637916 -0.408451
C 6.041495 3.472374 -1.750538
H 6.954916 3.287973 -1.167835
H 6.066432 2.90281 -2.691479
H 5.925132 4.546677 -1.951258

catB-ts2
Imaginary frequencies=1
SCF energy=-4838.4574552
C 5.741728 3.330751 1.897982
H 6.317576 3.976839 1.212488
H 5.441736 3.961462 2.749468
C 4.499537 2.811288 1.177844
H 3.899426 3.649014 0.789137
H 3.857374 2.255773 1.883023
C 4.855021 1.880778 0.014157
H 5.448076 2.446491 -0.733958
C 5.738007 0.712562 0.510559
H 5.154463 0.145936 1.258092
C 6.98965 1.258993 1.206439
H 7.598014 0.409725 1.555613
H 7.595625 1.803964 0.462149
C 6.631095 2.181426 2.367872

H 7.549084 2.572048 2.834112
H 6.101766 1.603075 3.145299
N 3.647625 1.34585 -0.572777
N 6.162314 -0.092644 -0.616526
C 5.814432 -1.301762 -0.798186
H 6.280159 -1.813137 -1.65748
C 3.423995 1.522012 -1.808499
H 4.108111 2.115003 -2.444613
C 4.880182 -2.176426 -0.030899
C 5.208199 -3.530654 0.132271
C 3.654675 -1.714459 0.455952
C 4.341858 -4.391023 0.804551
H 6.15062 -3.911375 -0.27068
C 2.766999 -2.58092 1.112325
H 3.368438 -0.673001 0.298127
C 3.12279 -3.926181 1.294363
H 4.61212 -5.440719 0.938089
H 2.438268 -4.604704 1.807406
C 2.263817 0.921152 -2.500382
C 2.08121 1.162533 -3.867038
C 1.374095 0.07544 -1.827414
C 1.031866 0.556609 -4.557176
H 2.772717 1.825228 -4.393952
C 0.340178 -0.563236 -2.522361
H 1.500705 -0.106865 -0.759255
C 0.170624 -0.312934 -3.896724
H 0.893978 0.750379 -5.622845
H -0.636717 -0.809423 -4.438391
C 1.507994 -2.05385 1.562673
C -0.511642 -1.500555 -1.845071
C 0.461669 -1.526764 1.895753
C -1.207998 -2.323402 -1.283805
I -1.246781 -0.498745 2.346081
I -2.299951 -3.71903 -0.352021
Br -3.806135 1.297549 2.817698
C -2.522446 1.853442 -0.649628
C -3.213026 0.878966 -1.470211
C -2.941764 0.647828 -2.832738
C -4.168637 0.074975 -0.811606
C -3.619727 -0.353118 -3.516372
H -2.179839 1.222402 -3.356027
C -4.844481 -0.92078 -1.502033
H -4.362586 0.248932 0.252521
C -4.570045 -1.134553 -2.855242
H -3.399031 -0.53465 -4.569964
H -5.578625 -1.542247 -0.985789
H -5.093791 -1.925339 -3.397527

C -1.333951 2.624987 -0.979135
C -1.096151 3.231712 -2.226764
C -0.379228 2.761658 0.045663
C 0.092074 3.914217 -2.449476
H -1.860041 3.21281 -3.004463
C 0.817368 3.429176 -0.190102
H -0.576182 2.321313 1.025625
C 1.055125 3.999946 -1.439038
H 0.269791 4.390281 -3.415778
H 1.562601 3.50645 0.603037
H 1.993273 4.527614 -1.626393
H -2.667575 1.691333 0.427169
C -4.681727 3.766079 0.344873
N -3.951522 3.346194 -0.44677
C -5.594413 4.286593 1.338725
H -5.406512 5.358037 1.491734
H -6.630118 4.132004 1.006734
H -5.414036 3.732399 2.272591

catB-ts1
Imaginary frequencies=1
SCF energy=-4705.8427887
C -5.855052 3.496951 -0.727546
H -6.487922 3.8813 0.091391
H -5.593924 4.360852 -1.358525
C -4.586154 2.884582 -0.140131
H -4.044872 3.619432 0.4766
H -3.905126 2.583112 -0.954593
C -4.89048 1.649408 0.714256
H -5.544366 1.947241 1.55937
C -5.657267 0.603257 -0.121381
H -5.011472 0.313723 -0.969843
C -6.93791 1.224208 -0.691842
H -7.4622 0.463122 -1.291145
H -7.603864 1.485346 0.148759
C -6.641879 2.463906 -1.531661
H -7.583503 2.898936 -1.901525
H -6.056816 2.17173 -2.421261
N -3.651611 1.078383 1.191843
N -6.030813 -0.512823 0.722091
C -5.584666 -1.693464 0.575123
H -6.016343 -2.457531 1.24355
C -3.392428 1.08676 2.433543
H -4.084602 1.534249 3.171635
C -4.574226 -2.254601 -0.369512
C -4.803079 -3.535109 -0.894399
C -3.376377 -1.6011 -0.675038

C -3.8666 -4.132016 -1.735959
H -5.723923 -4.066395 -0.639159
C -2.41272 -2.211067 -1.493564
H -3.172073 -0.621111 -0.240332
C -2.672009 -3.480998 -2.034539
H -4.060718 -5.123699 -2.150289
H -1.92775 -3.958771 -2.674964
C -2.14446 0.508195 2.977099
C -1.764614 0.782141 4.296341
C -1.337989 -0.321413 2.190872
C -0.585457 0.247134 4.815419
H -2.395686 1.422868 4.917732
C -0.168301 -0.882974 2.714399
H -1.626154 -0.543705 1.163942
C 0.211745 -0.585291 4.035667
H -0.289898 0.473372 5.841927
H 1.126352 -1.017172 4.446378
C -1.164649 -1.54056 -1.739338
C 0.621785 -1.760581 1.897845
C -0.103312 -0.966663 -1.911965
C 1.285175 -2.495978 1.193665
I 1.681436 0.026577 -2.104558
I 2.397783 -3.694349 0.038848
Br 4.349042 1.652828 -2.154468
C 3.012664 2.928978 0.522489
H 3.693913 3.715502 0.184413
C 1.68202 3.032968 0.030583
C 0.565714 2.363885 0.592239
C 1.484976 3.865824 -1.100865
C -0.686498 2.493588 0.010408
H 0.67191 1.776254 1.504616
C 0.235352 3.977969 -1.683078
H 2.345054 4.379902 -1.533599
C -0.847322 3.286253 -1.129701
H -1.55006 1.978207 0.436811
H 0.094796 4.601302 -2.567746
H -1.835708 3.376122 -1.586254
C 3.572665 2.019467 1.471071
C 4.750466 2.432309 2.139184
C 3.045565 0.734353 1.739064
C 5.339979 1.617471 3.093243
H 5.180016 3.409482 1.906936
C 3.660964 -0.086931 2.670747
H 2.193587 0.358072 1.17241
C 4.794916 0.357936 3.357999
H 6.235234 1.950686 3.621233
H 3.264106 -1.087119 2.854374

H 5.270669 -0.294086 4.09421

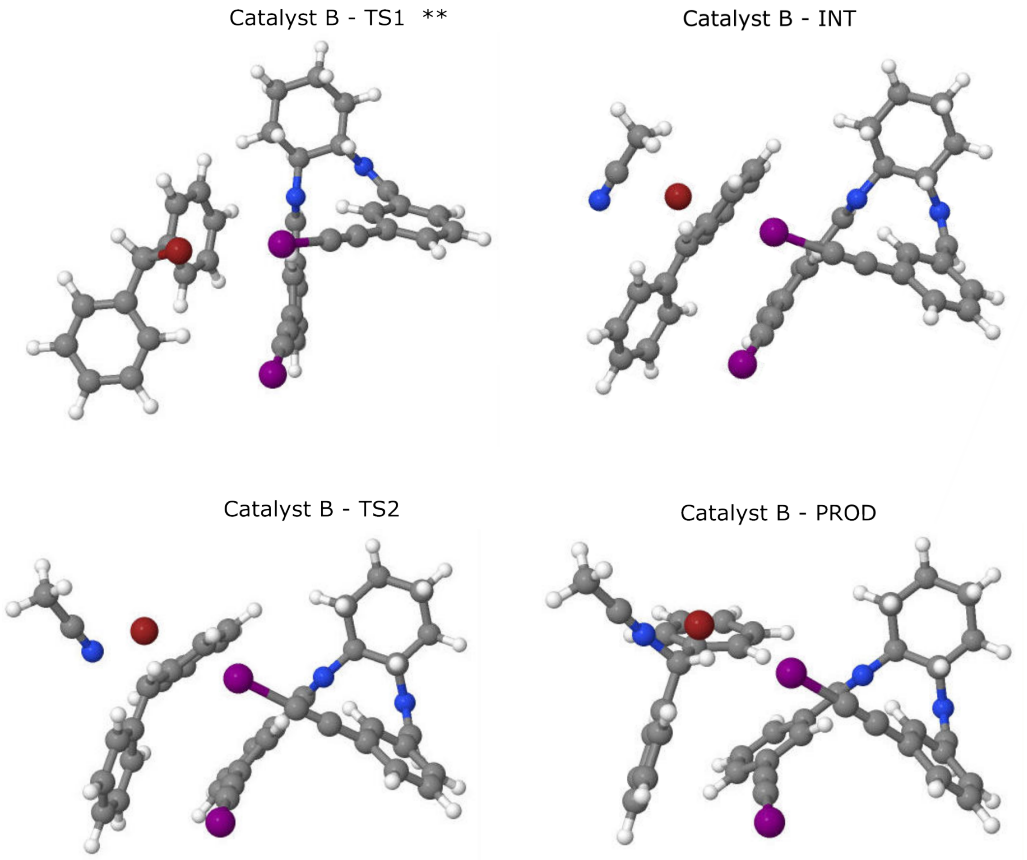

Figure A.3: Halide abstraction: catalyst B, cat-complex structures. ** Acetonitrile is not included in the TS1 structure as it was difficult to achieve this structure.

Table A.8: The ρ(BCP) (a.u.) and the $\nabla^2\rho$ (a.u.) calculated for the TS1 structure of catalyst B.

Atoms	**ρ(BCP) (a.u.)**	**$\nabla^2\rho$ (a.u.)**
I48 - H69	0.007	0.019
I47 - Br49	0.024	0.063
I47 - I48	0.005	0.012
I47 - C52	0.006	0.017
H56 - C65	0.011	0.039
C35 - H60	0.008	0.027
H39 - C59	0.006	0.027
H39 - C43	0.003	0.009
N17 - H62	0.011	0.027
H6 - H61	0.002	0.009
N17 - H29	0.020	0.053
H10 - C25	0.012	0.047

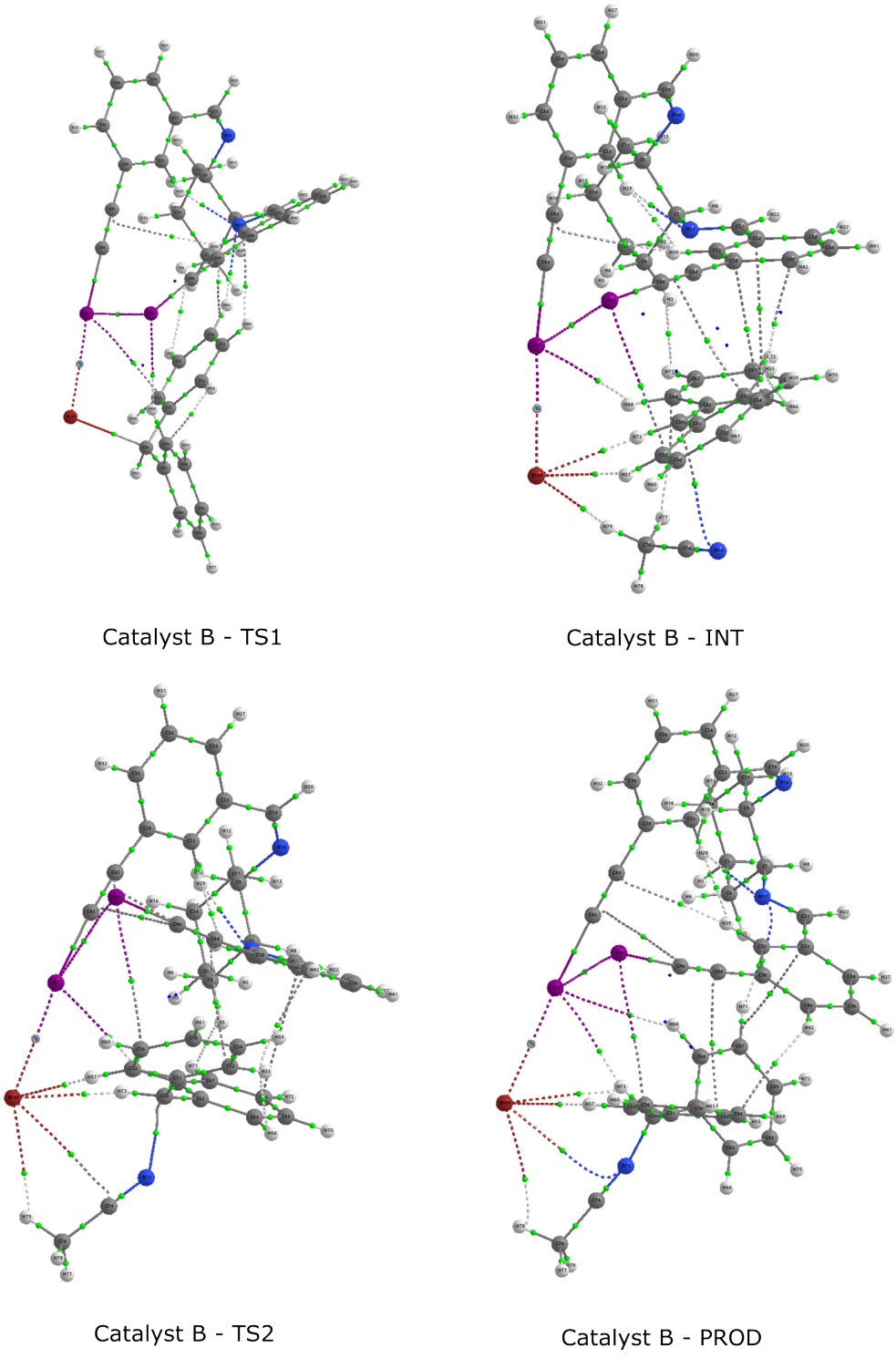

Figure A.4: Halide abstraction: catalyst B, QTAIM molecular graphs of the cat-complex structures showing the I–O electron density at BCP.

Table A.9: The ρ(BCP) (a.u.) and the $\nabla^2\rho$ (a.u.) calculated for the INT structure of catalyst B.

Atoms	**ρ(BCP) (a.u.)**	**$\nabla^2\rho$ (a.u.)**
I47 - I48	0.005061	0.011671
I47 - H68	0.00682	0.019874
I47 - Br49	0.022626	0.052303
C50 - N75	0.006234	0.018628

Table A.10: The ρ(BCP) (a.u.) and the $\nabla^2\rho$ (a.u.) calculated for the TS2 structure of catalyst B.

Atoms	**ρ(BCP) (a.u.)**	**$\nabla^2\rho$ (a.u.)**
I47 - I48	0.004479	0.01049
I47 - H68	0.006374	0.017799
I47 - Br49	0.02251	0.052274
C50 - N75	0.054636	0.116018

Table A.11: The ρ(BCP) (a.u.) and the $\nabla^2\rho$ (a.u.) calculated for the PROD structure of catalyst B.

Atoms	**ρ(BCP) (a.u.)**	**$\nabla^2\rho$ (a.u.)**
I47 - I48	0.004479	0.01049
I47 - H68	0.006374	0.017799
I47 - Br49	0.02251	0.052274
C50 - N75	0.054636	0.116018

Table A.12: Perturbation energies E(2) of the LP_{Br} to σ^*_{C-I} in the cat-complex B structures, calculated at the ωb97xD/def2SVP computational level (solvent = acetonitrile, SMD model and T = 273K).

Name	**Orb(1)**	**Orb(2)**	**E(2)(kJ/mol)**
TS1	$LP_{Br_{37}}$	$\sigma^*_{C_{47}-I_{47}}$	86.48
INT	$LP_{Br_{37}}$	$\sigma^*_{C_{47}-I_{47}}$	98.70
TS2	$LP_{Br_{37}}$	$\sigma^*_{C_{47}-I_{47}}$	99.45
PROD	$LP_{Br_{37}}$	$\sigma^*_{C_{47}-I_{47}}$	102.97

croto-mono
Imaginary frequencies=0
SCF energy=-461.8222608
C 3.049798 0.758628 0.08851
C 3.389445 -0.594314 0.015944
C 2.386356 -1.558976 -0.069531
C 1.044975 -1.177136 -0.076375
C 0.693804 0.178181 -0.004692
C 1.712269 1.139697 0.074251
H 3.832377 1.517866 0.154858
H 4.439529 -0.896324 0.024637
H 2.647112 -2.617798 -0.132741
H 0.279721 -1.950906 -0.149581
H 1.431566 2.193282 0.125358
C -0.728547 0.669533 -0.027157
O -0.952952 1.864305 -0.124107
C -1.834566 -0.316567 0.0748
H -1.602251 -1.371021 0.238801
C -3.113365 0.076418 -0.024291
H -3.300184 1.144631 -0.18784
C -4.302412 -0.814691 0.061803
H -4.028331 -1.863751 0.242841
H -4.974826 -0.477939 0.867898
H -4.887634 -0.757118 -0.870952

indole-mono
Imaginary frequencies=0
SCF energy=-363.4564184
C 0.500021 0.615008 0
C 0 -0.714545 0
C -1.373959 -0.99613 0
C -2.248712 0.080332 0
C -1.773649 1.410487 0
C -0.414514 1.686106 0
C 1.935237 0.516034 0
C 2.236159 -0.822057 0
H -1.738119 -2.025916 0
H -3.325938 -0.103704 0
H -2.49294 2.233185 0
H -0.056022 2.718658 0
H 2.651063 1.335597 0
N 1.080089 -1.559898 0
H 1.03296 -2.571215 0
H 3.204874 -1.318735 0

I2-mono
Imaginary frequencies=0

SCF energy=-595.5667936
I 0 0 1.346434
I 0 0 -1.346434

cat1-mono
Imaginary frequencies=0
SCF energy=-1679.9327357
C 2.939513 -0.517344 0.000944
C 3.305443 1.287386 1.214324
C 4.361339 0.446824 1.36826
N 4.116539 -0.674288 0.602925
N 2.41863 0.667364 0.353757
C 4.999343 -1.829301 0.469885
H 4.503455 -2.723406 0.867748
H 5.259101 -1.976369 -0.585908
H 5.907829 -1.624368 1.045233
C 1.178329 1.214973 -0.115076
C 1.207932 2.286336 -1.004004
C -0.018524 0.66817 0.337275
C 0.006637 2.823933 -1.45842
H 2.165335 2.689988 -1.337786
C -1.203316 1.212477 -0.149585
H -0.025101 -0.156863 1.051693
C -1.206493 2.283833 -1.040111
H 0.015918 3.661908 -2.156732
H -2.153756 2.686322 -1.403453
N -2.457385 0.670783 0.285876
C -3.415313 1.347862 1.01813
C -2.923975 -0.560655 0.028729
C -4.45712 0.494557 1.194826
N -4.132358 -0.692298 0.571845
C -4.973576 -1.883292 0.508663
H -4.452219 -2.732397 0.967832
H -5.891269 -1.671651 1.065403
H -5.221273 -2.107711 -0.536319
Cl -2.12391 -1.748348 -0.861449
Cl 2.228037 -1.622465 -1.054874
H -5.40415 0.6238 1.711495
H -3.258653 2.371066 1.348325
H 3.095555 2.264765 1.639839
H 5.269796 0.543253 1.956266

cat2-mono
Imaginary frequencies=0
SCF energy=-5907.6277919
C -3.008324 -0.110072 -0.27488
C -3.277043 1.965285 -0.97834

C -4.360042 1.240024 -1.362787
N -4.175887 -0.049943 -0.915558
N -2.437677 1.105688 -0.298193
C -5.108499 -1.15569 -1.113486
H -4.64082 -1.931355 -1.733356
H -5.407974 -1.569812 -0.142193
H -5.991035 -0.761199 -1.626727
C -1.190904 1.47 0.313219
C -1.207734 2.181294 1.510773
C 0.000042 1.114303 -0.311821
C -0.000005 2.541226 2.103309
H -2.160597 2.444799 1.973592
C 1.190965 1.470042 0.313241
H 0.000062 0.584517 -1.265337
C 1.20775 2.181337 1.510793
H -0.00002 3.098526 3.040852
H 2.16059 2.44488 1.973637
N 2.437752 1.105731 -0.298144
C 3.277083 1.965263 -0.97842
C 3.008364 -0.110039 -0.274804
C 4.360034 1.239946 -1.362906
N 4.175878 -0.049983 -0.915579
C 5.108407 -1.155799 -1.113484
H 4.641049 -1.930939 -1.734256
H 5.991453 -0.761152 -1.625718
H 5.406968 -1.570643 -0.142227
H 5.248929 1.526913 -1.918421
H 3.02299 3.011336 -1.12547
H -3.022911 3.011351 -1.125379
H -5.248965 1.527039 -1.918229
Br 2.301878 -1.61323 0.521151
Br -2.3019 -1.613268 0.52111

cat3-mono
Imaginary frequencies=0
SCF energy=-1355.3839425
C -3.00531 0.273533 -0.387463
C -3.216766 2.431141 -0.861446
C -4.296353 1.778534 -1.363912
N -4.148463 0.442152 -1.060503
N -2.419617 1.479268 -0.258658
C -5.096226 -0.605206 -1.425376
H -4.626104 -1.303011 -2.130256
H -5.41953 -1.14186 -0.524557
H -5.961502 -0.130376 -1.89895
C -1.183549 1.754722 0.415961
C -1.216833 2.29627 1.698825

C 0.017015 1.481171 -0.231044
C -0.017538 2.566945 2.352949
H -2.176182 2.496303 2.179301
C 1.200593 1.748347 0.450653
H 0.02976 1.066751 -1.240378
C 1.198798 2.289818 1.733564
H -0.030879 2.989584 3.358512
H 2.144916 2.485621 2.241266
N 2.453971 1.473392 -0.191217
C 3.286341 2.434428 -0.728488
C 3.014723 0.261745 -0.368909
C 4.359984 1.7819 -1.243294
N 4.173325 0.436111 -1.013427
C 5.104922 -0.613651 -1.41155
H 4.594831 -1.332429 -2.065384
H 5.930624 -0.143742 -1.955679
H 5.492809 -1.124369 -0.520906
H 5.241718 2.155804 -1.756641
H 3.032304 3.49035 -0.698604
H -2.938925 3.481281 -0.877856
H -5.159754 2.146801 -1.91141
I 2.247255 -1.536582 0.282003
I -2.274941 -1.505519 0.353569

cat4-mono
Imaginary frequencies=0
SCF energy=-1662.3679767
C -3.042192 -0.383533 -0.187918
N -4.17516 -0.026307 -0.799088
N -2.436958 0.703689 0.324114
C -5.089149 -0.918077 -1.501216
H -6.011265 -0.370499 -1.71929
H -4.632532 -1.256592 -2.440683
H -5.326459 -1.780244 -0.865792
C -1.195182 0.744563 1.035759
C -1.204072 0.844995 2.425278
C -0.006045 0.713273 0.314174
C 0.00728 0.908536 3.110153
H -2.154305 0.871229 2.961442
C 1.189683 0.761057 1.023011
H -0.011104 0.647328 -0.774942
C 1.211845 0.863397 2.412199
H 0.012657 0.988096 4.198126
H 2.167385 0.903354 2.937971
N 2.425401 0.724056 0.300969
C 3.037961 -0.37032 -0.187314
N 4.161912 -0.01765 -0.81664

C 5.129395 -0.910117 -1.439766
H 5.651412 -0.35889 -2.229292
H 5.853022 -1.259705 -0.691278
H 4.608801 -1.764203 -1.887264
I 2.342257 -2.296407 0.056242
I -2.326072 -2.311572 -0.03228
C -4.322556 1.354766 -0.683647
C -5.312673 2.23035 -1.138289
C -3.217028 1.819164 0.033178
C -5.137049 3.574114 -0.840441
H -6.18121 1.881581 -1.697971
C -3.034731 3.169514 0.333495
C -4.018034 4.037045 -0.118243
H -5.886117 4.293522 -1.17608
H -2.164462 3.515462 0.89252
H -3.923479 5.104549 0.089249
C 4.300801 1.365956 -0.728032
C 5.286425 2.233248 -1.206315
C 3.195107 1.8394 -0.017965
C 5.105802 3.583008 -0.939573
H 6.153044 1.868352 -1.75855
C 3.008068 3.195629 0.251091
C 3.986843 4.056474 -0.223987
H 5.850465 4.298595 -1.292904
H 2.138556 3.551964 0.80472
H 3.888406 5.127825 -0.039273

cat5-mono
Imaginary frequencies=0
SCF energy=-1999.0571606
C 5.459586 -0.594153 -1.172686
N 4.365112 0.115597 -0.519704
C 3.260313 -0.435963 -0.021109
I 2.806868 -2.445594 -0.045042
N 2.456321 0.515717 0.487142
C 1.197821 0.013012 2.480322
C -0.000603 -0.150827 3.163387
C -1.201465 0.008564 2.485122
N -2.474436 0.50688 0.502627
C -3.281799 -0.445181 0.001119
I -2.795188 -2.447931 -0.054795
N -4.39092 0.107744 -0.487428
C -5.490103 -0.576482 -1.156071
C -4.308526 1.4875 -0.306933
C -5.185769 2.521691 -0.642781
C -4.777049 3.806262 -0.3158
C -3.543733 4.058099 0.320915

C -2.673763 3.031901 0.656865
C -3.090564 1.742746 0.325593
C 0.003992 0.853856 -1.073158
F -1.10786 0.487525 -1.707595
F 1.015883 0.282964 -1.727162
F 0.127632 2.174397 -1.210305
C 3.080002 1.750248 0.319284
C 2.677849 3.037704 0.676853
C 3.553655 4.062264 0.353414
C 4.779748 3.810822 -0.297103
C 5.174943 2.528901 -0.648312
C 4.29268 1.494544 -0.324664
H 5.097223 -1.077225 -2.089604
H 6.234104 0.132722 -1.433667
H 5.882909 -1.338046 -0.485727
H 2.156023 -0.090549 2.99189
H 0.001831 -0.389423 4.227476
H -2.157279 -0.098071 3.00054
H -6.401329 0.014225 -1.015804
H -5.640053 -1.564304 -0.705685
H -5.270452 -0.676289 -2.227573
H -6.138131 2.332054 -1.138312
H -5.427278 4.647706 -0.561851
H -3.268888 5.088674 0.552784
H -1.716418 3.213997 1.146541
H 1.72597 3.218353 1.177757
H 3.290073 5.090612 0.607083
H 5.43668 4.650013 -0.532584
H 6.123951 2.342597 -1.151761
C -1.201466 0.313915 1.125853
C 1.189072 0.31813 1.122195
C -0.008391 0.468155 0.403851

uncat-ts
Imaginary frequencies=1
SCF energy=-825.2407204
C -1.980578 0.356671 -0.430476
C -3.383499 0.354525 -0.339417
C -4.132303 1.490626 -0.044248
C -3.424488 2.67175 0.16062
C -2.022519 2.701553 0.071985
C -1.289504 1.55329 -0.222137
C -1.545972 -1.028796 -0.670813
C -2.771338 -1.739031 -0.82832
H -5.221137 1.454184 0.023122
H -3.968224 3.590607 0.39107
H -1.499414 3.646715 0.234244

H -0.201141 1.586525 -0.293328
H -0.691279 -1.277589 -1.326516
N -3.812239 -0.951727 -0.589179
H -4.781237 -1.259088 -0.571322
H -2.911525 -2.79844 -1.042165
C 4.684476 0.645816 -1.2149
C 5.193316 1.145142 -0.014756
C 4.504807 0.909085 1.17648
C 3.311508 0.187102 1.166815
C 2.787182 -0.311906 -0.033862
C 3.495371 -0.08083 -1.220086
H 5.218815 0.822424 -2.151981
H 6.128042 1.71136 -0.006087
H 4.9033 1.286385 2.121749
H 2.794289 -0.003874 2.109885
H 3.087815 -0.489882 -2.14687
C 1.498588 -1.10168 -0.113458
O 1.285894 -1.777854 -1.151868
C 0.555857 -0.996413 0.923405
H 0.652887 -0.23192 1.697763
C -0.692048 -1.702766 0.80041
H -0.569078 -2.716751 0.398074
C -1.621575 -1.644188 1.992295
H -1.84253 -0.603748 2.276458
H -2.573083 -2.166568 1.814504
H -1.131653 -2.125128 2.85337

I2-ts
Imaginary frequencies=1
SCF energy=-1420.8270414
C -4.251852 -0.704895 -0.615299
C -5.327032 -1.59227 -0.419809
C -6.661049 -1.209494 -0.546711
C -6.903355 0.117815 -0.886427
C -5.845858 1.023011 -1.086424
C -4.51781 0.625958 -0.953269
C -3.024392 -1.437863 -0.309192
C -3.454156 -2.763944 -0.075126
H -7.474537 -1.919598 -0.38755
H -7.933438 0.462442 -1.001407
H -6.073352 2.057777 -1.352525
H -3.702105 1.334333 -1.11016
H -2.043697 -1.225927 -0.746998
N -4.784449 -2.833863 -0.091265
H -5.32538 -3.666106 0.126597
H -2.850932 -3.641013 0.156887
C 0.643827 3.897847 -1.138876

C 0.480607 4.86045 -0.141383
C -0.118507 4.509757 1.069448
C -0.556273 3.203496 1.281385
C -0.39465 2.230245 0.286156
C 0.213727 2.590499 -0.924155
H 1.111025 4.16664 -2.089181
H 0.823865 5.884586 -0.306311
H -0.239811 5.257638 1.85671
H -1.010526 2.931515 2.237037
H 0.338225 1.833601 -1.701525
C -0.853422 0.81825 0.479895
O -0.237206 -0.121829 -0.125973
C -1.989289 0.546025 1.244748
H -2.640663 1.360102 1.570202
C -2.399053 -0.801805 1.457148
H -1.574845 -1.521739 1.481553
C -3.495836 -1.053614 2.454889
H -4.386385 -0.44361 2.241493
H -3.790089 -2.110652 2.506529
H -3.127408 -0.762114 3.451707
I 4.911638 -1.008071 -0.102038
I 2.182986 -0.470099 -0.130951

cat1-ts
Imaginary frequencies=1
SCF energy=-2505.1915621
C 3.530215 1.75808 -0.102968
C 5.655011 1.525944 0.459069
C 5.478058 2.778818 -0.032988
N 4.147657 2.905563 -0.377678
N 4.425328 0.893594 0.407256
C 3.50984 4.096979 -0.928701
H 3.069347 3.865528 -1.906707
H 2.730892 4.450934 -0.241215
H 4.278592 4.86786 -1.043301
C 4.12779 -0.425751 0.876609
C 4.412109 -0.763959 2.198001
C 3.525842 -1.331021 0.008933
C 4.072444 -2.032723 2.661694
H 4.880365 -0.033974 2.860814
C 3.145647 -2.569813 0.514212
H 3.342899 -1.077616 -1.035995
C 3.416363 -2.937109 1.829953
H 4.289117 -2.305782 3.69539
H 3.103544 -3.914361 2.202018
N 2.431542 -3.468964 -0.341969
C 2.825136 -4.744381 -0.702428

C 1.247258 -3.212754 -0.92371
C 1.858254 -5.242537 -1.51521
N 0.883471 -4.27377 -1.642954
C -0.337077 -4.38416 -2.434409
H -1.213854 -4.281031 -1.783563
H -0.348448 -3.607039 -3.209129
H -0.345468 -5.372111 -2.905264
Cl 0.359979 -1.784676 -0.754194
Cl 1.887458 1.45172 -0.338221
H 6.183361 3.593153 -0.173675
H 6.540104 1.018705 0.832846
H 3.761821 -5.170615 -0.354149
H 1.777032 -6.200197 -2.021374
C -4.637448 -0.37307 -0.091386
C -5.547726 -1.370796 0.298141
C -6.920685 -1.157318 0.392896
C -7.378861 0.116939 0.070995
C -6.489538 1.130059 -0.326361
C -5.11816 0.899729 -0.410883
C -3.286799 -0.938968 0.022245
C -3.516945 -2.304748 0.346692
H -7.602334 -1.950595 0.704495
H -8.448165 0.331646 0.127858
H -6.885615 2.117442 -0.573966
H -4.434119 1.691425 -0.720794
H -2.466132 -0.659087 -0.652286
N -4.808759 -2.528244 0.554695
H -5.203204 -3.405392 0.885221
H -2.782656 -3.095195 0.499454
C -0.591812 4.700694 -1.828388
C -0.704801 5.702104 -0.861801
C -1.034256 5.361025 0.450985
C -1.257424 4.027395 0.793892
C -1.146567 3.015378 -0.168441
C -0.803244 3.368016 -1.480496
H -0.338868 4.960858 -2.859421
H -0.535037 6.747771 -1.129774
H -1.1154 6.138523 1.214546
H -1.499262 3.769112 1.82755
H -0.704023 2.574674 -2.224299
C -1.344787 1.556714 0.162125
O -0.74053 0.707653 -0.553121
C -2.217088 1.202331 1.200069
H -2.872628 1.951519 1.649943
C -2.427874 -0.179719 1.513432
H -1.519523 -0.787388 1.420653
C -3.237409 -0.483899 2.751197

H -4.220736 0.009164 2.71867
H -3.389215 -1.561019 2.908952
H -2.702029 -0.090015 3.629268

cat2-ts
Imaginary frequencies=1
SCF energy=-6732.8953595
C 3.531938 1.874278 -0.32136
C 5.730323 1.638988 -0.172635
C 5.467609 2.873338 -0.673511
N 4.096741 3.001254 -0.759486
N 4.511551 1.023092 0.039192
C 3.380445 4.17766 -1.241327
H 2.725287 4.567104 -0.451458
H 4.12008 4.938552 -1.508912
H 2.787627 3.917551 -2.127859
C 4.317297 -0.273904 0.614544
C 4.788173 -0.524666 1.901249
C 3.634376 -1.244536 -0.111701
C 4.558397 -1.77135 2.477758
H 5.316487 0.257933 2.448949
C 3.371276 -2.462039 0.508202
H 3.309037 -1.054957 -1.135761
C 3.830711 -2.741581 1.792799
H 4.923374 -1.977273 3.484892
H 3.609163 -3.705371 2.254354
N 2.589458 -3.441143 -0.187983
C 3.021269 -4.69806 -0.564521
C 1.303476 -3.299594 -0.560036
C 1.974319 -5.308111 -1.177781
N 0.916586 -4.42277 -1.168719
C -0.408689 -4.68167 -1.719388
H -1.142908 -4.761259 -0.907392
H -0.691495 -3.875982 -2.408265
H -0.369657 -5.628005 -2.267864
H 6.135329 3.672767 -0.982487
H 6.668788 1.13627 0.044575
H 4.037189 -5.032369 -0.372692
H 1.888368 -6.293285 -1.62736
C -4.848609 -0.378695 -0.335437
C -5.854764 -1.332433 -0.103427
C -7.213356 -1.052108 -0.229301
C -7.552183 0.243433 -0.60872
C -6.563943 1.213934 -0.847188
C -5.209488 0.917411 -0.713607
C -3.563524 -1.01203 -0.023916
C -3.901756 -2.364999 0.245052

H -7.973204 -1.812424 -0.041007
H -8.605181 0.508384 -0.725874
H -6.866902 2.220226 -1.145295
H -4.447632 1.675593 -0.902305
H -2.637246 -0.755498 -0.548876
N -5.220392 -2.524879 0.252184
H -5.700504 -3.383783 0.508466
H -3.240717 -3.19246 0.501393
C -0.933466 4.715833 -1.303366
C -1.094617 5.676386 -0.302994
C -1.443081 5.278436 0.988547
C -1.633865 3.927563 1.278505
C -1.46581 2.956436 0.283472
C -1.110484 3.365713 -1.009218
H -0.669681 5.021376 -2.319058
H -0.949281 6.73548 -0.529121
H -1.564176 6.025388 1.776856
H -1.895697 3.62216 2.294559
H -0.976736 2.608046 -1.784918
C -1.635811 1.486951 0.560172
O -0.861089 0.684782 -0.045558
C -2.673119 1.079694 1.405154
H -3.409011 1.812775 1.743084
C -2.926468 -0.305276 1.643588
H -2.024794 -0.928239 1.662566
C -3.92809 -0.648629 2.716861
H -4.898762 -0.164157 2.531385
H -4.086674 -1.730895 2.821608
H -3.550761 -0.270161 3.679967
Br 1.713883 1.538834 -0.219113
Br 0.260988 -1.797087 -0.27251

cat3-ts
Imaginary frequencies=1
SCF energy=-2180.6526778
C 3.682676 1.88797 -0.457853
C 5.863402 1.471811 -0.303962
C 5.703973 2.68592 -0.88944
N 4.348998 2.925465 -0.975551
N 4.596773 0.984378 -0.045324
C 3.74811 4.125729 -1.544562
H 4.552854 4.823924 -1.797471
H 3.185988 3.86685 -2.45138
H 3.076345 4.58768 -0.810134
C 4.317806 -0.253576 0.62149
C 4.699855 -0.403303 1.952992
C 3.662318 -1.272345 -0.064476

C 4.409521 -1.593071 2.61589
H 5.210067 0.4138 2.466261
C 3.348599 -2.436466 0.631541
H 3.388499 -1.154351 -1.113831
C 3.718813 -2.610887 1.963043
H 4.702557 -1.719087 3.659135
H 3.458216 -3.534849 2.482317
N 2.624419 -3.484392 -0.030409
C 3.15345 -4.716601 -0.361969
C 1.323742 -3.452594 -0.387415
C 2.152162 -5.432197 -0.934738
N 1.028506 -4.633406 -0.94191
C -0.274076 -5.033319 -1.460217
H -1.000441 -5.090429 -0.639127
H -0.612822 -4.308299 -2.210879
H -0.167819 -6.01913 -1.924821
H 6.435187 3.401285 -1.255562
H 6.756943 0.907018 -0.052182
H 4.194075 -4.961305 -0.16818
H 2.139253 -6.438831 -1.343478
C -5.039875 -0.312203 -0.483313
C -6.027356 -1.301338 -0.328752
C -7.391464 -1.0355 -0.426493
C -7.75516 0.280723 -0.695215
C -6.785682 1.286002 -0.855469
C -5.425942 1.004413 -0.750598
C -3.745621 -0.944485 -0.221827
C -4.053181 -2.319518 -0.065547
H -8.137509 -1.821814 -0.29888
H -8.813333 0.535285 -0.785859
H -7.108209 2.307906 -1.067111
H -4.678185 1.789525 -0.875578
H -2.812515 -0.625038 -0.694604
N -5.369628 -2.506004 -0.073215
H -5.831659 -3.394049 0.103919
H -3.371463 -3.15063 0.112058
C -1.28739 4.93022 -0.95478
C -1.402859 5.78796 0.140776
C -1.670472 5.263704 1.405951
C -1.827533 3.888439 1.576124
C -1.702515 3.020298 0.484444
C -1.428088 3.554875 -0.782017
H -1.088756 5.337173 -1.949197
H -1.284189 6.865811 0.007495
H -1.755183 5.930765 2.267173
H -2.030113 3.480185 2.569271
H -1.334099 2.879691 -1.636134

C -1.842697 1.531833 0.637302
O -1.0196 0.797863 0.000572
C -2.904559 1.046376 1.404202
H -3.654577 1.753067 1.766856
C -3.162463 -0.348835 1.544129
H -2.271155 -0.984975 1.548077
C -4.209275 -0.763025 2.544187
H -5.159911 -0.234967 2.376972
H -4.397439 -1.845233 2.540857
H -3.853173 -0.489489 3.550204
I 1.617191 1.67743 -0.297682
I 0.056895 -1.822991 -0.140742

cat4-ts
Imaginary frequencies=1
SCF energy=-2487.6380474
C -2.953763 -2.26603 -0.216023
N -3.605633 -3.308266 -0.739836
N -3.849686 -1.360949 0.235138
C -3.038309 -4.508139 -1.334732
H -3.457097 -4.639033 -2.340636
H -1.950346 -4.406673 -1.4033
H -3.289495 -5.376989 -0.712103
C -3.54804 -0.129238 0.900141
C -3.817019 -0.011962 2.262725
C -2.980283 0.919094 0.180928
C -3.500238 1.173276 2.921504
H -4.26322 -0.84993 2.801207
C -2.628977 2.07604 0.87062
H -2.787817 0.824586 -0.888839
C -2.890078 2.218079 2.23204
H -3.706868 1.2746 3.987916
H -2.607857 3.138759 2.74579
N -1.975771 3.143635 0.173107
C -0.688548 3.161141 -0.234316
N -0.423445 4.336568 -0.811729
C 0.83211 4.78658 -1.390484
H 1.586383 3.999355 -1.289835
H 0.678897 5.011433 -2.453986
H 1.168025 5.68941 -0.863991
C 5.717473 0.350497 -0.502632
C 6.672693 1.350425 -0.247092
C 8.042047 1.153996 -0.412373
C 8.445239 -0.100256 -0.860314
C 7.508299 -1.114103 -1.126451
C 6.14314 -0.90347 -0.950542
C 4.410216 0.8925 -0.128742

C 4.671365 2.248142 0.192731
H 8.761913 1.946706 -0.201637
H 9.508581 -0.298885 -1.010408
H 7.861974 -2.084732 -1.481464
H 5.421522 -1.695048 -1.160037
H 3.477888 0.594214 -0.613188
N 5.979674 2.485467 0.177097
H 6.415494 3.358926 0.461649
H 3.967247 3.022238 0.495666
C 2.683908 -5.561458 0.882755
C 2.316287 -5.953773 -0.404945
C 2.059653 -4.98595 -1.377813
C 2.158215 -3.633119 -1.059276
C 2.531019 -3.230096 0.230709
C 2.798248 -4.207561 1.19724
H 2.880226 -6.314797 1.649254
H 2.230205 -7.015 -0.650109
H 1.782107 -5.287161 -2.390953
H 1.95129 -2.872452 -1.815868
H 3.078276 -3.905619 2.209464
C 2.61689 -1.762412 0.542006
O 1.711443 -1.010161 0.054135
C 3.707768 -1.309487 1.286638
H 4.508714 -2.013489 1.523254
C 3.909144 0.069787 1.580525
H 2.991387 0.658374 1.681432
C 4.973873 0.412454 2.588088
H 5.938033 -0.050078 2.32945
H 5.118399 1.494256 2.710839
H 4.666211 0.004323 3.564037
I -0.888437 -1.995938 -0.102061
I 0.59338 1.533608 -0.018219
C -1.57406 5.118998 -0.782721
C -1.821403 6.408426 -1.256961
C -2.564852 4.363162 -0.153927
C -3.106318 6.899353 -1.068827
H -1.046448 6.996029 -1.750353
C -3.857766 4.85228 0.036055
C -4.105974 6.135007 -0.433724
H -3.349399 7.90316 -1.422183
H -4.626709 4.25599 0.528856
H -5.101947 6.564016 -0.308271
C -4.974838 -3.087549 -0.620767
C -6.070436 -3.864039 -1.003386
C -5.134042 -1.847078 -0.000894
C -7.326028 -3.333353 -0.738952
H -5.945789 -4.835583 -1.482617

C -6.393821 -1.308959 0.263521
C -7.484946 -2.077955 -0.118511
H -8.214452 -3.902818 -1.018796
H -6.509493 -0.337737 0.746223
H -8.492408 -1.700233 0.065928

cat5-ts
Imaginary frequencies=1
SCF energy=-2824.3291301
C 0.208893 2.908995 -0.180003
N -0.116618 4.098182 -0.686763
N 1.513102 2.921432 0.181456
C -1.404788 4.519181 -1.214054
H -1.761204 5.386659 -0.643646
H -1.287985 4.791108 -2.271066
H -2.125663 3.699929 -1.124167
C 2.186038 1.835892 0.828367
C 2.205023 1.844136 2.220496
C 2.734808 0.773835 0.091832
C 2.743493 0.76876 2.915944
H 1.770432 2.695206 2.747287
C 3.188274 -0.337202 0.820184
C 3.211465 -0.334164 2.212652
H 2.762337 0.773284 4.006572
H 3.581632 -1.217942 2.734803
N 3.582389 -1.550084 0.167993
C 2.735698 -2.540518 -0.197605
N 3.439444 -3.556047 -0.700338
C 2.938036 -4.820062 -1.217505
H 1.855872 -4.879607 -1.065024
H 3.163823 -4.888119 -2.289787
H 3.427722 -5.643676 -0.682505
C -5.230161 -0.326165 -1.291411
C -6.218529 -0.484002 -2.280596
C -7.484599 0.09097 -2.186406
C -7.746412 0.852117 -1.051111
C -6.773829 1.025896 -0.050674
C -5.514149 0.441981 -0.157592
C -4.08104 -1.132444 -1.694069
C -4.421454 -1.618953 -2.97613
H -8.23439 -0.050174 -2.967003
H -8.724732 1.323753 -0.935905
H -7.01458 1.631321 0.826236
H -4.764835 0.581529 0.624326
H -3.048425 -0.912909 -1.407155
N -5.673661 -1.284094 -3.284694
H -6.168308 -1.589145 -4.118568

H -3.827718 -2.23988 -3.645927
C -1.378869 -0.294839 4.45871
C -2.523905 0.069787 5.169
C -3.781197 -0.11252 4.592596
C -3.895806 -0.661691 3.316164
C -2.752247 -1.031884 2.593855
C -1.49316 -0.833994 3.17994
H -0.390902 -0.157313 4.904961
H -2.43576 0.499465 6.169633
H -4.681549 0.179106 5.138411
H -4.885776 -0.781919 2.870977
H -0.596355 -1.112889 2.622711
C -2.827029 -1.592545 1.203486
O -1.841795 -1.365058 0.419395
C -3.956925 -2.287484 0.779113
H -4.829668 -2.367465 1.429668
C -4.055187 -2.767224 -0.557725
H -3.109516 -3.094523 -1.001628
C -5.25092 -3.606624 -0.914864
H -6.192219 -3.061576 -0.744676
H -5.225683 -3.957367 -1.95492
H -5.264456 -4.492078 -0.259184
I -0.970148 1.208986 0.089097
I 0.673295 -2.367371 0.037821
C 4.79358 -3.227963 -0.657524
C 5.926456 -3.935919 -1.062664
C 4.888344 -1.95436 -0.094985
C 7.149476 -3.307444 -0.869973
H 5.852687 -4.928345 -1.508078
C 6.113073 -1.317597 0.098725
C 7.241465 -2.0224 -0.298591
H 8.064559 -3.821646 -1.169714
H 6.174919 -0.32012 0.535545
H 8.22553 -1.568344 -0.16773
C 1.003526 4.926529 -0.643304
C 1.184896 6.251152 -1.043721
C 2.042349 4.181476 -0.082708
C 2.45203 6.786299 -0.853085
H 0.37373 6.833436 -1.482054
C 3.317474 4.71174 0.106451
C 3.499136 6.03052 -0.288581
H 2.642575 7.820151 -1.146913
H 4.124044 4.118566 0.539023
H 4.478613 6.494809 -0.159269
C 2.806413 0.81413 -1.431255
F 1.711322 0.31893 -2.00767
F 3.845295 0.115057 -1.889107

F 2.9598 2.060843 -1.878656

uncat-prod
Imaginary frequencies=0
SCF energy=-825.3016544
C -2.103417 0.090518 0.296993
C -3.162871 0.592178 -0.502025
C -3.771341 1.8293 -0.246667
C -3.300977 2.563345 0.831544
C -2.247186 2.084079 1.64008
C -1.645976 0.860864 1.383543
C -1.725748 -1.188734 -0.26223
C -2.556355 -1.388352 -1.341504
H -4.584281 2.197592 -0.876148
H -3.753309 3.531726 1.058908
H -1.900931 2.690742 2.480302
H -0.826968 0.501361 2.010431
H -0.237244 -0.538284 -1.609292
N -3.414318 -0.329822 -1.48493
H -4.108551 -0.235306 -2.215769
H -2.594313 -2.230554 -2.03127
C 4.175396 1.734533 -0.72143
C 5.134071 1.133996 0.094461
C 4.841027 -0.078463 0.721186
C 3.599126 -0.68242 0.537758
C 2.622363 -0.078737 -0.268574
C 2.931846 1.132332 -0.904935
H 4.39538 2.681867 -1.219652
H 6.109802 1.604743 0.236302
H 5.590016 -0.565365 1.350361
H 3.395195 -1.643989 1.013866
H 2.183436 1.604188 -1.5434
C 1.279643 -0.685887 -0.463135
O 0.705279 -0.303919 -1.627125
C 0.683946 -1.498356 0.431395
H 1.219501 -1.708106 1.359635
C -0.675556 -2.147649 0.254057
H -0.581808 -2.943609 -0.508278
C -1.12994 -2.814674 1.557959
H -1.254768 -2.069532 2.359344
H -2.09232 -3.328879 1.418605
H -0.389142 -3.555735 1.896701

I2-prod
Imaginary frequencies=0
SCF energy=-1420.8418082
C -3.873747 -0.876529 -0.199722

C -4.599345 -2.040587 -0.469415
C -5.908829 -2.050497 -0.928746
C -6.507649 -0.804816 -1.111853
C -5.806806 0.378834 -0.844507
C -4.485659 0.35887 -0.392109
C -2.500102 -1.279537 0.249162
C -2.588224 -2.748188 0.225678
H -6.437818 -2.982364 -1.13405
H -7.537494 -0.752076 -1.470721
H -6.304034 1.338939 -0.997987
H -3.945983 1.286545 -0.196086
H -1.733276 -0.99719 -0.515661
N -3.752981 -3.139072 -0.18869
H -4.02406 -4.116439 -0.307608
H -1.808349 -3.462203 0.493915
C 0.318074 4.435478 -1.310454
C 0.186919 5.376372 -0.289174
C -0.257238 4.966882 0.969775
C -0.572013 3.630069 1.203837
C -0.457721 2.677434 0.179826
C 0.001335 3.09843 -1.076256
H 0.671701 4.744149 -2.297431
H 0.436438 6.424743 -0.469531
H -0.348252 5.694296 1.780242
H -0.892343 3.32306 2.202032
H 0.104166 2.355406 -1.869268
C -0.793168 1.233018 0.377903
O -0.300146 0.385183 -0.520176
C -1.61449 0.795647 1.364271
H -2.105178 1.511795 2.027151
C -1.920807 -0.665518 1.561696
H -0.969476 -1.203366 1.723113
C -2.835679 -0.910577 2.757003
H -3.805602 -0.405571 2.62595
H -3.025687 -1.984637 2.909476
H -2.374155 -0.517021 3.674928
I 4.557025 -1.292929 -0.020806
I 1.821509 -0.30735 -0.286698

cat1-prod
Imaginary frequencies=0
SCF energy=-2505.1963327
C 3.397514 1.741736 -0.29671
C 5.594273 1.60711 -0.082489
C 5.283356 2.859104 -0.504346
N 3.910604 2.924296 -0.632008
N 4.403053 0.91382 0.04182

C 3.137656 4.088304 -1.053542
H 3.8376 4.911506 -1.228103
H 2.598009 3.858593 -1.981019
H 2.426978 4.369292 -0.265806
C 4.254715 -0.423096 0.527908
C 4.866283 -0.786364 1.725757
C 3.480544 -1.326313 -0.193377
C 4.684614 -2.07689 2.217189
H 5.46623 -0.060273 2.276948
C 3.264279 -2.587044 0.352005
H 3.04546 -1.055287 -1.155202
C 3.863715 -2.979952 1.546239
H 5.161821 -2.370592 3.153149
H 3.680383 -3.977113 1.950227
N 2.393271 -3.494177 -0.332668
C 2.719369 -4.775545 -0.737179
C 1.11411 -3.25655 -0.673965
C 1.616585 -5.297528 -1.330982
N 0.627322 -4.336916 -1.28526
C -0.725197 -4.485374 -1.809382
H -0.764527 -5.419767 -2.378496
H -1.445906 -4.530751 -0.98267
H -0.961608 -3.643095 -2.471104
Cl 0.259517 -1.827076 -0.380428
Cl 1.750861 1.364925 -0.286048
H 5.917024 3.711136 -0.734243
H 6.550701 1.137076 0.129056
H 3.711905 -5.18756 -0.577503
H 1.448315 -6.265771 -1.794411
C -4.524707 -0.270109 0.055612
C -5.374753 -1.373867 -0.077441
C -6.682131 -1.297243 -0.540112
C -7.144102 -0.027016 -0.879065
C -6.316239 1.098028 -0.755176
C -5.002997 0.99148 -0.294172
C -3.208744 -0.756794 0.574249
C -3.442849 -2.193568 0.704772
H -7.31073 -2.184582 -0.631159
H -8.164627 0.092431 -1.248523
H -6.709115 2.079793 -1.028219
H -4.363714 1.870809 -0.20717
H -2.36394 -0.55913 -0.144098
N -4.651066 -2.511996 0.338581
H -5.033821 -3.457595 0.358103
H -2.749171 -2.948367 1.077397
C -0.623413 4.623441 -1.650203
C -0.5388 5.650745 -0.707746

C -0.725954 5.358728 0.644266
C -1.00115 4.052009 1.049894
C -1.093119 3.013813 0.112804
C -0.88828 3.317894 -1.24043
H -0.477923 4.841772 -2.711535
H -0.326261 6.67471 -1.024857
H -0.652643 6.1535 1.391066
H -1.130208 3.832579 2.112677
H -0.93447 2.50364 -1.96678
C -1.374466 1.583174 0.503022
O -0.849228 0.663703 -0.23127
C -2.221128 1.328838 1.556895
H -2.735601 2.14351 2.071957
C -2.611869 -0.077054 1.877046
H -1.709428 -0.680897 2.084101
C -3.567446 -0.182444 3.059145
H -4.504102 0.363048 2.863562
H -3.822727 -1.229267 3.290481
H -3.106796 0.258507 3.956278

cat2-prod
Imaginary frequencies=0
SCF energy=-6732.9020606
C 3.382326 1.842072 -0.724543
C 5.592798 1.694628 -0.60487
C 5.277613 2.851692 -1.240786
N 3.901777 2.925228 -1.306791
N 4.399319 1.071161 -0.291016
C 3.141786 4.023444 -1.892803
H 3.851258 4.707831 -2.369022
H 2.446522 3.636819 -2.648568
H 2.587056 4.555208 -1.108553
C 4.263595 -0.163948 0.419934
C 4.807555 -0.283286 1.6969
C 3.56522 -1.211921 -0.171413
C 4.638027 -1.474164 2.399126
H 5.346038 0.555841 2.140639
C 3.35934 -2.367661 0.574208
H 3.18074 -1.127482 -1.188483
C 3.895016 -2.516957 1.85119
H 5.062867 -1.578361 3.398491
H 3.718989 -3.436679 2.411827
N 2.557304 -3.417606 0.018944
C 2.988093 -4.70155 -0.254919
C 1.251005 -3.323862 -0.293756
C 1.919537 -5.379674 -0.746198
N 0.850505 -4.507349 -0.765082

C -0.497311 -4.834908 -1.212381
H -0.473537 -5.833032 -1.661169
H -1.185681 -4.837854 -0.357177
H -0.827664 -4.108294 -1.965095
H 5.910781 3.629094 -1.659417
H 6.551643 1.247067 -0.358597
H 4.017547 -5.004841 -0.085351
H 1.824348 -6.405084 -1.092072
C -4.751195 -0.176742 -0.281601
C -5.689987 -1.142018 -0.659381
C -6.96593 -0.848934 -1.12037
C -7.297656 0.50294 -1.196808
C -6.377234 1.493124 -0.82757
C -5.097386 1.169136 -0.372266
C -3.504476 -0.883662 0.158957
C -3.869274 -2.292557 -0.041522
H -7.667439 -1.633342 -1.407796
H -8.288458 0.792634 -1.552555
H -6.666658 2.543486 -0.902533
H -4.385308 1.94647 -0.093528
H -2.624587 -0.618353 -0.474067
N -5.084803 -2.406863 -0.483127
H -5.5502 -3.295409 -0.672616
H -3.263739 -3.175402 0.169184
C -0.991998 4.821122 -0.575215
C -0.882999 5.586953 0.587729
C -0.990072 4.96582 1.832702
C -1.207994 3.590015 1.915727
C -1.318172 2.812177 0.755793
C -1.200348 3.446124 -0.489497
H -0.91307 5.300105 -1.554653
H -0.714364 6.664678 0.522831
H -0.898384 5.555415 2.748417
H -1.279452 3.10849 2.894178
H -1.274388 2.840097 -1.395725
C -1.564587 1.326953 0.794132
O -0.93845 0.607452 -0.08442
C -2.503264 0.845543 1.669866
H -3.062476 1.541216 2.300098
C -2.968162 -0.574687 1.619742
H -2.116057 -1.266856 1.741656
C -4.012031 -0.889851 2.685239
H -4.89416 -0.238792 2.581254
H -4.351756 -1.936976 2.637752
H -3.587557 -0.718325 3.685894
Br 1.575265 1.474838 -0.515427
Br 0.205164 -1.799214 -0.106072

cat3-prod
Imaginary frequencies=0
SCF energy=-2180.6619482
C 3.625433 1.832202 -0.587143
C 5.811827 1.430806 -0.444683
C 5.640715 2.630339 -1.055686
N 4.28329 2.860593 -1.13387
N 4.549652 0.94315 -0.163072
C 3.670287 4.044207 -1.723925
H 4.466772 4.750182 -1.981489
H 3.117252 3.765659 -2.630582
H 2.986929 4.506955 -1.000748
C 4.283898 -0.278025 0.539314
C 4.704383 -0.399446 1.862125
C 3.599491 -1.308236 -0.100685
C 4.424157 -1.569931 2.562713
H 5.234208 0.425634 2.341423
C 3.2925 -2.450372 0.634207
H 3.29339 -1.21421 -1.14355
C 3.70271 -2.595652 1.957497
H 4.749056 -1.673092 3.59906
H 3.44778 -3.503111 2.507806
N 2.535389 -3.50543 0.02278
C 3.039249 -4.755885 -0.280885
C 1.228715 -3.459846 -0.313361
C 2.017465 -5.470603 -0.816558
N 0.908052 -4.651475 -0.829681
C -0.406595 -5.038885 -1.322244
H -0.322693 -6.031541 -1.776828
H -1.121666 -5.07672 -0.489987
H -0.746939 -4.31851 -2.076566
H 6.365169 3.340988 -1.443882
H 6.710783 0.876512 -0.188929
H 4.078739 -5.012271 -0.096257
H 1.980721 -6.488115 -1.195826
C -5.001364 -0.159753 -0.296597
C -5.947685 -1.157662 -0.545837
C -7.250491 -0.91057 -0.953324
C -7.601597 0.429498 -1.114313
C -6.672945 1.451266 -0.878122
C -5.365948 1.17191 -0.471497
C -3.726563 -0.820593 0.143697
C -4.084742 -2.249346 0.059786
H -7.959334 -1.719121 -1.136987
H -8.61515 0.683267 -1.431072
H -6.977435 2.490689 -1.017458

H -4.64842 1.973607 -0.294488
H -2.884261 -0.609933 -0.546172
N -5.318013 -2.402729 -0.307087
H -5.781896 -3.307168 -0.40689
H -3.453198 -3.107312 0.295538
C -1.196306 4.946759 -0.734189
C -1.130566 5.744241 0.410336
C -1.266667 5.155971 1.66811
C -1.468237 3.78002 1.782624
C -1.532555 2.970191 0.641369
C -1.389613 3.571763 -0.617714
H -1.095473 5.40062 -1.72336
H -0.972473 6.821679 0.320876
H -1.210366 5.771744 2.569324
H -1.562824 3.322676 2.770638
H -1.432293 2.944631 -1.511841
C -1.746203 1.48295 0.721988
O -1.008901 0.748666 -0.064695
C -2.740484 1.02007 1.537875
H -3.353469 1.740944 2.084359
C -3.170946 -0.412883 1.569497
H -2.299391 -1.072798 1.720501
C -4.1874 -0.689616 2.67242
H -5.095015 -0.079642 2.541947
H -4.487847 -1.749363 2.704276
H -3.753248 -0.435499 3.65081
I -0.009957 -1.787394 -0.102142
I 1.553008 1.603907 -0.400884

cat4-prod
Imaginary frequencies=0
SCF energy=-2487.6477175
C -2.900594 -2.236821 -0.368627
N -3.540781 -3.263058 -0.938093
N -3.810246 -1.336641 0.067414
C -2.961944 -4.453516 -1.540174
H -3.162605 -4.451334 -2.619807
H -1.881144 -4.470649 -1.366468
H -3.416865 -5.340325 -1.080911
C -3.5277 -0.132243 0.788577
C -3.839791 -0.070055 2.145642
C -2.931903 0.941913 0.132895
C -3.535856 1.082983 2.864826
H -4.307133 -0.9272 2.633694
C -2.593095 2.064947 0.883021
H -2.70731 0.891673 -0.933487
C -2.895477 2.150303 2.240694

H -3.774326 1.13965 3.927921
H -2.619892 3.045015 2.802194
N -1.906112 3.154812 0.256385
C -0.611115 3.16697 -0.127328
N -0.316137 4.367306 -0.635944
C 0.962408 4.820742 -1.155461
H 1.383245 5.57886 -0.481223
H 1.648676 3.971243 -1.232593
H 0.810575 5.255476 -2.151552
C 5.659788 0.147109 -0.451875
C 6.513567 1.214328 -0.74445
C 7.791763 1.068307 -1.263541
C 8.21872 -0.239629 -1.490788
C 7.385367 -1.329311 -1.207029
C 6.099688 -1.151484 -0.690264
C 4.378576 0.707747 0.096254
C 4.635771 2.160376 0.036716
H 8.424527 1.929348 -1.483784
H 9.215968 -0.414137 -1.89937
H 7.749379 -2.341357 -1.396153
H 5.456465 -2.006053 -0.477617
H 3.514995 0.470569 -0.55705
N 5.823193 2.406655 -0.418501
H 6.218942 3.342436 -0.523617
H 3.968918 2.965593 0.348626
C 2.030682 -5.146591 -0.81232
C 2.037054 -5.977163 0.310645
C 2.20824 -5.420512 1.578285
C 2.372407 -4.042335 1.724595
C 2.362084 -3.199935 0.605782
C 2.185196 -3.769858 -0.663822
H 1.904599 -5.576365 -1.809355
H 1.907691 -7.056047 0.196374
H 2.208223 -6.063333 2.462276
H 2.495401 -3.608692 2.720201
H 2.170648 -3.117453 -1.540705
C 2.523227 -1.708955 0.723551
O 1.6865 -0.985468 0.028604
C 3.562732 -1.231203 1.469529
H 4.243137 -1.946654 1.938042
C 3.936176 0.217995 1.531946
H 3.049793 0.829962 1.770896
C 5.014844 0.492137 2.575439
H 5.928267 -0.086448 2.366151
H 5.288558 1.558684 2.619681
H 4.65451 0.196101 3.571871
I 0.639451 1.492824 0.034377

I -0.828802 -1.946426 -0.191807
C -4.91202 -3.030267 -0.877641
C -5.996885 -3.782369 -1.33263
C -5.087437 -1.804139 -0.234079
C -7.258378 -3.245309 -1.110692
H -5.860378 -4.739778 -1.83662
C -6.35236 -1.260574 -0.009812
C -7.433001 -2.006694 -0.461854
H -8.138419 -3.795953 -1.448462
H -6.480015 -0.301483 0.493848
H -8.443947 -1.622944 -0.311831
C -1.449208 5.173672 -0.576269
C -1.662418 6.495285 -0.971784
C -2.465147 4.403391 -0.007387
C -2.939124 7.002853 -0.770724
H -0.86701 7.096416 -1.413638
C -3.750416 4.908143 0.192537
C -3.964692 6.222832 -0.199708
H -3.154071 8.033074 -1.060616
H -4.540261 4.299904 0.635307
H -4.953324 6.664906 -0.062138

cat5-prod
Imaginary frequencies=0
SCF energy=-2824.3433260
C -0.307279 2.81096 0.277686
N -0.825888 3.97645 -0.113323
N 1.002902 2.988711 0.564539
C -2.201822 4.239553 -0.501262
H -2.642199 4.965033 0.195248
H -2.219322 4.646541 -1.520565
H -2.774141 3.306243 -0.469166
C 1.858482 1.961408 1.074101
C 1.987128 1.879325 2.45923
C 2.460661 1.016277 0.230453
C 2.688745 0.829095 3.036283
H 1.504472 2.63853 3.076845
C 3.081446 -0.083767 0.842978
C 3.211669 -0.171064 2.225033
H 2.791837 0.765519 4.120166
H 3.708536 -1.042056 2.655179
N 3.550272 -1.195961 0.069376
C 2.806942 -2.285397 -0.245612
N 3.592399 -3.196289 -0.820761
C 3.206927 -4.510045 -1.309569
H 2.151161 -4.688171 -1.080455
H 3.365214 -4.556744 -2.394903

H 3.822664 -5.270367 -0.812212
C -4.361911 -0.542693 -1.749063
C -4.480137 -0.03542 -3.046946
C -5.210638 1.099447 -3.372884
C -5.85875 1.741124 -2.318912
C -5.762873 1.252308 -1.008402
C -5.012411 0.114406 -0.706582
C -3.44318 -1.725488 -1.79978
C -3.156064 -1.834651 -3.232341
H -5.273089 1.467213 -4.398185
H -6.450034 2.636812 -2.519586
H -6.285514 1.77532 -0.204592
H -4.934655 -0.253841 0.317116
H -2.472165 -1.437347 -1.306825
N -3.724218 -0.873691 -3.89668
H -3.629497 -0.733763 -4.903523
H -2.537856 -2.582708 -3.730898
C -1.745528 -1.277713 4.634688
C -2.964728 -1.233458 5.311013
C -4.147027 -1.470346 4.608299
C -4.110336 -1.751327 3.243408
C -2.890273 -1.807701 2.552255
C -1.710811 -1.557148 3.26953
H -0.812519 -1.093342 5.173243
H -2.995469 -1.011649 6.380443
H -5.108802 -1.425676 5.124953
H -5.048321 -1.911808 2.707154
H -0.753236 -1.588396 2.746207
C -2.809404 -2.093091 1.081107
O -1.763045 -1.590965 0.447376
C -3.776673 -2.804252 0.44359
H -4.607389 -3.217546 1.0194
C -3.792851 -3.039702 -1.044432
H -2.983283 -3.74185 -1.319202
C -5.120569 -3.627323 -1.516138
H -5.95691 -2.94857 -1.28624
H -5.118799 -3.81589 -2.60129
H -5.315582 -4.58382 -1.008176
I -1.210901 0.90987 0.41864
I 0.741842 -2.356059 0.099089
C 4.893544 -2.700649 -0.881212
C 6.069637 -3.256998 -1.386253
C 4.87198 -1.429878 -0.305269
C 7.216146 -2.480446 -1.280306
H 6.083974 -4.24797 -1.841057
C 6.019577 -0.646408 -0.19506
C 7.191683 -1.199207 -0.69386

H 8.160807 -2.872335 -1.661852
H 5.990119 0.346681 0.2545
H 8.119051 -0.626579 -0.63273
C 0.169999 4.951087 -0.078204
C 0.143724 6.31098 -0.391492
C 1.338243 4.323161 0.358966
C 1.340146 7.002266 -0.246747
H -0.768311 6.802651 -0.731737
C 2.541542 5.010933 0.503959
C 2.517319 6.364321 0.192091
H 1.370132 8.068623 -0.478539
H 3.448164 4.507807 0.842668
H 3.434347 6.948602 0.288509
C 2.468475 1.131699 -1.287583
F 1.682456 0.226019 -1.872575
F 3.706039 0.936579 -1.753743
F 2.079093 2.32751 -1.720479

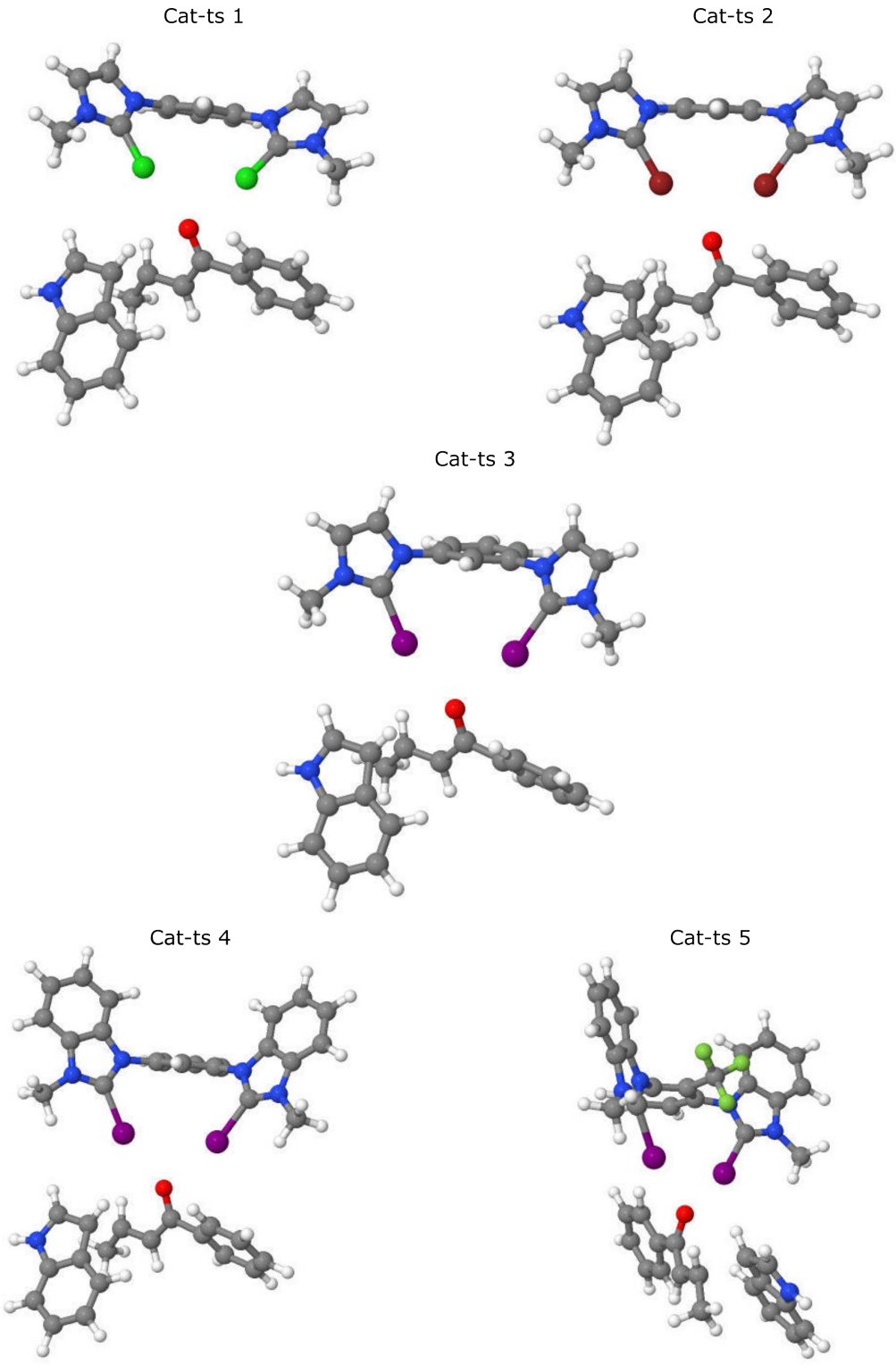

Figure A.5: Michael addition: catalysts 1 to 5, cat-ts structures.

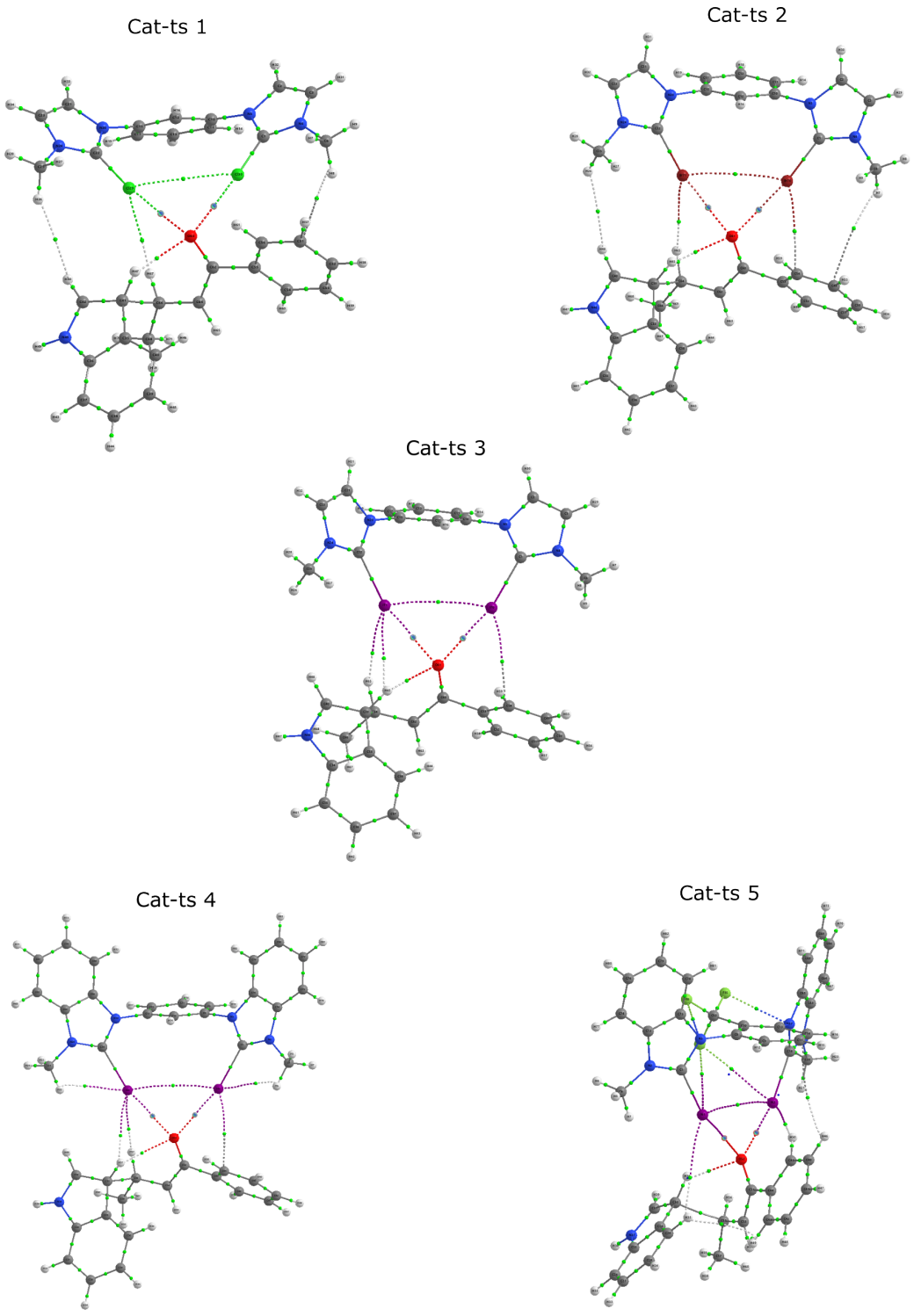

Figure A.6: Michael addition: catalysts 1 to 5, QTAIM molecular graphs of the cat-ts structures showing the X–O electron density at BCP.

Table A.13: The ρ(BCP) (a.u.) and the $\nabla^2\rho$ (a.u.) calculated for the cat1-ts structure

Atoms	**ρ(BCP) (a.u.)**	**$\nabla^2\rho$ (a.u.)**
H8 - C51	0.001368	0.004907
Cl30 - O63	0.018697	0.061125
Cl29 - Cl30	0.005879	0.02045
Cl29 - O63	0.017581	0.064643
Cl29 - H67	0.00472	0.01764
H47 - O63	0.018503	0.04907
H26 - H50	0.000956	0.004419

Table A.14: The ρ(BCP) (a.u.) and the $\nabla^2\rho$ (a.u.) calculated for the cat1-prod structure

Atoms	**ρ(BCP) (a.u.)**	**$\nabla^2\rho$ (a.u.)**
H27 - H50	0.001336	0.006059
H46 - C64	0.007896	0.023018
H47 - O63	0.03154	0.084452
Cl29 - O63	0.017891	0.064757
Cl29 - Cl30	0.006875	0.022714
Cl30 - O63	0.02099	0.06799
Cl30 - C55	0.00786	0.025971
H9 - C52	0.002986	0.009722

Table A.15: The ρ(BCP) (a.u.) and the $\nabla^2\rho$ (a.u.) calculated for the cat2-ts structure

Atoms	**ρ(BCP) (a.u.)**	**$\nabla^2\rho$ (a.u.)**
H26 - H50	0.000956	0.004419
H65 - Br71	0.004786	0.015593
H45 - O61	0.013982	0.039418
O61 - Br71	0.019649	0.075092
O61 - Br70	0.022248	0.074517
Br70 - Br71	0.007945	0.021171
C54 - Br70	0.007039	0.020012
H7 - C49	0.001089	0.003919

Table A.16: The ρ(BCP) (a.u.) and the $\nabla^2\rho$ (a.u.) calculated for the cat2-prod structure

Atoms	**ρ(BCP) (a.u.)**	**$\nabla^2\rho$ (a.u.)**
H27 - H48	0.001755	0.008278
H44 - C62	0.008259	0.024635
H65 - Br71	0.006448	0.019197
H45 - O61	0.022374	0.058563
O61 - Br71	0.024028	0.085148
Br70 - Br71	0.008824	0.024247
O61 - Br70	0.024066	0.077479
C54 - Br70	0.007877	0.022573
H9 - C49	0.001229	0.004349

Table A.17: The ρ(BCP) (a.u.) and the $\nabla^2\rho$ (a.u.) calculated for the cat3-ts structure

Atoms	**ρ(BCP) (a.u.)**	**$\nabla^2\rho$ (a.u.)**
H65 - I71	0.007328	0.022331
H45 - I71	0.005213	0.018845
H45 - O61	0.012506	0.036625
O61 - I71	0.020165	0.066474
O61 - I70	0.023269	0.068913
C54 - I70	0.006537	0.0182
I70 - I71	0.008872	0.024425

Table A.18: The ρ(BCP) (a.u.) and the $\nabla^2\rho$ (a.u.) calculated for the cat3-prod structure

Atoms	**ρ(BCP) (a.u.)**	**$\nabla^2\rho$ (a.u.)**
H44 - C62	0.007986	0.024551
H65 - I70	0.007822	0.023432
H45 - O61	0.013814	0.039571
C54 - I71	0.007681	0.021873
O61 - I70	0.02607	0.080357
O61 - I71	0.027739	0.077266
I70 - I71	0.010133	0.028951

Table A.19: The ρ(BCP) (a.u.) and the $\nabla^2\rho$ (a.u.) calculated for the cat4-ts structure

Atoms	**ρ(BCP) (a.u.)**	**$\nabla^2\rho$ (a.u.)**
H22 - I63	0.010479	0.036121
H37 - I63	0.006026	0.020589
H57 - I63	0.006359	0.020175
H37 - O53	0.010536	0.033043
O53 - I63	0.022295	0.074404
I62 - I63	0.008842	0.02462
O53 - I62	0.023785	0.070157
C44 - I62	0.006756	0.019046
H6 - I62	0.010618	0.036448

Table A.20: The ρ(BCP) (a.u.) and the $\nabla^2\rho$ (a.u.) calculated for the cat4-prod structure

Atoms	**ρ(BCP) (a.u.)**	**$\nabla^2\rho$ (a.u.)**
H36 - C54	0.007669	0.023626
H37 - I62	0.006074	0.022005
H57 - I62	0.007402	0.022544
H37 - O53	0.012613	0.037399
C46 - I63	0.007701	0.022128
O53 - I62	0.027737	0.08578
O53 - I63	0.028845	0.08
I62 - I63	0.009975	0.028805
H23 - I62	0.010306	0.035935

Table A.21: The ρ(BCP) (a.u.) and the $\nabla^2\rho$ (a.u.) calculated for the cat5-pts structure

Atoms	**ρ(BCP) (a.u.)**	**$\nabla^2\rho$ (a.u.)**
H35 - I61	0.001506	0.004777
H35 - H49	0.003665	0.014808
H49 - H54	0.010558	0.045735
H36 - O52	0.017423	0.048136
O52 - I61	0.025789	0.077784
O52 - I62	0.024327	0.081539
H50 - I62	0.006047	0.018426
I61 - I62	0.00733	0.020867
C11 - H46	0.000757	0.002759
I61 - F84	0.006115	0.0238
I62 - F84	0.005909	0.023192
N3 - F86	0.015566	0.062551
N17 - F85	0.015576	0.062582

Table A.22: The ρ(BCP) (a.u.) and the $\nabla^2\rho$ (a.u.) calculated for the cat5-prod structure

Atoms	**ρ(BCP) (a.u.)**	**$\nabla^2\rho$ (a.u.)**
H49 - H54	0.010508	0.046594
H35 - C53	0.008046	0.022816
H7 - C28	0.001083	0.003963
C29 - I61	0.003715	0.008445
H50 - I62	0.00628	0.020074
H36 - O52	0.036007	0.104762
O52 - I61	0.036689	0.106445
O52 - I62	0.030437	0.095758
I61 - I62	0.008834	0.027507
I61 - F84	0.006244	0.02408
I62 - F84	0.006117	0.023822
N17 - F85	0.014967	0.060078
N3 - F86	0.01552	0.062356

Table A.23: The ρ(BCP) and $\nabla^2\rho$ values in the cat-ts structures of catalysts 1 to 5, calculated at the ωb97xD/def2SVP computational level (solvent = DCM, SMD model and T = 273K).

Complex	**ρ(BCP) (a.u.)**	**$\nabla^2\rho$ (a.u.)**
Cat-ts 1	0.018	0.065
	0.019	0.061
Cat-ts 2	0.020	0.075
	0.022	0.075
Cat-ts 3	0.020	0.066
	0.023	0.069
Cat-ts 4	0.022	0.074
	0.024	0.070
Cat-ts 5	0.024	0.082
	0.026	0.078

Table A.24: The dihedral α angle and the X–X distance measure for all catalysts 1 to 5

Catalyst	**I_1 α-angle**	**I_2 α-angle**	**X-X distance (Å)**
1	72.4	72.8	4.5
2	88.3	88.2	5.1
3	85.8	73.4	4.7
4	81.9	80.9	4.7
5	97.9	97.4	5.6

Table A.25: Perturbation energies E(2) of the LP_{Br} to σ^*_{C-I} in the cat-ts structures of catalysts 1 to 5, calculated at the ωb97xD/def2SVP computational level (solvent = DCM, SMD model and T = 273K).

Complex	**Orb(1)**	**Orb(2)**	**E(2)(kJ/mol)**
Cat-ts 1	LP_O	$\sigma^*_{C_{47}-Cl_{29}}$	13.2
	LP_O	$\sigma^*_{C_{47}-Cl_{30}}$	7.5
Cat-ts 2	LP_O	$\sigma^*_{C_{47}-Br_{70}}$	35.2
	LP_O	$\sigma^*_{C_{47}-Br_{71}}$	28.6
Cat-ts 3	LP_O	$\sigma^*_{C_{47}-I_{70}}$	52.9
	LP_O	$\sigma^*_{C_{47}-I_{71}}$	42.7
Cat-ts 4	LP_O	$\sigma^*_{C_{47}-I_{62}}$	53.6
	LP_O	$\sigma^*_{C_{47}-I_{63}}$	50.4
Cat-ts 5	LP_O	$\sigma^*_{C_{47}-I_{61}}$	64.4
	LP_O	$\sigma^*_{C_{47}-I_{62}}$	57.1

Table A.26: Perturbation energies E(2) of the LP_{Br} to σ^*_{C-I} in the cat-prod structures of catalysts 1 to 5, calculated at the ωb97xD/def2SVP computational level (solvent = DCM, SMD model and T = 273K).

Complex	**Orb(1)**	**Orb(2)**	**E(2)(kJ/mol)**
Cat-prod 1	LP_O	$\sigma^*_{C_{47}-Cl_{29}}$	14.9
	LP_O	$\sigma^*_{C_{47}-Cl_{30}}$	19.0
Cat-prod 2	LP_O	$\sigma^*_{C_{47}-Br_{70}}$	40.9
	LP_O	$\sigma^*_{C_{47}-Br_{71}}$	45.1
Cat-prod 3	LP_O	$\sigma^*_{C_{47}-I_{70}}$	69.2
	LP_O	$\sigma^*_{C_{47}-I_{71}}$	70.8
Cat-prod 4	LP_O	$\sigma^*_{C_{47}-I_{62}}$	77.2
	LP_O	$\sigma^*_{C_{47}-I_{63}}$	75.3
Cat-prod 5	LP_O	$\sigma^*_{C_{47}-I_{61}}$	112.2
	LP_O	$\sigma^*_{C_{47}-I_{62}}$	75.3

cat6-mono
Imaginary frequencies=0
SCF energy=-1999.0633527
C 5.158526 -1.552657 -1.632078
N 4.205219 -0.54044 -1.201144
C 3.047847 -0.713589 -0.558936
I 2.224663 -2.513625 0.023235
N 2.470779 0.484517 -0.33432
C 1.236321 1.162722 1.650153
C 0.02358 1.410266 2.287363
C -1.184138 1.218135 1.617486
N -2.393545 0.590661 -0.400234
C -3.07481 -0.564331 -0.537178
I -2.485915 -2.344539 0.325182
N -4.170846 -0.354519 -1.270074
C -5.197651 -1.312078 -1.655227
C -4.217863 0.993578 -1.617536
C -5.151093 1.721434 -2.3586
C -4.890695 3.075445 -2.517681
C -3.747448 3.683074 -1.959251
C -2.821645 2.958565 -1.221414
C -3.087797 1.598153 -1.065659
C 3.294607 1.479015 -0.857439
C 3.158604 2.866794 -0.898089
C 4.186494 3.564581 -1.517056
C 5.302785 2.905574 -2.071583
C 5.432638 1.524191 -2.029034
C 4.396608 0.823578 -1.407881
H 5.304861 -1.464666 -2.716023
H 6.111943 -1.390455 -1.113003
H 4.774142 -2.549076 -1.392481
H 2.186233 1.305514 2.167269
H -2.139961 1.403851 2.111095
H -6.119073 -1.103675 -1.095618
H -4.856554 -2.330362 -1.44421
H -5.384593 -1.208563 -2.731304
H -6.036518 1.250427 -2.786223
H -5.590027 3.687808 -3.089808
H -3.587545 4.752089 -2.111171
H -1.93707 3.421051 -0.781968
H 2.292323 3.368217 -0.464681
H 4.12881 4.652959 -1.577809
H 6.08607 3.49833 -2.547566
H 6.294977 1.013347 -2.458165
C -1.160022 0.776597 0.299177
C 1.226747 0.724987 0.328684
C 0.037854 0.538484 -0.366961

C 0.000611 1.84234 3.735603
F -0.272541 0.81011 4.540624
F -0.934828 2.769316 3.952162
F 1.171123 2.349329 4.121781
H 0.042936 0.206416 -1.406278

cat7-mono
Imaginary frequencies=0
SCF energy=-2257.1637766
C 5.316882 -0.496367 -1.106537
N 4.238034 0.325903 -0.575315
C 3.147004 -0.163044 0.064536
I 2.646735 -2.135532 0.404024
N 2.386018 0.859759 0.452575
C 1.205325 0.710596 2.580495
C 0.013762 0.63775 3.296884
C -1.206898 0.631552 2.626356
N -2.477978 0.720227 0.548447
C -3.119577 -0.333884 0.034952
I -2.329292 -2.240039 0.113492
N -4.283801 0.100301 -0.506849
C -5.314186 -0.647017 -1.210489
C -4.376621 1.494663 -0.344238
C -5.340647 2.426787 -0.732805
C -5.084093 3.749474 -0.398293
C -3.919941 4.13407 0.294517
C -2.962589 3.205593 0.675781
C -3.223334 1.879811 0.333533
C 2.979542 2.05971 0.060096
C 2.548978 3.372777 0.242273
C 3.371553 4.363738 -0.270105
C 4.570075 4.045895 -0.935552
C 4.994365 2.736356 -1.115793
C 4.166672 1.734633 -0.598722
H 2.169323 0.715383 3.091975
H 0.036253 0.584805 4.386101
H -2.148447 0.572774 3.175258
H -6.244996 2.143708 -1.269801
H -5.809596 4.513591 -0.682469
H -3.768063 5.187637 0.535516
H -2.056126 3.487104 1.212782
H 1.616901 3.597605 0.762187
H 3.085354 5.410633 -0.155692
H 5.191163 4.8541 -1.32583
H 5.923426 2.520064 -1.636383
C -1.217859 0.702449 1.235872
C 1.157751 0.774594 1.189884

C -0.04489 0.782876 0.492553
F -5.142325 -1.939042 -1.081401
F -5.290222 -0.325759 -2.490286
F -6.489443 -0.31497 -0.711388
F 5.900084 -1.166881 -0.132601
F 6.205006 0.276708 -1.686198
F 4.844099 -1.350564 -1.992392
H -0.068057 0.841005 -0.596796

cat6-ts
Imaginary frequencies=1
SCF energy=-2824.3361587
C 1.744905 -5.263813 -1.387078
N 2.539558 -4.080166 -1.097788
C 2.117267 -2.910977 -0.612514
I 0.173934 -2.330618 -0.138325
N 3.170583 -2.073045 -0.48659
C 3.576281 -0.527165 1.342646
C 3.506402 0.755157 1.876478
C 2.970379 1.806662 1.132542
N 1.944601 2.632381 -0.908571
C 0.623965 2.801905 -1.142029
I -0.793615 1.423499 -0.473596
N 0.441554 3.927895 -1.834852
C -0.816181 4.492135 -2.297818
C 1.680431 4.524609 -2.057601
C 2.031298 5.701683 -2.720697
C 3.385597 6.006452 -2.763372
C 4.353072 5.171194 -2.169647
C 4.00213 4.001153 -1.509049
C 2.641031 3.700902 -1.467943
C 4.323369 -2.736106 -0.903014
C 5.655938 -2.329282 -0.972702
C 6.560672 -3.265603 -1.455033
C 6.152646 -4.55501 -1.851535
C 4.825065 -4.95544 -1.780439
C 3.91688 -4.013057 -1.294739
H 2.098726 -6.096154 -0.765156
H 0.692058 -5.061079 -1.165482
H 1.85553 -5.518741 -2.448951
H 3.963143 -1.362031 1.928245
H 2.877803 2.807834 1.558827
H -0.751796 4.666072 -3.379405
H -1.002525 5.441707 -1.779219
H -1.630322 3.790986 -2.088074
H 1.280926 6.347094 -3.178457
H 3.710188 6.917086 -3.270263

H 5.406325 5.451447 -2.231562
H 4.744639 3.349268 -1.046892
H 5.964778 -1.329581 -0.664065
H 7.616063 -2.997047 -1.530177
H 6.900399 -5.257599 -2.224131
H 4.507284 -5.952592 -2.086731
C 2.531781 1.562354 -0.163339
C 3.128622 -0.743667 0.041425
C 2.631725 0.296155 -0.736538
C 3.976296 1.032071 3.285242
F 2.970364 1.463165 4.056339
F 4.91363 1.9838 3.302127
F 4.489663 -0.050931 3.865763
H 2.296811 0.119132 -1.759501
C -5.801435 -0.073152 -0.868766
C -6.924354 -0.420577 -1.642493
C -8.190148 0.121698 -1.429023
C -8.309724 1.050582 -0.399735
C -7.201209 1.415816 0.384617
C -5.943679 0.86064 0.162558
C -4.686724 -0.896758 -1.328589
C -5.19813 -1.593195 -2.446093
H -9.045734 -0.168337 -2.041641
H -9.281906 1.50665 -0.200539
H -7.331758 2.152766 1.180386
H -5.086147 1.15085 0.772793
H -3.634722 -0.607742 -1.249424
N -6.501248 -1.353194 -2.588438
H -7.103534 -1.800635 -3.273949
H -4.685068 -2.293684 -3.103963
C -0.840494 0.720491 4.074327
C -1.826661 1.211708 4.931062
C -3.172471 1.011795 4.621668
C -3.532585 0.32145 3.465058
C -2.550379 -0.17562 2.596278
C -1.200994 0.037675 2.915467
H 0.215741 0.872604 4.306761
H -1.546898 1.751674 5.838728
H -3.949475 1.399325 5.284671
H -4.590544 0.18544 3.230351
H -0.427876 -0.344247 2.245535
C -2.889322 -0.911408 1.333406
O -2.066287 -0.831915 0.3561
C -4.075058 -1.636241 1.232701
H -4.812884 -1.603413 2.036376
C -4.402819 -2.327275 0.032616
H -3.54376 -2.722774 -0.518953

C -5.618705 -3.211809 0.039928
H -6.525518 -2.648353 0.30862
H -5.783035 -3.713249 -0.922893
H -5.47982 -3.990232 0.807344

cat7-ts
Imaginary frequencies=1
SCF energy=-3082.4385115
C 3.787304 3.063849 -1.647847
N 2.685745 3.304152 -0.731451
C 1.790591 2.35799 -0.359438
I 1.616237 0.346429 -0.921281
N 0.938925 2.90632 0.512661
C 0.028794 1.80407 2.485432
C -0.991118 1.088121 3.107604
C -2.148209 0.761401 2.404599
N -3.45205 0.7848 0.345937
C -3.521084 -0.237215 -0.513118
I -1.844869 -1.3998 -0.957261
N -4.794337 -0.326002 -0.969873
C -5.267834 -1.347722 -1.890044
C -5.579554 0.675989 -0.361671
C -6.928951 1.031359 -0.450374
C -7.339606 2.109714 0.321957
C -6.453737 2.818319 1.153949
C -5.115884 2.465429 1.245709
C -4.708228 1.379986 0.472094
C 1.284534 4.240101 0.735732
C 0.695718 5.198332 1.558626
C 1.290764 6.450775 1.56953
C 2.427423 6.72553 0.787684
C 3.007952 5.76967 -0.036041
C 2.407268 4.507587 -0.050494
H 0.956716 2.032379 3.012638
H -0.871009 0.759836 4.140949
H -2.942161 0.175867 2.871479
H -7.634049 0.501092 -1.085143
H -8.38662 2.414793 0.277071
H -6.827435 3.661055 1.737986
H -4.413592 2.999328 1.886944
H -0.183757 4.964005 2.159837
H 0.871664 7.23786 2.198812
H 2.872091 7.72146 0.827035
H 3.8881 6.006045 -0.628769
C -2.281492 1.178279 1.081673
C -0.137499 2.214904 1.164845
C -1.299109 1.935348 0.451067

F -5.282432 -2.527399 -1.297608
F -4.485203 -1.409214 -2.947954
F -6.486912 -1.048692 -2.278352
F 4.705543 2.305158 -1.078896
F 4.328856 4.213326 -1.985213
F 3.348868 2.461424 -2.734963
H -1.416935 2.260533 -0.583553
C 1.767365 -2.202329 2.746094
C 1.448003 -2.439193 4.095591
C 2.412712 -2.538179 5.096338
C 3.739664 -2.383922 4.705886
C 4.082184 -2.144345 3.363208
C 3.107088 -2.053211 2.373689
C 0.518478 -2.243109 1.991665
C -0.487473 -2.377224 2.975359
H 2.140581 -2.727083 6.136259
H 4.529088 -2.449723 5.457661
H 5.134662 -2.026182 3.096121
H 3.377606 -1.868987 1.33209
H 0.35812 -1.679325 1.071861
N 0.058795 -2.542415 4.179214
H -0.459076 -2.751394 5.028609
H -1.56709 -2.425302 2.83882
C 3.922477 -2.46525 -3.918067
C 5.152489 -2.942712 -3.463138
C 5.2568 -3.468932 -2.175204
C 4.13747 -3.523159 -1.346157
C 2.896222 -3.04763 -1.794055
C 2.805739 -2.512854 -3.087338
H 3.833113 -2.052391 -4.925671
H 6.030871 -2.903056 -4.111768
H 6.218342 -3.836261 -1.809059
H 4.243764 -3.922155 -0.335293
H 1.841434 -2.135717 -3.434262
C 1.663953 -3.053266 -0.93604
O 0.776761 -2.168432 -1.203675
C 1.550569 -3.954996 0.119692
H 2.385389 -4.617928 0.352076
C 0.431119 -3.962668 0.99852
H -0.527081 -3.692916 0.543462
C 0.350503 -5.074092 2.009262
H 1.229569 -5.079528 2.671984
H -0.558156 -5.022863 2.623563
H 0.3408 -6.035196 1.471172

cat6-prod-front
Imaginary frequencies=0

SCF energy=-2824.3506313
C -2.521052 4.834075 -1.889586
N -3.077637 3.538217 -1.53912
C -2.46187 2.531845 -0.915267
I -0.479914 2.386563 -0.253792
N -3.329958 1.505168 -0.767623
C -3.407297 0.136415 1.237942
C -3.053023 -1.024777 1.921509
C -2.327782 -2.028494 1.284576
N -1.143784 -2.851642 -0.671093
C 0.201143 -2.758171 -0.78453
I 1.212716 -1.022071 -0.137585
N 0.666046 -3.867981 -1.362205
C 2.050856 -4.185922 -1.67206
C -0.403675 -4.719329 -1.634609
C -0.452304 -5.982931 -2.225286
C -1.709232 -6.561481 -2.348894
C -2.873922 -5.907279 -1.900839
C -2.824445 -4.650058 -1.312414
C -1.560663 -4.073396 -1.19169
C -4.558371 1.870602 -1.311952
C -5.771047 1.188991 -1.410398
C -6.810105 1.868882 -2.032198
C -6.645554 3.174899 -2.535626
C -5.436316 3.850308 -2.433763
C -4.393169 3.165864 -1.807287
H -2.594134 4.977902 -2.97533
H -3.085114 5.621588 -1.373011
H -1.471347 4.876123 -1.581862
H -3.936052 0.947796 1.740925
H -2.003771 -2.918984 1.825268
H 2.333163 -5.110088 -1.151036
H 2.696686 -3.366822 -1.33784
H 2.159864 -4.32363 -2.755798
H 0.449643 -6.488986 -2.570812
H -1.798271 -7.549199 -2.805099
H -3.839794 -6.401922 -2.019577
H -3.721143 -4.137955 -0.960929
H -5.891092 0.1788 -1.016718
H -7.780275 1.379196 -2.135064
H -7.492109 3.668303 -3.016733
H -5.307127 4.861416 -2.821438
C -1.979688 -1.867885 -0.053031
C -3.045065 0.272131 -0.098303
C -2.353943 -0.733699 -0.768135
C -3.445597 -1.179511 3.371804
F -4.691976 -1.647829 3.492752

F -3.400492 -0.010197 4.017287
F -2.639622 -2.025083 4.015824
H -2.063834 -0.609914 -1.812546
C 4.964898 0.639594 -0.967152
C 5.509638 0.467438 -2.243601
C 6.265166 -0.633608 -2.623721
C 6.478162 -1.603412 -1.645357
C 5.946869 -1.456838 -0.356241
C 5.182771 -0.342743 -0.00345
C 4.165698 1.907594 -0.975348
C 4.397086 2.411502 -2.33212
H 6.66911 -0.732542 -3.632434
H 7.068137 -2.489508 -1.888422
H 6.133994 -2.233204 0.388658
H 4.76566 -0.240403 0.999138
H 3.07547 1.63098 -0.911543
N 5.128288 1.585652 -3.018013
H 5.387542 1.7187 -3.99655
H 4.018395 3.335067 -2.772261
C 0.464284 0.12428 4.30046
C 1.410208 -0.272568 5.246202
C 2.764786 -0.052227 4.995145
C 3.170449 0.56058 3.810088
C 2.23026 0.971664 2.852984
C 0.872284 0.734051 3.115664
H -0.598732 -0.044832 4.485223
H 1.093128 -0.756896 6.17277
H 3.514825 -0.370297 5.723267
H 4.236685 0.704131 3.620352
H 0.125096 1.035753 2.379511
C 2.636489 1.611453 1.55631
O 1.851602 1.378535 0.517261
C 3.771085 2.35452 1.467765
H 4.362725 2.532676 2.368172
C 4.293642 2.939693 0.182025
H 3.653384 3.786464 -0.130124
C 5.724607 3.451082 0.331645
H 6.408174 2.637295 0.620531
H 6.098341 3.897991 -0.603116
H 5.772013 4.221936 1.115379

cat7-prod-back1
Imaginary frequencies=0
SCF energy=-3082.4531693
C 3.846238 2.449114 -2.102824
N 2.768424 2.948821 -1.271015
C 1.84777 2.153852 -0.675105

I 1.570315 0.047641 -0.709702
N 1.019176 2.937718 0.025751
C 0.048744 2.436494 2.205085
C -1.000878 1.941325 2.976045
C -2.154868 1.456162 2.364977
N -3.425706 0.948961 0.344423
C -3.501503 -0.252615 -0.240307
I -1.821414 -1.517957 -0.343654
N -4.758277 -0.409481 -0.720491
C -5.230637 -1.609151 -1.388572
C -5.529092 0.729132 -0.407576
C -6.861881 1.082506 -0.635646
C -7.263192 2.327252 -0.168069
C -6.382092 3.196347 0.500421
C -5.060363 2.844512 0.731445
C -4.66277 1.5925 0.265917
C 1.409849 4.273234 -0.093833
C 0.857626 5.429265 0.453923
C 1.495048 6.622766 0.14729
C 2.63668 6.650489 -0.673658
C 3.180162 5.496499 -1.223776
C 2.536138 4.29441 -0.918797
H 0.972293 2.783394 2.671893
H -0.909669 1.915792 4.062806
H -2.970435 1.036123 2.956498
H -7.56145 0.427719 -1.149247
H -8.297727 2.636713 -0.327051
H -6.747223 4.164907 0.846657
H -4.363725 3.503593 1.250654
H -0.027892 5.388549 1.089459
H 1.10387 7.557695 0.55216
H 3.114827 7.607978 -0.888131
H 4.062974 5.54181 -1.856687
C -2.257111 1.498226 0.97605
C -0.084591 2.474642 0.819004
C -1.244917 2.03695 0.18655
F -5.399415 -2.585737 -0.516148
F -4.363299 -1.997 -2.301523
F -6.379381 -1.352601 -1.975278
F 4.749372 1.829827 -1.365604
F 4.418038 3.457598 -2.725024
F 3.377322 1.605377 -3.000811
H -1.341409 2.074068 -0.899626
C 2.176327 -1.690349 2.867223
C 1.96782 -0.896004 3.998818
C 2.971521 -0.186657 4.644915
C 4.252828 -0.305845 4.108942

C 4.492214 -1.099427 2.978637
C 3.461687 -1.794205 2.342404
C 0.848559 -2.237854 2.436615
C -0.051427 -1.719315 3.47657
H 2.766428 0.424022 5.525539
H 5.082691 0.224508 4.580099
H 5.508158 -1.174867 2.585416
H 3.656318 -2.402193 1.457935
H 0.547764 -1.721058 1.492604
N 0.591267 -0.966118 4.314635
H 0.161407 -0.486271 5.106961
H -1.123339 -1.897787 3.576081
C 2.446243 -3.565814 -3.950298
C 3.612662 -4.327689 -3.880283
C 4.067215 -4.775666 -2.638718
C 3.360308 -4.467786 -1.477635
C 2.181391 -3.709259 -1.536147
C 1.741238 -3.256764 -2.788465
H 2.081525 -3.209417 -4.916946
H 4.168768 -4.568322 -4.789518
H 4.986756 -5.362258 -2.572402
H 3.741511 -4.811474 -0.513223
H 0.828252 -2.660052 -2.838568
C 1.382171 -3.348252 -0.320968
O 0.635465 -2.259871 -0.437302
C 1.435909 -4.084088 0.819061
H 2.046395 -4.989247 0.839468
C 0.686495 -3.743624 2.081086
H -0.398529 -3.87255 1.906938
C 1.097756 -4.638422 3.247759
H 2.171893 -4.531513 3.465441
H 0.53638 -4.39746 4.164412
H 0.908125 -5.694476 3.004637

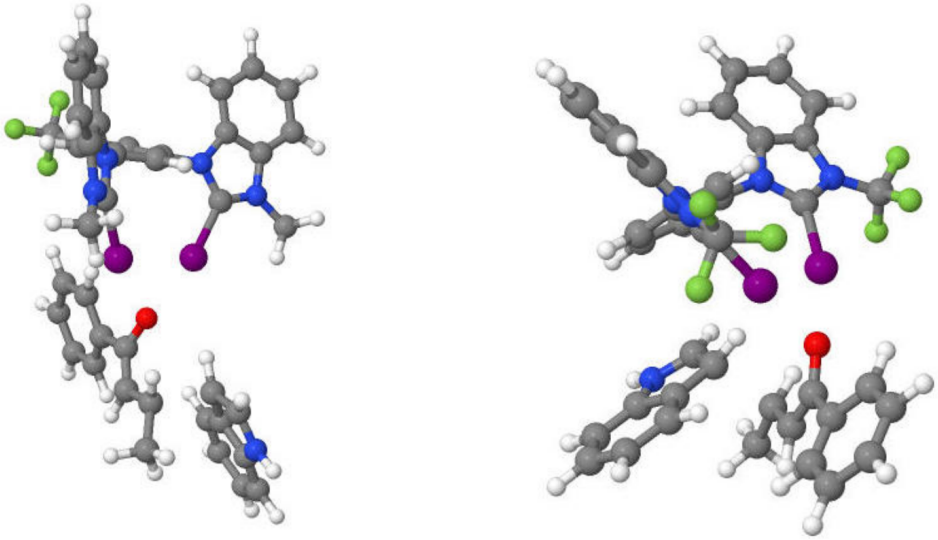

Cat-ts 6 Cat-ts 7

Figure A.7: Michael addition: catalysts 6 and 7, cat-ts structures.

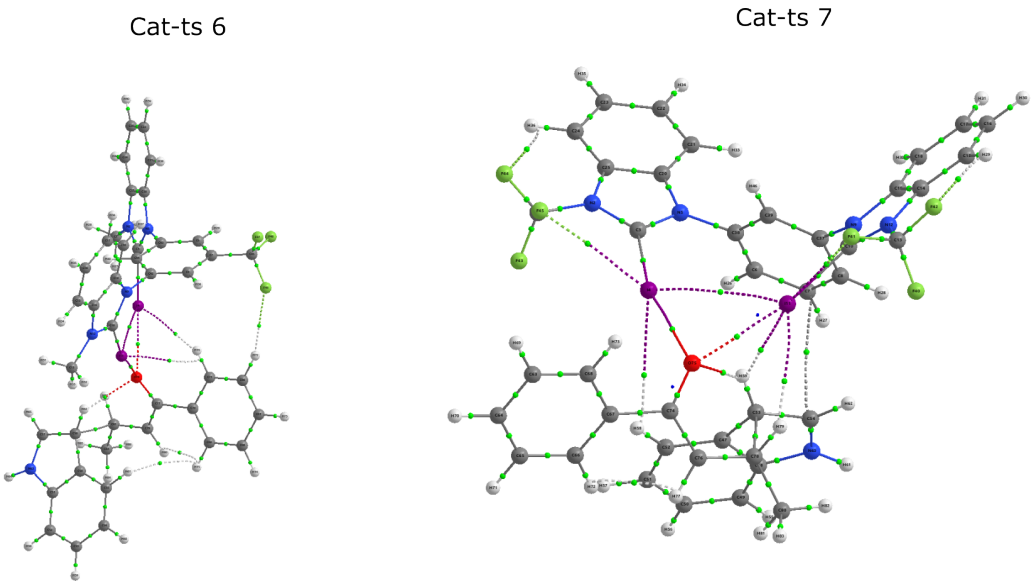

Figure A.8: Michael addition: catalysts 6 and 7, QTAIM molecular graphs of the cat-ts structures showing the X–O electron density at BCP.

Table A.27: The ρ(BCP) (a.u.) and the $\nabla^2\rho$ (a.u.) calculated for the cat6-ts structure

Atoms	**ρ(BCP) (a.u.)**	**$\nabla^2\rho$ (a.u.)**
H61 - H75	0.003041	0.012383
H75 - H80	0.010255	0.045232
H62 - O78	0.016642	0.045821
F46 - H72	0.002879	0.014875
I11 - H76	0.006044	0.021395
I4 - H76	0.00587	0.018201
I4 - O78	0.024489	0.079708
I11 - O78	0.026508	0.081226
I4 - I11	0.007949	0.022538

Table A.28: The ρ(BCP) (a.u.) and the $\nabla^2\rho$ (a.u.) calculated for the cat6-prod structure

Atoms	**ρ(BCP) (a.u.)**	**$\nabla^2\rho$ (a.u.)**
F47 - H72	0.003135	0.015672
F48 - H72	0.002923	0.015371
I4 - H76	0.00765	0.022423
H61 - C79	0.008241	0.023382
I11 - C55	0.003533	0.008234
H62 - O78	0.03487	0.101302
I4 - O78	0.029972	0.093409
I11 - O78	0.036964	0.105269
I4 - I11	0.008989	0.02758

Table A.29: The ρ(BCP) (a.u.) and the $\nabla^2\rho$ (a.u.) calculated for the cat7-ts structure

Atoms	**ρ(BCP) (a.u.)**	**$\nabla^2\rho$ (a.u.)**
H72 - H77	0.011274	0.046986
I4 - H58	0.002768	0.008518
C7 - C54	0.004408	0.010799
I11 - H59	0.007853	0.024707
H59 - O75	0.013627	0.039263
I11 - H79	0.00687	0.02147
I11 - O75	0.024195	0.079905
I4 - O75	0.029634	0.087832
I4 - I11	0.007977	0.023092
I11 - F41	0.009524	0.034573
I4 - F45	0.009985	0.036042
H29 - F42	0.014487	0.062843
H36 - F44	0.013819	0.06036

Table A.30: The ρ(BCP) (a.u.) and the $\nabla^2\rho$ (a.u.) calculated for the cat7-prod structure

Atoms	**ρ(BCP) (a.u.)**	**$\nabla^2\rho$ (a.u.)**
H72 - H77	0.010145	0.045285
H58 - C76	0.007345	0.02101
I4 - C47	0.004088	0.009696
C7 - N60	0.003417	0.009783
H59 - O75	0.028593	0.079455
I4 - O75	0.041407	0.119064
I11 - O75	0.035128	0.1113
I4 - F45	0.009514	0.034893
H36 - F44	0.013987	0.060918
I11 - F41	0.010595	0.037887
I11 - F41	0.010595	0.037887

Table A.31: The ρ(BCP) and $\nabla^2\rho$ values in the cat-ts structures of catalysts 6 and 7, calculated at the ωb97xD/def2SVP computational level (solvent = acetonitrile, SMD model and T = 273K).

Complex	**ρ(BCP) (a.u.)**	**$\nabla^2\rho$ (a.u.)**
Cat-ts 6	0.018	0.065
	0.019	0.061
Cat-ts 7	0.020	0.075
	0.022	0.075

Table A.32: Perturbation energies E(2) of the LP_{Br} to σ^*_{C-I} in the cat-ts structures of catalysts 6 and 7, calculated at the ωb97xD/def2SVP computational level (solvent = DCM, SMD model and T = 273K).

Complex	**Orb(1)**	**Orb(2)**	**E(2)(kJ/mol)**
Cat-ts 6	LP_O	$\sigma^*_{C_{47}-I_4}$	56.44
	LP_O	$\sigma^*_{C_{47}-I_{11}}$	69.32
Cat-ts 7	LP_O	$\sigma^*_{C_{47}-I_4}$	71.76
	LP_O	$\sigma^*_{C_{47}-I_{11}}$	55.94

B Published papers

- Garcia, M. R., Iribarren, I., Rozas, I., Trujillo, C., *Cover Profile.* Chem. Eur. J. 2023, e202300717.[96]
- Garcia, M. R., Iribarren, I., Rozas, I., Trujillo, C., *Cover Picture.* Chem. Eur. J. 2023, e202300716.[97]
- Garcia, M.R., Iribarren, I., Rozas, I. and Trujillo, C. (2023), *Simultaneous Hydrogen Bonds with Different Binding Modes: the Acceptor "Rules" but the Donor "Chooses".* Chem. Eur. J. 2023, e202203577.[98]
- N. Melnyk, M. R. Garcia, I. Iribarren and C. Trujillo, *Evolution of design approaches in asymmetric organocatalysis over the last decade.* Tetrahedron Chem, 2023, 5, 100035.[99]
- Iribarren, I, Garcia, MR, Trujillo, C. *Catalyst design within asymmetric organocatalysis.* WIREs Comput Mol Sci. 2022; 12:e1616.[100]